

1 **ExIFFI and EIF⁺: Interpretability and Enhanced Generalizability to Extend the**
2 **Extended Isolation Forest**

3
4 ALESSIO ARCUDI, University of Padova, Italy
5

6 DAVIDE FRIZZO, University of Padova, Italy
7

8 CHIARA MASIERO, Statwolf Data Science Srl, Italy
9

10 GIAN ANTONIO SUSTO, University of Padova, Italy
11

12 Anomaly [Detection](#) involves identifying unusual behaviors within complex datasets and systems. While Machine Learning algorithms
13 and Decision Support Systems (DSSs) offer effective solutions for this task, simply pinpointing anomalies [may prove insufficient](#)
14 in real-world applications. Users require insights into the rationale behind these predictions to facilitate root cause analysis and
15 foster trust in the model. However, the unsupervised nature of AD presents a challenge in developing interpretable tools. This paper
16 addresses this challenge by introducing ExIFFI, a novel interpretability approach specifically designed to explain the predictions made
17 by Extended Isolation Forest. ExIFFI leverages feature importance to provide explanations at both global and local levels. This work
18 also introduces EIF⁺, an enhanced variant of Extended Isolation Forest, conceived to improve its generalization capabilities through
19 a different splitting hyperplanes design strategy. A comprehensive comparative analysis is conducted, employing both synthetic
20 and real-world datasets to evaluate various unsupervised AD approaches. The analysis demonstrates the effectiveness of ExIFFI in
21 providing explanations for AD predictions. Furthermore, the paper explores the utility of ExIFFI as a feature selection technique in
22 unsupervised settings. Finally, this work contributes to the research community by providing open-source code, facilitating further
23 investigation and reproducibility.
24

25 **ACM Reference Format:**

26 Alessio Arcudi, Davide Frizzo, Chiara Masiero, and Gian Antonio Susto. 2023. ExIFFI and EIF⁺: Interpretability and Enhanced
27 Generalizability to Extend the Extended Isolation Forest. *J. ACM* 37, 4, Article 111 (August 2023), 78 pages. <https://doi.org/XXXXXXX>.
28 XXXXXXXX
29

30 **1 INTRODUCTION**

31 Machine Learning (ML) and Artificial Intelligence (AI) play a central role in the ongoing socio-economic change,
32 revolutionizing various sectors such as manufacturing [20, 45], medicine [17], and the Internet of Things [19]. With the
33 increasing deployment of ML across various industries, new problems have emerged due to the widespread application
34 of these systems, which are often complex and opaque.
35

36 Moreover, the end users of these systems are becoming more diverse, including people from various backgrounds
37 who may not have a knowledge in data-driven methods. Therefore, it is essential to develop explanation algorithms
38 that provide a deeper understanding of the model structure and predictions to ensure that these systems can be used
39

40 Authors' addresses: Alessio Arcudi, alessio.arcudi@phd.unipd.it, University of Padova, Italy; Davide Frizzo, davide.frizzo.1@phd.unipd.it, University of
41 Padova, Italy; Chiara Masiero, chiara.masiero@statwolf.com, Statwolf Data Science Srl, Italy; Gian Antonio Susto, gianantonio.susto@unipd.it, University
42 of Padova, Italy.
43

44 Permission to make digital or hard copies of all or part of this work for personal or classroom use is granted without fee provided that copies are not
45 made or distributed for profit or commercial advantage and that copies bear this notice and the full citation on the first page. Copyrights for components
46 of this work owned by others than ACM must be honored. Abstracting with credit is permitted. To copy otherwise, or republish, to post on servers or to
47 redistribute to lists, requires prior specific permission and/or a fee. Request permissions from permissions@acm.org.

48 © 2023 Association for Computing Machinery.

49 Manuscript submitted to ACM

50 Manuscript submitted to ACM

effectively by a wide range of users. Many scientific works identify explainability¹ as a key factor to enable the successful adoption of ML-based systems [11, 12, 25].

In the case of tabular data, there are various methods for explaining the outcomes of a model [31]. One common approach is to calculate the importance of each feature in the model's predictions. This involves evaluating the influence of each feature on both individual predictions (referred to as "Local Importance") and the overall dataset ("Global Importance"). By understanding the relative importance of each feature, users can gain insight into how the model is using the input data to inform its predictions.

Despite the remarkable recent advancements in eXplainable Artificial Intelligence (XAI), most approaches are designed for supervised tasks, leaving unsupervised tasks, like Anomaly Detection (AD), rarely discussed in the literature.

AD, also referred to as Outlier Detection², is a field of ML that focuses on identifying elements that live outside the standard "normal" behavior observed in the majority of the dataset [16].

Explainability for AD approaches has paramount importance. A simple example is given by the AD approaches used to monitor industrial machinery. Effective interpretation of the reasons for the rise of an anomaly enables Root Cause Analysis, leading to the reduction of machine failures, energy loss, waste of resources, and production costs. Another argument for the need for interpretable algorithms is that the lack of explanations hinders the trust in the model's output by the ones who benefit from its services, **in particular in the case of high-stakes decisions. In the latter scenarios explainability is not only a need but it is also required by the law** [10].

Isolation Forest (IF) [26] is one of the most popular AD approaches due to its high accuracy, low computational costs, and relatively simple inner mechanisms. This method relies on an iterative process. Recursively splitting the feature space along axis-aligned hyper-planes chosen at random, IF can isolate anomalous points using few space partitions.

Some ad hoc interpretability approaches are available for IF [26]. The first approach to provide explainability features for IF, named Depth-based Isolation Forest Feature Importance (DIFI) [8] takes advantage of the inner structure of the IF to supply global and local model explanations.

Unfortunately, the one-dimensional partition process that IF relies on causes the creation of artifacts that degrade the detection of anomalies and negatively affect feature explanation. Thus, the Extended Isolation Forest (EIF) has been proposed [15]. EIF improves over the IF using oblique partitions that avoid creating the previously discussed artifacts. According to the literature, EIF is one of the best unsupervised AD approaches [3]. However, it lacks built-in interpretability features. To address this gap and promote the adoption of isolation-based unsupervised AD approaches, **this paper makes three key contributions:**

- (1) We propose the Extended Isolation Forest Feature Importance (ExIFFI), the first (to the best of our knowledge) model-specific approach which can provide explanations about the Extended Isolation Forest.
- (2) We present EIF⁺, a refined version of the EIF designed to optimally model the space around the training data distribution, enhancing the algorithm's performance on unseen data. This innovation aims to bolster the model's generalization ability, reliably identifying anomalies even without prior knowledge of their potential locations or without being present in the training dataset. ExIFFI applies to EIF⁺, too.

¹While authors in the literature use the term 'interpretability' and 'explainability' associated with slightly different concepts when associated to Machine Learning/Artificial Intelligence as presented in [14], in this work we will use both terms interchangeably.

²In this paper, we will refer to 'Outlier Detection' and 'Anomaly Detection' alternatively, always referring to the same unsupervised task of finding anomalous data points.

105 (3) We benchmark the novel EIF⁺ and ExIFFI against state-of-the-art isolation based AD and explainability ap-
 106 proaches on 15 public datasets and showcase their effectiveness and computational efficiency. To facilitate
 107 further investigation and reproducibility, we introduce a functionally-grounded quantitative evaluation of
 108 interpretability by using Feature Selection as a proxy task and provide open-source code for the experiments.
 109

110 The rest of the paper is organized as follows. First, Section 2 surveys existing relevant research results. Then, a
 111 general introduction of the IF algorithm is provided in Section 3.1. Then, in Section 3.2, the EIF proposed in [15] is
 112 discussed. The newly introduced EIF⁺ model will be instead presented in Section 3.3. Successively, the DIFFI and ExIFFI
 113 interpretation algorithms are presented in Section 4.1 and 4.2 together with an explanation on the graphical tools
 114 exploited to easily illustrate their results.
 115

116 In Section 5 a detailed description of the experimental setup, used to assess the effectiveness of EIF⁺ and ExIFFI as
 117 AD and interpretability methods, is provided.

118 Successively, Section 6 present in details the experimental evaluation conducted on 6 datasets, both synthetic and
 119 real-world, together with an ablation study on the hyperparameters of ExIFFI and the Time Scaling Experiments,
 120 exploited to test the scalability of the presented methods on large-scale datasets.

121 The comprehensive results of experiments conducted on the remaining 9 datasets are detailed in the Appendix A.4,A.5.
 122 This Appendix includes also an extensive analysis highlighting the EIF model’s enhancements over the traditional IF
 123 A.1.3 and provides a thorough description of the datasets utilized in the study and a detailed description of the datasets
 124 used A.1.

125 Finally, conclusions and future research directions are discussed in Section 7.

131 2 RELATED WORK

132 Feature importance has been widely exploited and popularized in recent years, particularly thanks to the widespread
 133 application of Random Forest (RF) algorithm. RF provides built-in approaches to provide a ranking of the most important
 134 features [21]. Moreover, due to the rise of many post-hoc methods [40], like permutation importance [2] or SHAP [28],
 135 feature ranking as an interpretability measure has been extended also to models that are not tree-based.

136 Still, explainability for unsupervised AD approaches remains a challenging problem. In particular, eXplainable
 137 Anomaly Detection (XAD) is defined as the extraction of relevant knowledge from an anomaly detection model
 138 concerning relationships either contained in data or learned by the model. Several intrerpretability methods were
 139 adopted to enrich the capabilities of AD models. In [24], the authors provide a detailed survey on the state-of-the-art.

140 The need for explainability is particularly required in deep learning based Anomaly Detection methods which are
 141 considered, because of their inherent structure, black-box models. The majority of deep learning based AD models
 142 are based on the Anomaly Autoencoder (AE) model [9]. Oliveira et al. introduced RXP (Residual eXPlainer) [34], an
 143 interpretable method to deal with the shortcomings of AE-based AD models where the explanations are produced
 144 performing a deviation analysis of the reconstructed input features.

145 ECOD (Empirical-Cumulative-distribution-based Outlier Detection) [23] is another common approach for Anomaly
 146 Detection based on the empirical cumulative distribution of the data points and the fact that outliers are points placed in
 147 the tails of the estimated distribution. Differently from other XAD approaches ECOD has the advantage of possessing an
 148 intrinsic local interpretability. In fact, given a data point, it is necessary to simply observe the estimated tail probabilities
 149 of each dimension to have a clear measure of the contribution of each one of them in the detection of abnormal samples.

157 However, isolation-based AD approaches are often the go-strategy in practical applications, due to their efficiency
 158 and low computational burden which make them particularly suitable to be used in Decision Support Systems.
 159

160 As discussed in 1, DIFFI is the reference method for the explainability of these approaches. DIFFI belongs to Model-
 161 specific interpretation tools, i.e., approaches that are designed to work for specific model classes. Instead, Model-
 162 agnostic tools can be used on any machine learning model and are applied after the model has been trained [31].

163 Another similar model-specific approach for the interpretation of the IF model is proposed by Kartha et al. in [18]
 164 which however provides only local explainability. Moreover, differently from this method, DIFFI is also proven to be
 165 effective in industrial settings [6], [4].
 166

167 As introduced in 1, EIF is a modification of IF that overcomes some of its limitations, e.g. artifacts in the anomaly score
 168 function due to the one-dimensional partitions defined in IF. However, to the best of our knowledge, no model-specific
 169 interpretability tool exists for EIF. Drawing inspiration from DIFFI, this work aims at addressing this gap by proposing
 170 ExIFFI. Moreover, we also propose EIF⁺, an enhancement of EIF with better generalization properties that can still be
 171 explained via ExIFFI.
 172

174 3 ISOLATION-BASED APPROACHES FOR ANOMALY DETECTION

175 Next, we provide some notions about isolation-based approaches for AD. This family of methodologies, stemming
 176 from the Isolation Forest [26], identifies outliers as samples that can be easily separated from the others, i.e., through a
 177 reduced number of splitting hyperplanes.
 178

181 3.1 Isolation Forest

182 Isolation Forest is a widely used ML model for AD [26]. It generates a set of N random trees, called isolation trees, that
 183 are able to identify anomalous elements in a dataset based on their position in the tree structure. The idea behind this
 184 approach is that anomalies, on average, are located at the beginning of the trees because they are easier to separate
 185 from the rest of the dataset.
 186

187 Assume that we have n training data $\mathbf{X} = \{\mathbf{x}_1, \dots, \mathbf{x}_n\}$, where $\mathbf{x}_i \in \mathbb{R}^d$. The IF algorithm chooses at random one
 188 dimension $q \in \{1, \dots, d\}$ and a split value $p \in [\min_{i \in \{1, \dots, n\}} x_{i,q}, \max_{i \in \{1, \dots, n\}} x_{i,q}]$. The dataset is then divided into
 189 two subsets, the left one $L = \{\mathbf{x}_i | x_{i,q} \leq p\}$ and the right one $R = \{\mathbf{x}_i | x_{i,q} > p\}$. This procedure is calculated iteratively
 190 until the whole forest is built. Suppose the size of the dataset is excessive, meaning that the number of samples makes
 191 the construction of the trees too slow; in that case, it is demonstrated by Liu et al. [26] that it is better to build the forest
 192 using only a random subsample $\tilde{\mathbf{X}}$ with \tilde{n} elements for each tree. Not only does this keep the computational cost low. It
 193 also improves IF's ability to identify anomalies clearly. Once the model has built an isolation forest, to determine which
 194 data points live outside the dataset distribution, the algorithm computes an anomaly score for each of them. This value
 195 is based on the average depth among trees where each data point is isolated.
 196

197 The depth of a point x in a tree t , denoted by $h_t(x)$, is the cardinality of the set of nodes \mathcal{P}_x^t that it has to pass to
 198 reach the leaf node, i.e.:
 199

$$200 h_t(x) = |\mathcal{P}_x^t| \quad \text{where} \quad \mathcal{P}_x^t = \{k_{s_1}, k_{s_2}, \dots, k_{s_h}\}, \quad (1)$$

201 Let $E(h(x))$ be the mean value of depths reached among all trees for a single data point x . Then, according to [35],
 202 the anomaly score is defined by the function:
 203

$$204 s(x, \tilde{n}) = 2^{-\frac{E(h(x))}{c(\tilde{n})}}, \quad (2)$$

where $c(N)$ is the normalizing factor defined as the average depth of an unsuccessful search in a Binary Search Tree [15], i.e.:

$$c(N) = 2H(N - 1) - \frac{2(N - 1)}{N}. \quad (3)$$

and $H(i)$ is the harmonic number that can be estimated by:

$$H(i) = \ln(i) + 0.5772156649 \text{ (Euler constant).} \quad (4)$$

If's fast execution with low memory requirement is a direct result of building partial models and requiring only a significantly small sample size as compared to the given training set. This capability is due to the fact IF has the main goal to quickly isolate anomalies more than modelling the normal distribution, contrarily to what other detection methods do [38].

3.2 Extended Isolation Forest

Although IF is one of the most popular and effective AD algorithms, it has some drawbacks due to its partition strategy. One of them is related to considering only hyper-planes that are orthogonal with respect to the directions of the feature space, as Hariri et al. show in [15]. In some cases, this bias leads to the formation of some artifacts where points are associated with low anomaly scores even if they are clearly anomalous. These areas are in the intersection of the hyperplanes orthogonal to the dimensions associated with the detection of inliers (Figure 24), creating misleading score maps and, in some cases, wrong predictions.

As a consequence, Hariri et al. in [15] tried to improve the AD algorithm by correcting this bias with a different and more general algorithm called Extended IF. Instead of selecting a hyper-plane orthogonal to a single input dimension chosen at random, they suggested picking a random point p and a random vector v that are consequently used to build a hyperplane that will split the space at each node of the binary tree into two smaller subspaces, as the IF does. Therefore, they proposed a more generic and extended paradigm, while maintaining the fast execution and low memory requirements of the original IF.

In the following, we will briefly describe the working principle of the EIF model. Let's consider a set X of n elements $\mathbf{x}_i \in \mathbb{R}^d$ with $i \in \{1, \dots, n\}$. In order to evaluate the anomaly score of the samples, the EIF model [15] generates a forest of N binary trees:

$$\mathcal{T} = \{t_0, t_1, \dots, t_N\}. \quad (5)$$

Every tree $t \in \mathcal{T}$ is built from a bootstrap sample $X_t \subset X$. At each node k of t , a random hyperplane \mathcal{H}_k^t is selected by picking a random point p inside the distribution space limits, and a normalized random vector v defined as

$$v \sim \frac{\mathbf{Z}}{\|\mathbf{Z}\|_2}, \quad \text{where } \mathbf{Z} = (Z_1, \dots, Z_d)^\top \quad \text{and} \quad Z_i \sim \mathcal{N}(0, 1) \forall i \in \{1, \dots, d\}. \quad (6)$$

Lesouple et al. in [22] pointed out that this way of drawing a random hyperplane may lead to the creation of empty branches, that are merely artifacts of the algorithm. To avoid this problem, they propose a particular way of selecting random hyperplanes, that we also use in our implementation of the EIF model.

As done in [15, 22], we first select a random hyperplane by drawing a unit vector v defined as in (6). which will serve as the normal vector of the hyperplane. Then, as done in [22], the point where the hyperplane passes is obtained by a scalar α drawn uniformly between the minimum value and the maximum value of the points of the dataset X in the

direction of the random vector previously drawn. Therefore,

$$\alpha \in [\min \{x \cdot v \mid \forall x \in X\}, \max \{x \cdot v \mid \forall x \in X\}], \quad p = \alpha v. \quad (7)$$

The algorithm starts by generating a random hyperplane $\mathcal{H}_{k_0}^t$ defined by the intercept point p and v as described in Equations 6 and 7.

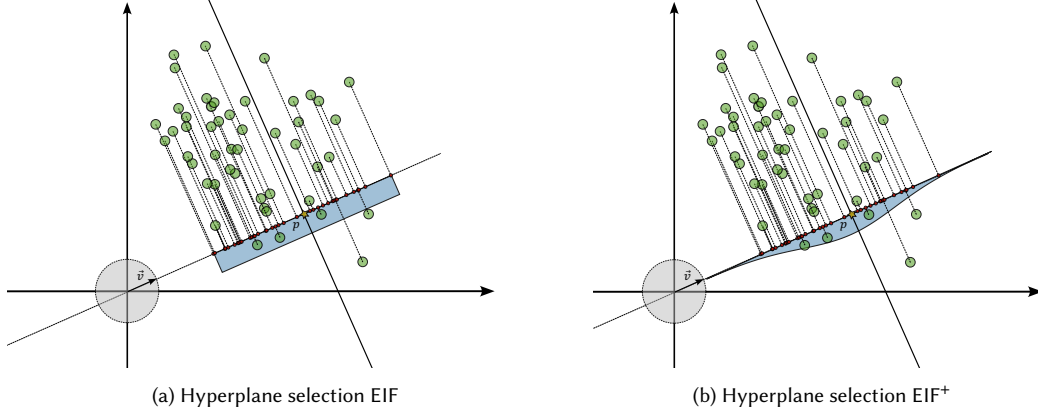


Fig. 1. Figure 1a illustrates the process of hyperplane selection utilized by the algorithm developed by Lesouple et al. [22]. This algorithm selects the point p by uniformly sampling it from an interval depicted in light blue within the figure. In Figure 1b, a novel approach is presented for drawing the point p . This new method involves sampling the point p from a normal distribution centered around the mean point of the dataset projection onto the direction described by vector v (represented as red dots in the figure). The distribution is visually depicted as a blue bell shape.

Thus the hyperplane splits the dataset X_t into two subsets,

$$\begin{aligned} L_{k_0}^t &= \{\mathbf{x} \mid \mathbf{x} \in X_{k_0}^t, \mathbf{v}_{k_0}^t \cdot \mathbf{x} > \mathbf{v}_{k_0}^t \cdot \mathbf{p}_{k_0}^t\}, \\ R_{k_0}^t &= X_t \setminus L_{k_0}^t. \end{aligned} \quad (8)$$

The root node of the tree, k_0 , is the space splitting made by the hyperplane $\mathcal{H}_{k_0}^t$. Then, this method is applied recursively to the subsets $L_{k_0}^t$ and $R_{k_0}^t$ until the max number of splits is reached, which corresponds to the preset max depth of the tree or when the set to split has only one element.

Thanks to this hierarchical tree structure, to evaluate if an element is an anomaly, the model extracts the path of the point $x \in X_t$ from the root to the leaf nodes down the tree. Then, as IF does [38], the EIF algorithm uses the average depth of the point in each tree to evaluate the anomaly score, according to the paradigm that the anomalies can be isolated with few partitions. The average depth of the point in the trees will be translated to an anomaly score according to Equation (2), as in IF.

3.3 EIF⁺ a novel enhancement of EIF algorithm

Lesouple et al. [22] shown that the EIF algorithm presented by Hariri et al. in [15] can create misleading empty branches. On the other hand, we observed that the solution proposed in [22] hinders the ability to generalize well in the space around the distribution. Actually, generalization ability is very important in the context of AD, since an anomaly is a point that is outside the normal distribution of the data.

313 Therefore, we propose EIF⁺, a novel approach that enhances the EIF methodology, based on the modification
 314 introduced by Lesouple et al. [22]. EIF⁺ aims to better describe the space surrounding the training data distribution.
 315 This goal is achieved by choosing splitting hyperplanes with an *ad hoc* procedure.

316 Let $\mathcal{A} = \{\mathbf{x} \cdot \mathbf{v} \mid \mathbf{x} \in X\}$ be the set of the point projections along the hyperplane's orthogonal direction \mathbf{v} . As in
 317 [22], the point \mathbf{p} is defined as $\mathbf{p} = \alpha\mathbf{v}$. However, instead of drawing α using the interval defined by the minimum and
 318 maximum values of \mathcal{A} , EIF⁺ draws it from a normal distribution $N(\mathbb{E}[\mathcal{A}], \eta\sigma(\mathcal{A}))$ as shown in Figure 1b. Even if EIF⁺
 319 can generate empty branches, they contribute to the formation of a model that exhibits enhanced generalizability, as
 320 will be shown in Section 6.

323 4 INTERPRETABILITY FOR ISOLATION-BASED ANOMALY DETECTION APPROACHES

324 Next, we delve into interpreting the predictions computed by the isolation-based models introduced in Section 3.
 325 Interpretation algorithms aim to explain the latent patterns identified by the models, thereby enriching our comprehen-
 326 sion of their outputs. Drawing inspiration from the DIFFI algorithm developed by Carletti et al. [8] for the IF, we
 327 introduce ExIFFI, a novel model-specific algorithm designed to interpret the results generated by the Extended Isolation
 328 Forest (EIF), along with its variant, the EIF⁺.

329 4.1 Depth-based Isolation Forest Feature Importance

330 Depth-based Isolation Forest Feature Importance (DIFFI) was the first unsupervised model-specific method addressing
 331 the need to interpret the IF model [8]. It exploits the structure of the trees in the IF algorithm to understand which
 332 features are the most relevant to discriminate whether a point is an outlier or not. In particular, a meaningful feature
 333 should isolate the anomalies as soon as possible, and create a high imbalance when isolating anomalous points (the
 334 opposite being true for inliers).

335 We briefly explain how DIFFI works and we introduce the related notation, as we will leverage it when introducing
 336 the novel ExIFFI approach to explain EIF and EIF⁺ predictions. From [8], we define:

337 **Induced Imbalance Coefficients** λ : given an internal node k of an isolation tree, as defined in Section 3.1, let
 338 $n(k)$ be the number of points that the node divides, being $n_l(k)$ and $n_r(k)$ the number of points on the left and
 339 the right child, respectively. The coefficient measuring the induced imbalance of the node v is:

$$340 \quad \lambda(v) = \begin{cases} 0 & \text{if } n_l(k) = 0 \text{ or } n_r(k) = 0 \\ 341 \quad \tilde{\lambda}(k) & \text{otherwise} \end{cases} \quad (9)$$

342 where

$$343 \quad \tilde{\lambda}(k) = g\left(\frac{\max(n_l(k), n_r(k))}{n(k)}\right) \quad \text{and} \quad g(a) = \frac{a - \lambda_{\min}(n)}{2(\lambda_{\max}(n) - \lambda_{\min}(n))} + 0.5. \quad (10)$$

344 In the previous equation, λ_{\min} and λ_{\max} denote the minimum and maximum scores that can be obtained a
 345 priori given the number of data $n(k)$.

346 **Cumulative feature importances** \mathbf{I} : it is a vector of dimension d (i.e., the number of features) where the j -th
 347 component is the feature importance of the j -th feature. In [8], authors distinguish between \mathbf{I}_I , created based
 348 on predicted inliers, and \mathbf{I}_O , based on the outliers. Concerning \mathbf{I}_I , the procedure starts with the initialization
 349 $\mathbf{I}_I = \mathbf{0}_d$. Considering the subset of predicted inliers for the tree t , $\mathcal{P}_{I,t}$, for each predicted inlier $x_I \in \mathcal{P}_{I,t}$, DIFFI
 350 iterates over the internal nodes in its path $Path(x_I, t)$. If the splitting feature associated with the generic internal
 351 node k is f_j , then \mathbf{I}_I is updated as follows:

node v is f_j , then we update the j -th component of \mathbf{I}_I by adding the quantity:

$$\Delta = \frac{1}{h_t(x_I)} \lambda_I(v) \quad (11)$$

The same procedure applies for $x_O \in \mathcal{P}_{O,t}$ and \mathbf{I}_O . Intuitively, at each point and each step, the vector accumulates the imbalance produced by each feature. The imbalance is measured by the previously defined λ and weighted by the depth of the node. This means that, according to DIFFI, features that allowed to isolate the points sooner, are considered to be more useful.

Features counter \mathbf{V} : it is used to compensate for uneven random feature sampling that might bias the calculated cumulative feature importance. At each passage of a point through a node, the entry of the counter corresponding to the splitting feature is incremented by one. As for the cumulative feature importance, two feature counters are calculated, the one for predicted inliers \mathbf{V}_I and the one for outliers \mathbf{V}_O .

Based on the above-introduced quantities, DIFFI computes the Global Feature Importance by looking at the weighted ratio between outliers and inliers cumulative feature importance:

$$GFI = \frac{\mathbf{I}_O/\mathbf{V}_O}{\mathbf{I}_I/\mathbf{V}_I}$$

4.2 Extended Isolation Forest Feature Importance (ExIFFI)

Drawing inspiration from DIFFI, we introduce ExIFFI, the Extended Isolation Forest Feature Importance, to rank the importance of the features in deciding whether a sample is an anomaly or not for the EIF model.

As seen in Section 3.2, a node $k \in \mathcal{K}_t$ in an EIF tree $t \in \mathcal{T}$ corresponds to an hyperplane \mathcal{H}_k^t , that splits the subset $X_k^t \subseteq X^t \subseteq X$. Using the Lesouple et al. [22] correction of the EIF, \mathcal{H}_k^t is completely defined by means of a vector orthogonal to its direction \mathbf{v}_k^t , defined as in (6), and a point \mathbf{p}_k^t that belongs to it, defined as in (7).

The hyperplane \mathcal{H}_k^t separates the points in a set of elements on the left side of the hyperplane and a set of elements on the right side of the hyperplane.

$$\begin{aligned} L_k^t &= \{\mathbf{x} | \mathbf{x} \in X_k^t, \mathbf{v}_k^t \cdot \mathbf{x} > \mathbf{v}_k^t \cdot \mathbf{p}_k^t\}, \\ R_k^t &= X_k^t \setminus L_k^t. \end{aligned} \quad (12)$$

ExIFFI computes a vector of feature importances for each node of the tree, based on two intuitions:

- The importance of the node k for a point x is higher when k creates a greater inequality between the number of elements on each side of the hyperplane, and x is in the smaller subset. Indeed, greater inequality means a higher grade of isolation for the points in the smaller set.
- For node k , the relative importance of the j -th feature is determined by the projection of the normal vector of the splitting hyperplane onto that feature. If the split occurs along a single feature, that feature will receive the entire importance score. If the splitting hyperplane is oblique, the importance scores of multiple features will be calculated based on their respective projections onto the normal vector of the hyperplane.

Thus, we assign an importance value function to every node of the trees that is the projection on the normal vector of the splitting hyperplane of the quotient between the cardinality of the sample before a particular node and after it, following the path of a sample \mathbf{x} . Thus, knowing that the splitting hyperplane \mathcal{H}_k^t of that node is determined by the

417 pair $\{\mathbf{v}_k^t, \mathbf{p}_k^t\}$ ³:

$$\lambda_k^t(\mathbf{x}) = \begin{cases} \left(\frac{|X_k^t|}{|L_k^t|} \right) \text{abs}(\mathbf{v}_k^t), & \text{if } \mathbf{v}_k^t \cdot \mathbf{x} > \mathbf{v}_k^t \cdot \mathbf{p}_k^t \\ \left(\frac{|X_k^t|}{|R_k^t|} \right) \text{abs}(\mathbf{v}_k^t), & \text{otherwise} \end{cases} \quad (13)$$

422 The vector of importances evaluated in the tree t for a point x is the sum of all the importance vectors of all the
423 nodes that the element x passed through on its path to the leaf node in the tree t defined in Equation (1):
424

$$\mathbf{I}_t(x) = \sum_{k \in \mathcal{P}_x^t} \lambda_{t,k}(x). \quad (14)$$

425 We then calculate the sum of the importance vector of the point x for all the trees in \mathcal{T} :

$$\mathbf{I}(x) = \sum_{t \in T} \mathbf{I}_t(x) \quad (15)$$

432 We define $\mathbf{V}(x)$ as the sum of the vectors orthogonal to the hyperplanes of the nodes that an element x passes in a
433 tree, then we calculate the sum of the values in all the trees:

$$\mathbf{V}(x) = \sum_{t \in T} \sum_{k \in \mathcal{P}_x^t} \mathbf{v}_k^t \quad (16)$$

438 4.2.1 *ExIFFI: Global Feature Importance.* To globally evaluate the importance of the features, we divide X into the
439 subset of predicted inliers $Q_I = \{\mathbf{x}_i \in X | \hat{y}_i = 0\}$ and the one of predicted outliers $Q_O = \{\mathbf{x}_i \in X | \hat{y}_i = 1\}$ where
440 $\hat{y}_i \in \{0, 1\}$ is the binary label produced by the thresholding operation indicating whether the corresponding data point
441 \mathbf{x}_i is anomalous ($\hat{y}_i = 1$) or not ($\hat{y}_i = 0$).
442

443 We define the global importance vectors for the inliers and for the outliers by summing out the importance values
444 introduced in Equation (15):
445

$$\mathbf{I}_I = \sum_{\mathbf{x} \in Q_I} \mathbf{I}(\mathbf{x}), \quad \mathbf{I}_O = \sum_{\mathbf{x} \in Q_O} \mathbf{I}(\mathbf{x}). \quad (17)$$

448 Likewise the sum of the orthogonal vectors:
449

$$\mathbf{V}_I = \sum_{\mathbf{x} \in Q_I} \mathbf{V}(\mathbf{x}), \quad \mathbf{V}_O = \sum_{\mathbf{x} \in Q_O} \mathbf{V}(\mathbf{x}). \quad (18)$$

452 Due to stochastic sampling of hyperplanes, in order to avoid the bias generated by the fact that it is possible that
453 some dimensions are sampled more often than others, the vectors of importance have to be divided by the sum of the
454 orthogonal vectors.
455

$$\hat{\mathbf{I}}_I = \frac{\mathbf{I}_I}{\mathbf{V}_I}, \quad \hat{\mathbf{I}}_O = \frac{\mathbf{I}_O}{\mathbf{V}_O}. \quad (19)$$

459 To evaluate which are the most important features to discriminate a data as an outlier we divide the importance
460 vector of the outliers by the one of the inliers. Equation (19), and we obtain the global feature importance vector in the
461 same vein as in the DIFFI algorithm [8]:
462

$$\text{GFI} = \frac{\hat{\mathbf{I}}_O}{\hat{\mathbf{I}}_I}. \quad (20)$$

466
467 ³With $\text{abs}(\mathbf{v})$ we refer to the positive part of every element of the vector \mathbf{v}

469 470 471 472 473 474 475 476 *4.2.2 ExIFFI: Local Feature Importance.* The Local Feature Importance assumes significance primarily within the context of anomalous data points, especially from the point of view of applications. Indeed, providing explanations of samples deemed anomalous eases decision-making by domain experts, who can subsequently tailor their responses based on the salient features driving the anomaly of a single point. Let's take into account an element x , the Equation (15) gives a vector of importances $I(x)$ of the sample x for each feature. Then the vector $V(x)$ is the normalization factor of the feature importance. Thus, the Local Feature Importance (LFI) of an element x is the quotient:

$$\text{LFI}(x) = \frac{I(x)}{V(x)}. \quad (21)$$

477 478 479 480 481 482 *4.2.3 Visualizing Explanations.* Miller [30] defines interpretability in AI models as the extent to which a human can comprehend the rationale behind a decision. To be effective, interpretability should deliver a clear and comprehensible representation of how inputs influence outputs, even for individuals who are not experts in the field.

483 484 485 486 To bolster users' trust in the model, relying solely on a series of numerical Scores is insufficient. Providing a series of summary scores and comprehensible graphical representations of these scores may help the evaluation of the model outputs and evaluating its interpretational efficacy.

487 488 To achieve these goals, three distinct graphical representations are proposed, two for the GFI, and one to comprehend the Local Feature Importance.

489 490 491 492 493 494 495 The GFI in the plots discussed can accommodate several model runs, reflecting the inherent stochastic nature of the EIF/EIF⁺ model. This strategy acknowledges the inherent randomness of the model, advocating for the use of numerous runs to embrace these variations and yield more reliable interpretability outcomes. Such an approach deepens the insight into the impact of individual features on the model's output. For validating the algorithm, we will employ this approach of multiple model runs in Section 6.

496 497 498 499 500 501 502 503 504 505 506 507 508 **GFI Bar Plot** In this plot, we consider n runs of model training executions, and for each training we compute the GFI score vector as described in Section 4.2.1. Successively, the Bar Plot is obtained by showing the percentage distribution across all potential ranking positions for each distinct feature. To enhance visual clarity, the graphical representation is confined to the foremost six ranking positions. As it will be shown in Section 6.1 and Section 6.2, in the datasets the most important features are placed in the very first rankings, strongly dominating the output with respect to the other features. Thus, limiting the representation just to the top six ranking positions is more than sufficient in most cases. For each position, there is a vertical bar partitioned into distinct colors associated with the features that appeared in that rank in one of the runs. A feature can be considered important if it occupies a large portion of the vertical bar associated with the top rankings. A visual example of the GFI Bar Plot can be found in Figure 2a.

509 510 511 512 513 514 515 516 517 **GFI Score Plot** While the Bar Plot offers a comprehensive overview of feature rankings, it lacks the inclusion of precise quantitative Importance Scores. Incorporating these actual scores can offer valuable complementary insights. These scores provide a quantitative measure of how one feature's importance compares to another, and when computed across multiple runs, they reveal the consistency of the ranking. For a practical illustration, refer to Figure 2b. To address these nuances, we consider the Score Plot. This graphical representation consists in a horizontal bar plot with superimposed score uncertainty to depict the average Global Importance Score obtained for each feature among the n training executions.

518 519 **LFI Scoremap** In the Scoremap, the focus is on local interpretability. Given a pair of features, we define a grid of values and compute the Local Importance Score for the two selected features. Then, for each point in the grid,

we identify the feature with the highest value and assign the color accordingly: red for the first feature and blue for the second one. Furthermore, a darker color shape corresponds to a higher Feature Importance Score. To provide additional contextual insights, a scatter plot depicting the data points is overlaid on the score map, where points are distinguished among inliers (depicted as blue dots) and outliers (represented as red stars). This representation is enriched with the contour plot of the Anomaly Score, where the darker the contour line, the higher the Anomaly Score. Since it is not feasible to inspect all features pairs, selecting the most meaningful pair of features has paramount importance. In most cases, as will be described in the next sections, a common choice is to focus on the pair composed of the two most important features at global level so that it is possible to capture the dispersion of anomalous points along one or both axes of the plot. For example, this strategy was exploited for the local Scoremap of the Bisect3D dataset, depicted in Figure 2c. In cases in which the analysis of a pair of features is not enough to provide a reliable explanation of the model's outputs an extension of the Local Scoremap, called Complete Local Scoremap can be exploited. Additional details about Complete Scoremaps are reported in Appendix A.3.

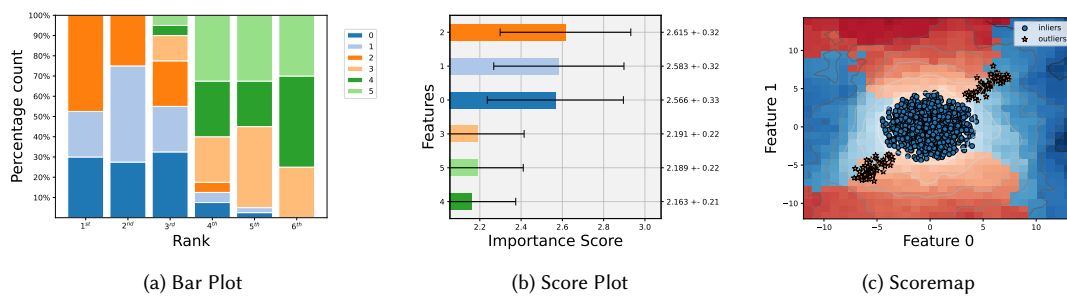


Fig. 2. Bar Plot 2a, Score Plot 2b, and Scoremap 2c of the dataset Bisect 3d

In order to explain how the interpretation of the graphical representation just described can be conducted, we present the example of the Bisect3D dataset, that will be commented deeply in the Section 6.1 in order to validate the interpretation algorithm. The dataset is built by anomalous points that are placed ad-hoc along the bisector line of the Feature 0, 1 and 2, while the inlier points are placed around the origin of the axes using a normal distribution along all the 6 dimensions.

As a consequence, Feature 0, 1 and 2 have a crucial role in the outlier's detection. Because of the stochasticity of the different executions performed the model will alternatively select one of the three features as the top-ranked one.

As a result, in the Bar Plot depicted in Figure 2a the importance is almost evenly shared among the three considered attributes. The Score Plot in Figure 2b shows three almost identical Importance Scores, while the remaining features are consistently lower than the first 3 features. The order of importance of the first three may probably change if another set of model executions is performed.

Looking at the scatter plot superimposed on the Scoremap, depicted in Figure 2c, it is clear that the stars representing the outliers deviate from the normal distribution represented by the ball of inliers.

The distribution of the red and blue colors provides useful insights on how the Local Importance Score changes in the different locations of the feature space identified by the two attributes under analysis. In particular, one can observe a distinct pattern in the Scoremap. Points located at the center occupy a region characterized by lighter shades, while

573 anomalies are concentrated in a darker area. Notably, these anomalies tend to align with the boundary where the most
 574 significant feature transition occurs, transitioning from Feature 0 to Feature 1.
 575

576 5 EXPERIMENTAL SETUP

577 To comprehensively assess the performance and interpretability of the EIF⁺ model and our proposed approach, we
 578 conduct a series of experiments using various benchmark datasets, detailed in Section 5.3. The implementation code for
 579 EIF⁺ and ExIFFI, along with the experimental setup to replicate our findings, is publicly accessible at <https://github.com/alessioarcudi/ExIFFI>. Our evaluation of a dataset is divided into two main sections. The initial segment presented
 580 in Section 5.1 assesses the EIF⁺ algorithm's performance, offering a comparative analysis against other AD models.
 581 The second evaluation presented in Section 5.2 delves into the results of the ExIFFI interpretation, comparing it with
 582 another ad-hoc interpretation method, DIFFI, and various post-hoc interpretation techniques. Following the evaluation
 583 of various datasets and considering the Isolation Forest models' speed and low memory requirements, we analyze the
 584 computational efficiency of these algorithms. In Section 6.4 we compare the algorithms considering the time needed to
 585 fit the model, predict the results and computing feature importances. This examination highlights the efficiency of the
 586 proposed models.
 587

588 5.1 Performance Evaluation

589 Initially, we conduct a thorough analysis of the EIF⁺ model's AD capabilities by benchmarking it against several other
 590 AD models. This comparison encompasses both well-established models widely recognized in the literature and a
 591 cutting-edge model representing the state-of-the-art in unsupervised AD. Specific models included in this comparative
 592 analysis are:

- 600 • Traditional Isolation-based approaches such as Isolation Forest (IF) and Extended Isolation Forest (EIF).
 601
- 602 • The novel Deep Isolation Forest (DIF), an advanced Isolation-based model integrating deep learning techniques
 603 for enhanced AD [44].
- 604 • The Anomaly AutoEncoder [9], a deep learning-based AD model, recognized for its robust performance in
 605 unsupervised AD scenarios.

606 The Performance evaluation aims to highlight the distinctive characteristics of the EIF⁺ model relative to analogous
 607 models in the AD field. Central to our evaluation is the EIF⁺ model's enhanced generalization capability towards
 608 novel anomalies, an improvement over the EIF. Our analysis methodically examines how anomaly contamination level
 609 influence the average precision metric, with a particular focus on delineating the performance disparities between
 610 EIF and EIF⁺. This rigorous assessment not only benchmarks the EIF⁺ model against traditional approaches but also
 611 highlights its advanced generalization properties in specific scenarios.
 612

613 With reference to the analysis of the performances varying the contamination, we consider two distinct experimental
 614 scenarios chosen to mirror the varied conditions under which AD models might be deployed, offering a comprehensive
 615 understanding of their adaptability and effectiveness:
 616

- 617 • Scenario I: We fit and evaluate the models using the entire dataset.
- 618 • Scenario II: We fit the models exclusively on the inliers within the dataset, that correspond to the scenario of 0
 619 contamination of outliers. Subsequently, we assess the Average Precision scores of these models when applied
 620 to the entirety of the dataset.

625 In both scenarios, we conducted multiple iterations for each model. Repeated runs are necessary to take into account
 626 the impact of the random generation of the isolation trees.
 627

628 Our analysis will not only compare the AD performance of EIF⁺ with other models but also evaluate their compu-
 629 tational efficiency. Given the value placed on speed for Isolation-based models, it's crucial to weight the comparison
 630 with other more complex models in terms of computational costs. This comprehensive evaluation will present the
 631 trade-off between higher performances and the required computational resources, offering insights into the practical
 632 applicability of EIF⁺ in contexts where both precision and speed are important.
 633

634 5.2 Interpretability Evaluation

635 Following the performance assessment, we shift our focus to the interpretability aspects of AD, focusing particularly on
 636 the evaluation of the ExIFFI algorithm. This algorithm enhances the EIF and EIF⁺ models with built-in interpretive
 637 capabilities.
 638

639 Our evaluation is carried out in two stages. Initially, we qualitatively examine the ExIFFI algorithm's interpretive
 640 method in two distinct scenarios through the plots detailed in section 4.2.3, observing how the resulting visualizations
 641 provide aspects on the nature of the anomalies. Given the lack of standardized benchmark datasets that provide a
 642 ground truth on the feature influence of the anomalies, we need to find strategies in order to assess the results coming
 643 from the ExIFFI. An initial evaluation utilizes synthetic datasets, crafted with the intention to provide complete insight
 644 into the anomalies generated and which are the features affecting the most anomalous samples. Subsequently, we
 645 extend our analysis to include real-world datasets, particularly underlying the datasets where some knowledge about
 646 the anomalies and their influencing features is available or comprehensible.
 647

648 We then proceed to assess our models' interpretive effectiveness by comparing them with alternative interpretation
 649 algorithms. Among these, we examine an ad-hoc algorithm named DIFFI, as introduced in section 4.1, and a post-hoc
 650 method that leverages Random Forest as a surrogate model. This approach involves using an inherently interpretable
 651 model to estimate the predictions of the initial Isolation Forest models (IF, EIF, or EIF⁺), with interpretations derived
 652 from the feature importance scores that the surrogate model provides.
 653

654 Now, the problem is to effectively compare the algorithms and evaluate the performances of the interpretations. In the
 655 absence of a one-size-fits-all metric or fully comprehensible prior knowledge on the features, assessing the performances
 656 of such algorithms is challenging due to the dependency on various factors, including input data complexity, model
 657 intricacies, and end-user interpretability, then the evaluation becomes a delicate balancing act between quantifiable
 658 measures and qualitative insights.
 659

660 To quantitatively evaluate model interpretability, a proxy task is often utilized as an indirect means to assess model
 661 performance or abilities when direct measurement is difficult. In this paper the Feature Selection acts as such a proxy,
 662 where Importance Scores from interpretability methods prioritize input features. Then we assess the interpretation
 663 algorithm performance based on how it prioritizes key features versus less important ones offering insight into its
 664 effectiveness using the Feature Selection. Additionally, we add to these results those from a casual feature selection to
 665 gauge the overall performance trends more broadly.
 666

667 We then introduce a metric to quantify the goodness of a Feature Selection, the Area Under the Curve of Feature
 668 Selection (AUC_{FS}), taking inspiration from the methodological evaluation used by Turbe et al. in [41]. AUC_{FS} is
 669 calculated as the difference between the area under the curve when shrinking the dimensions of the dataset on the
 670 most important features (AUC_M) and the area under the curve when considering the least important features (AUC_L),
 671 $AUC_{FS} = AUC_M - AUC_L$. This metric reflects the distinction in selecting significant features or dropping them, with
 672

677 a larger gap indicating more effective prioritization, as on one hand losing vital information leads to a noticeable
 678 performance decline when important features are excluded early on, on the other hand maintaining the most important
 679 information will result in maintaining the performances or even increasing them.
 680

681 There exist various post-hoc interpretation algorithms like SHAP [29] that could be integrated as a comparison in the
 682 proxy task. However, due to their computational burden, these algorithms are often less suitable for tree-based models,
 683 which are widely employed in industrial settings due to their speed and low memory requirements. Our experiment
 684 confirmed the unsuitability of SHAP in our evaluation. Even considering the faster variants of SHAP [27], the required
 685 computational time necessary to apply it to the benchmark datasets is excessive, making it not viable in practice.
 686

687 Our interpretability evaluation bypasses human experiments due to their high cost in terms of required time and effort,
 688 focusing instead on metric-based assessments. Like other studies [41, 42], we adopt, according to the Doshi-Velez's et al.
 689 taxonomy [12], a Functionally-grounded evaluation by using a proxy task (Feature Selection). This method is neither
 690 specific nor expensive, making it ideal for our purposes. It provides a practical framework for assessing interpretability
 691 without the significant resources required for human-based evaluations, aligning with our research constraints and
 692 objectives.
 693

694 5.3 Datasets

695 We use seventeen datasets with labeled anomalies to evaluate the performances and interpretations of the models. This
 696 benchmark includes six synthetic datasets, which were designed to highlight the differences in model performance and
 697 to provide a ground truth about anomalies and model interpretation, as well as eleven open source datasets based on
 698 real applications. In the rest of the paper, the datasets will be indicated using a typewriter font. Table 1 summarizes the
 699 key characteristics of the datasets that were examined. A detailed description can be found in Appendix A.1.
 700

701 Table 1. Experimental datasets overview: The first column lists the dataset names; the second specifies the total number of instances;
 702 the third details the count of outliers; the fourth shows contamination rates; the fifth indicates the total features; the final column
 703 reveals the dataset's dimensionality.
 704

| | n. data n | n. anomalies | contamination % | n. features d | (Dimensionality) | Dataset Type |
|------------|--------------|--------------|--------------------|------------------|------------------|--------------|
| Xaxis | 1100 | 100 | 9.09 | 6 | (Low) | Synthetic |
| Bisect | 1100 | 100 | 9.09 | 6 | (Low) | Synthetic |
| Bisec3D | 1100 | 100 | 9.09 | 6 | (Low) | Synthetic |
| Bisec6D | 1100 | 100 | 9.09 | 6 | (Low) | Synthetic |
| Annthyroid | 7200 | 534 | 7.56 | 6 | (Low) | Real |
| Breastw | 683 | 239 | 52.56 | 9 | (Middle) | Real |
| Cardio | 1831 | 176 | 9.60 | 21 | (High) | Real |
| Glass | 214 | 9 | 13.55 | 29 | (Middle) | Real |
| Ionosphere | 351 | 126 | 35.71 | 33 | (High) | Real |
| Pendigits | 6870 | 156 | 2.27 | 16 | (Middle) | Real |
| Pima | 768 | 268 | 34.89 | 8 | (Middle) | Real |
| Shuttle | 49097 | 3511 | 7.15 | 9 | (Middle) | Real |
| Wine | 129 | 10 | 7.75 | 13 | (Middle) | Real |
| Diabetes | 85916 | 8298 | 9.65 | 4 | (Low) | Real |
| Moodify | 276260 | 42188 | 15.27 | 11 | (Middle) | Real |

724 5.3.1 Remarks on Synthetic datasets. The synthetic datasets were meticulously engineered to elucidate the distinctions
 725 and advantages of the EIF and EIF⁺ algorithms compared to the IF methodology, reflecting the complex, multidimensional
 726 attributes of the data.
 727

These datasets comprise two distinct categories of data points: one, designated as *inliers*, adheres to the anticipated distribution pattern, while the second category, denoted as *outliers*, consists of points that markedly diverge from the inlier distribution along specific directions.

To accurately replicate the class imbalance prevalent in AD tasks, the proportion of anomalies (outliers) generated is significantly lower than that of inliers. This disparity mirrors real-world conditions, as validated in Section 5.3.2, where anomalous instances are infrequent. The datasets are characterized by a *contamination factor*, a metric quantifying the prevalence of outliers relative to the total dataset population. Typical contamination factor values range between 5 to 10%, although in certain contexts, such as Credit Card Fraud Detection, this percentage can be substantially below 1

5.3.2 *Remarks on Real-World Datasets.* Most of the considered Real-World Datasets are part of the widely used Outlier Detection DataSets (ODDS) library introduced in [37]. Unlike their computer-generated counterparts, these datasets reflect the complexity present in real world scenarios. However, it's essential to emphasize the origin of these datasets, as the majority comes from an adaptation to the AD task of datasets originated with a different purpose. In particular, the ODDS datasets are obtained after applying an alteration to datasets that originally came in the form of Multi-Class datasets. This is due to the fact that, unfortunately, the existing literature lacks dedicated Real-World benchmark Datasets specifically tailored for AD. Typically, the applied transformation involves undersampling the least-represented class, designating it as the outlier class, and merging the remaining classes into a single category representing the normal distribution of the data. As we will discuss in our experiments, this approach presents challenges, as an undersampled version of the minority class may not result in abnormally distributed samples. The considered AD approaches are designed to identify anomalies defined as isolated samples in an unsupervised manner. Obviously, the detected anomalies may not always align with the provided labels. It is worth noticing that this discrepancy makes it more difficult to evaluate the algorithm interpretability, as will be investigated in Section 6.2.

Many Real-World Datasets lack detailed information on features and labels, complicating model evaluation and interpretation of Feature Importance scores. Only the Glass dataset, detailed by Carletti et al. [7], allows us to analyze Feature influence on anomalies, discussed in Section 6.2.3. This gap in data detail poses significant challenges for complete qualitative model assessment and understanding the real impact of the features to the anomalies.

To overcome these limitations, two new datasets were added to the original list: the Diabetes and the Moodify datasets. The peculiarity of these two sets of data is that they are provided with highly detailed information on the semantics of the features and labels composing them. Thus, once AD and interpretation results are obtained, is possible to evaluate them by measuring how they are aligned with the provided domain knowledge.

6 EXPERIMENTAL EVALUATION OF EIF⁺ AND EXIFFI

In this section, we present the experimental evaluation of EIF⁺ and ExIFFI and showcase the capabilities and enhancements these models offer over traditional and state-of-the-art models. We leverage both synthetic and real-world datasets to provide a comprehensive analysis of their performance, emphasizing interpretability and the precise identification of anomalies. These experiments not only highlight the advancements of EIF⁺ and ExIFFI but also underscore their practical applicability in diverse settings through an analysis of computational time.

6.1 Synthetic Datasets

We evaluate the performance of EIF⁺ and ExIFFI in detecting anomalies and identifying the main features for the detection of anomalous points through the graphical representations illustrated in Section 4.2.3. We use synthetic

781 datasets first, as we have a complete knowledge of the mechanism generating the anomalies, and we can leverage this
 782 information to properly evaluate model interpretation performance.
 783

784 Next, we consider Xaxis, Bisec3D and Bisec6D. The results for the other synthetic datasets can be found in the
 785 Appendix A.4.

787 Xaxis

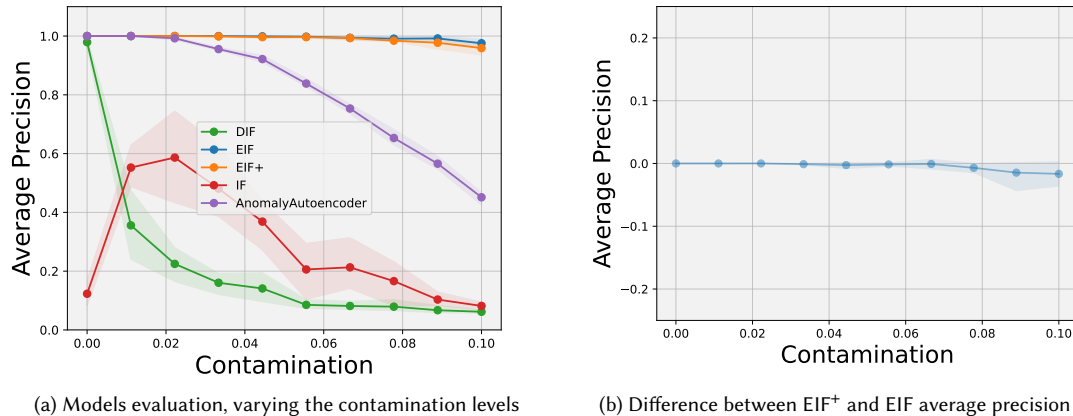
788 **6.1.1 Performance.** In Figure 3, we observe the changes in average precision across various models as we adjust the
 789 number of anomalies that contaminate the train set. The dataset, which is described in the Appendix A.1.1, is specifically
 790 designed to expose the limitations of the Isolation Forest (IF) model. It does this by distributing anomalies along a
 791 singular direction, knowing that in that bundle the anomalies are artificially influenced by the IF model's bias in its
 792 decision boundaries as presented in Appendix A.1.3.
 793

794 Contrastingly, the EIF and its improved version, EIF⁺, demonstrate high performance. Their effectiveness is not
 795 diminished by the anomalies' structured distribution, thus the enhanced generalization capabilities of EIF⁺ are not
 796 distinctly observable since both models achieve perfect precision (a score of 1) when there is no contamination.
 797

798 Additionally, we note that the DIF model struggles to detect anomalies as effectively as IF when anomalies are present
 799 in the dataset used to fit the model. Yet, when trained exclusively on inliers, its performance increase, aligning with
 800 that of EIF and EIF⁺.
 801

802 Finally, the AutoEncoder stays below the value of 0.6 of Avg Prec when the contamination of the training set reaches
 803 its maximum. On the other hand the performances of the model are similar to the ones of the Isolation based models
 804 (i.e. IF, EIF and EIF⁺) when the contamination factor is close (or equal) to 0.
 805

806 Figure 3b showcases the performance delta between EIF⁺ and EIF, highlighting their distinct characteristics. In this
 807 analysis, we note that EIF⁺ exhibits marginally lower performance when trained on datasets with a high contamination
 808 level of anomalies. However, its performance progressively improves as the contamination in the training dataset
 809 decreases, underlining EIF⁺'s enhanced adaptability and efficiency in environments with diminishing levels of anomaly
 810 contamination.
 811



830 Fig. 3. Figure 3a illustrates the average precision as the contamination level in the training set increases. Figure 3b compares the
 831 performance graphs of EIF and EIF⁺, using the difference of their scores in various contamination levels.
 832

In the Table 2, we detail the performance metrics of various models under the two Scenarios outlined in Section 5.1. This comparison reveals that in Scenario I, the EIF and EIF⁺ models surpass the performance of their counterparts, showcasing superior ability to discern the dataset's structure. Conversely, in Scenario 2, where the training dataset is made of inliers, the DIF model exhibits comparable effectiveness to the EIF and EIF⁺ models. A critical aspect of our analysis also includes the evaluation of fitting and prediction times. This highlights that the IF, EIF, and EIF⁺ models significantly outpace the DIF model, being over 20 times quicker in model fitting and 200 times faster in making predictions. Finally, the Autoencoder is 2 times slower than the DIF model fitting the dataset but its prediction times are comparable with the ones of IF, EIF and EIF⁺.

Table 2. Performances of 5 different Anomaly Detection models over Xaxis are compared using classical Classification metrics. Moreover, the last two columns contain the average time for a fit and predict operation. The highest metric values and the lowest execution times are highlighted in bold.

| AD Model | Scenario I | | | Scenario II | | | Time | |
|------------------|-------------|-------------|-------------|-------------|------------|------------|-------------|--------------|
| | Avg Prec | Prec | ROC AUC | Avg Prec | Prec | ROC AUC | fit | pred |
| IF | 0.09 | 0.11 | 0.51 | 0.10 | 0.0 | 0.45 | 0.07 | 0.007 |
| EIF | 0.97 | 0.89 | 0.93 | 0.99 | 1.0 | 1.0 | 0.07 | 0.004 |
| EIF ⁺ | 0.91 | 0.89 | 0.93 | 0.99 | 1.0 | 1.0 | 0.07 | 0.005 |
| DIF | 0.06 | 0.06 | 0.48 | 0.97 | 0.9 | 0.94 | 1.57 | 1.25 |
| AutoEncoder | 0.52 | 0.46 | 0.7 | 1.0 | 1.0 | 1.0 | 3.74 | 0.07 |

6.1.2 Importance Plots. The interpretation results of the EIF⁺ model across both scenarios are showcased in Figures 4. Across 40 algorithm iterations, feature 0 consistently emerges as the most significant, as depicted in Figures 4a and 4d. The primary distinction between the scenarios is observed in the importance scores; in the second scenario, these scores present an increased gap between the importance score of feature 0 and the one of the other features, indicating a clearer differentiation in feature importance.

6.1.3 Feature Selection. Figure 5c presents Feature Selection in Scenario II, comparing various interpretation algorithms across different isolation models. The IF model, showing lower average precision, suggests that DIFFI's ad-hoc interpretation, despite being slightly less effective than other algorithms, still manages above-average feature selection performance. The post-hoc interpretation using a surrogate Random Forest model reveals a significant Feature Selection performance impact, likely due to its close ties with the prediction of the model. Notably, Figure 5d demonstrates that prioritizing the removal of features deemed most important by the RandomForest (blue line) surprisingly enhances feature selection, indicating a reversal in the expected feature importance order. This phenomenon suggests the RandomForest model may inversely assess feature significance relative to optimal anomaly detection criteria.

Looking at the plots, a significant decline in performance is observed once Feature 0, the feature used to craft the anomalies in this dataset, is removed. For both EIF models, Feature Selection guided by the importance scores from ExIFFI and the Random Forest exhibits strong performance, acknowledging Feature 0 as the most crucial, underscoring its significance in accurate anomaly detection and interpretation within this context.

In the Table 3, we showcase the AUC_{FS} scores for Feature Selection across both scenarios, evaluated through the EIF and EIF⁺ models and considering various interpretation algorithms. In Scenario I, the performance across different interpretation algorithms is largely comparable, except in the case of feature importance derived from the Random Forest model fitted on the IF model's results. This exception is attributed to the IF model's under-performance. Moreover

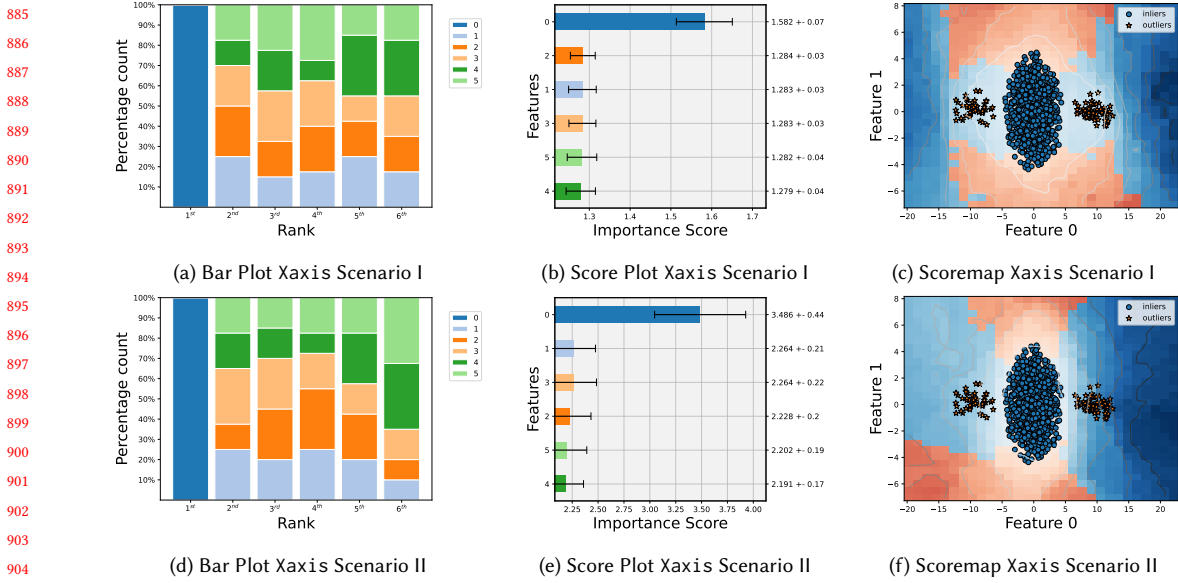


Fig. 4. Bar Plot, Score Plot and Scoremap of the dataset Xaxis in the two different Scenarios, using the EXIFFI algorithm applied to the EIF⁺ model.

in the Scenario II we observe a drop in performances even in the case of the DIFFI interpretation. It's important to highlight the efficiency aspect in our analysis: the EXIFFI algorithm demonstrates a notably quicker computation time for evaluating importance scores. This observation emphasizes the speed advantage of our proposed ad-hoc interpretation method over alternative approaches, illustrating not only its effectiveness in interpretation but also its operational efficiency.

Table 3. Quantitative evaluation of the effectiveness of 6 different interpretation algorithms on Xaxis through the AUC_{FS} metric, introduced in 5.2. In the last column the average time taken by the different models to produce the importance scores is reported. The highest AUC_{FS} and lowest Importance time values are highlighted in bold.

| Interpretation | Evaluation with EIF | | Evaluation with EIF ⁺ | | Importance time |
|----------------|--------------------------|---------------------------|----------------------------------|---------------------------|-----------------|
| | Scenario I AUC_{FS} | Scenario II AUC_{FS} | Scenario I AUC_{FS} | Scenario II AUC_{FS} | |
| DIFFI | 4.739 | 2.838 | 4.548 | 2.728 | 0.55 |
| EXIFFI | 4.721 | 4.701 | 4.571 | 4.609 | 0.07 |
| EXIFFI+ | 4.709 | 4.724 | 4.527 | 4.588 | 0.07 |
| IF_RF | -2.822 | -2.828 | -2.733 | -2.678 | 0.67 |
| EIF_RF | 4.718 | 4.71 | 4.535 | 4.517 | 0.67 |
| EIF+_RF | 4.706 | 4.722 | 4.527 | 4.531 | 0.67 |

Bisect 3D

6.1.4 Performance. From the analysis presented in plot 6a, we note that the DIF model struggles with accurately identifying the correct anomalies within the Bisect3D dataset, such dataset was thoroughly described in Appendix

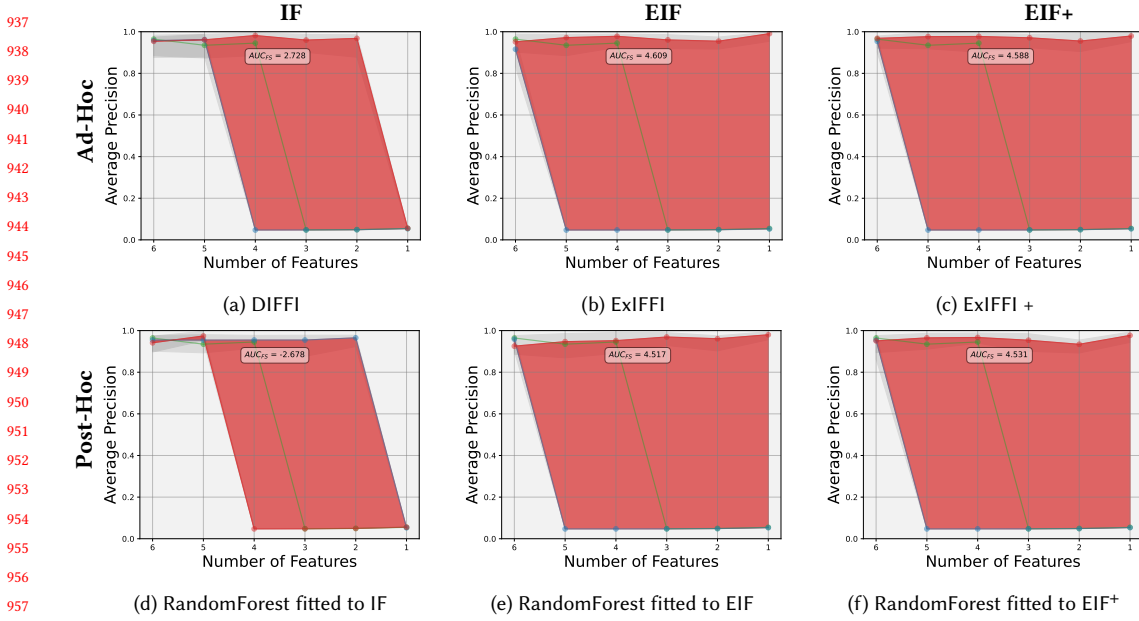


Fig. 5. Feature Selection of the different Ad-Hoc and Post-Hoc methods applied to the 3 Isolation Forest models: IF, EIF and EIF⁺. The blue line is the values of average precision, calculated with the EIF⁺ model in the Scenario II, dropping the most important feature at each step, the red line is the values of average precision dropping the least important feature at each step and the green line is the value of the feature selection dropping a random feature at each step.

A.1.1. Conversely, all other models demonstrate the capability to detect perfectly anomalies once the contamination level dips below 0.06, while still maintaining high performance across levels of contamination. This observation underscores the robustness of these models in handling anomaly detection in datasets with low contamination rates.

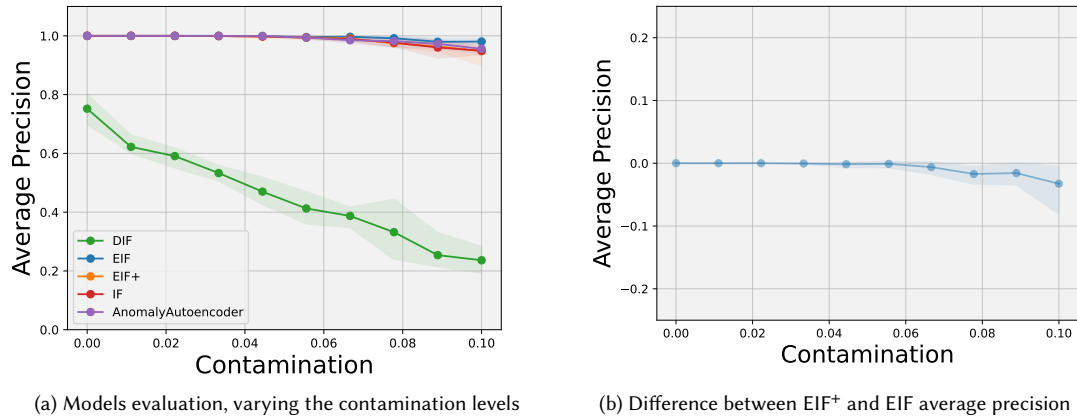


Fig. 6. Figure 6a illustrates the average precision as the contamination level in the training set increases. Figure 6b compares the performance graphs of EIF and EIF⁺, using the difference of their scores in various contamination levels.

From the analysis presented in Table 4, it's evident that the IF, EIF, and EIF⁺ models exhibit robust performance across both scenarios, effectively identifying anomalies within the Bisect3D dataset, as detailed in Appendix A.1.1. In contrast, the DIF model encounters significant challenges in Scenario I, struggling to accurately detect anomalies. Moving to Scenario II, even if it increased its Average Precision score, it remains remarkably lower than the other models. Instead, the Anomaly Autoencoder displays a perfect anomaly detection as the IF model.

Table 4. Performances of 5 different Anomaly Detection models over Bisec3D are compared using classical Classification metrics. Moreover, the last two columns contain the average time for a fit and predict operation. The highest metric values and the lowest execution times are highlighted in bold

| AD Model | Scenario I | | | Scenario II | | | Time | |
|-------------|-------------|-------------|-------------|-------------|------------|------------|-------------|--------------|
| | Avg Prec | Prec | ROC AUC | Avg Prec | Prec | ROC AUC | fit | pred |
| IF | 0.95 | 0.85 | 0.91 | 1.0 | 1.0 | 1.0 | 0.08 | 0.008 |
| EIF | 0.96 | 0.89 | 0.93 | 0.99 | 1.0 | 1.0 | 0.09 | 0.02 |
| EIF+ | 0.93 | 0.71 | 0.84 | 0.99 | 0.99 | 0.99 | 0.097 | 0.01 |
| DIF | 0.3 | 0.28 | 0.6 | 0.79 | 0.72 | 0.84 | 1.84 | 1.44 |
| AutoEncoder | 0.97 | 0.92 | 0.95 | 1.0 | 1.0 | 1.0 | 3.86 | 0.07 |

6.1.5 *Importance Plots.* The division of the dataset into two distinct scenarios does not significantly alter the relative importance of features, except for variations in the absolute scores of these importances. The results depicted in Figures 7a, 7b, 7d, and 7e align with the expected structure of the dataset, identifying features 0, 1, and 2 as the most crucial, each holding similar importance scores. Notably, the presence of multiple features contributing equally to the deviation of points from the dataset's normal distribution results in a smaller gap between scores of significant and less significant features. This contrast is evident when compared to observations from the Xaxis dataset shown in Figures 4b and 4e, where the disparity in importance scores between important and non important features is more pronounced.

6.1.6 *Feature Selection.* In the Figures 7 we can observe that the important features are preserved until the latter stages of feature selection, in fact the average precision remains high, underscoring the importance of these features in maintaining model accuracy. Conversely, when we consider the case in which we removed important features in the early phases of Feature Selection, there's a noticeable decrement in average precision with each step. This trend culminates in significantly reduced precision once the model is evaluated using the less important features, highlighting the pivotal role that the selected important feature features play in the model's ability to predict anomalies.

The Table 5 shows consistent performance across interpretation algorithms and Scenarios, except for DIFFI in Scenario II, likely due to not selecting all key features, as seen in Figure 8a. This highlights the importance of comprehensive Feature Selection for model accuracy. For what concerns the time performances the EIF and EIF⁺ models are almost 10 times faster than the other methods considered in the analysis, proving again their computational efficiency.

Bisect 6D

6.1.7 *Performance.* The contamination plot in Figure 9a reveals that all algorithms, except for DIF, deliver impressive performances. As the contamination level decreases, both EIF and EIF⁺ models exhibit a slight improvement in their ability to detect anomalies, ultimately achieving near-perfect anomaly detection.

Table 6 corroborates observations from the contamination plots, indicating that, across both scenarios, all algorithms exhibit high performance levels, with the notable exception of DIF. Specifically, the IF model and the Autoencoder stand

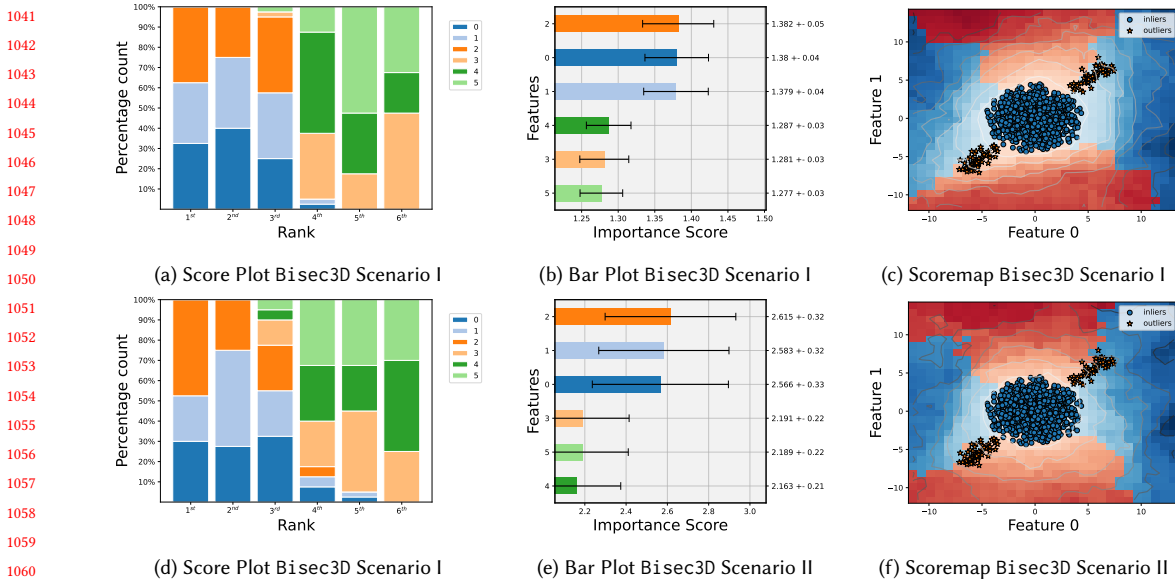


Fig. 7. Bar Plot, Score Plot and Scoremap of the dataset Bisec3D in the two different Scenarios, using the ExIFFI algorithm applied to the EIF⁺ model.

Table 5. Quantitative evaluation of the effectiveness of 6 different interpretation algorithms on Bisec3D through the AUC_{FS} metric, introduced in 5.2. In the last column the average time taken by the different models to produce the importance scores is reported. The highest AUC_{FS} and lowest Importance time values are highlighted in bold.

| Interpretation | Evaluation with EIF | | Evaluation with EIF ⁺ | | Importance time |
|----------------|--------------------------|---------------------------|----------------------------------|---------------------------|-----------------|
| | Scenario I AUC_{FS} | Scenario II AUC_{FS} | Scenario I AUC_{FS} | Scenario II AUC_{FS} | |
| DIFFI | 3.424 | 2.79 | 3.327 | 2.834 | 0.56 |
| EXIFFI | 3.413 | 3.413 | 3.445 | 3.454 | 0.07 |
| EXIFFI+ | 3.434 | 3.438 | 3.418 | 3.432 | 0.07 |
| IF_RF | 3.441 | 3.486 | 3.421 | 3.397 | 0.68 |
| EIF_RF | 3.417 | 3.457 | 3.35 | 3.462 | 0.68 |
| EIF+_RF | 3.417 | 3.4 | 3.371 | 3.474 | 0.68 |

out as the most effective across both scenarios, demonstrating their superior anomaly detection capabilities within the Bisec6D dataset context. Observing the execution time for a single fit and predict operation IF, EIF and EIF⁺ showcase the most efficient performances.

6.1.8 Importance Plots. Since the Bisect6D is crafted in such a way that the anomalies deviate along all the directions the resulting feature importance show as most important feature a blend of the six different features and the scores are very similar underlying this characteristic of the dataset.

6.1.9 Feature Selection. The Feature Selection plots reveal a consistent decrease in average precision, irrespective of the feature selection strategy employed. Whether features are dropped based on their deemed importance: least

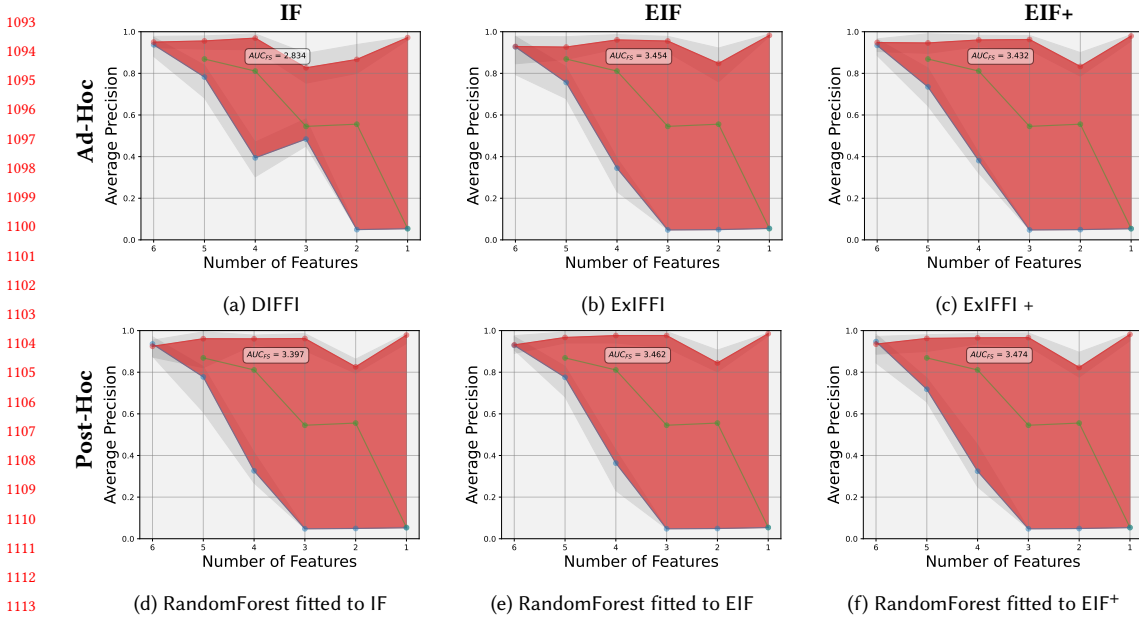


Fig. 8. Feature Selection of the different Ad-Hoc and Post-Hoc methods applied to the 3 Isolation Forest models: IF, EIF and EIF+. The blue line is the values of average precision, calculated with the EIF+ model in the Scenario II, dropping the most important feature at each step, the red line is the values of average precision dropping the least important feature at each step and the green line is the value of the feature selection dropping a random feature at each step.

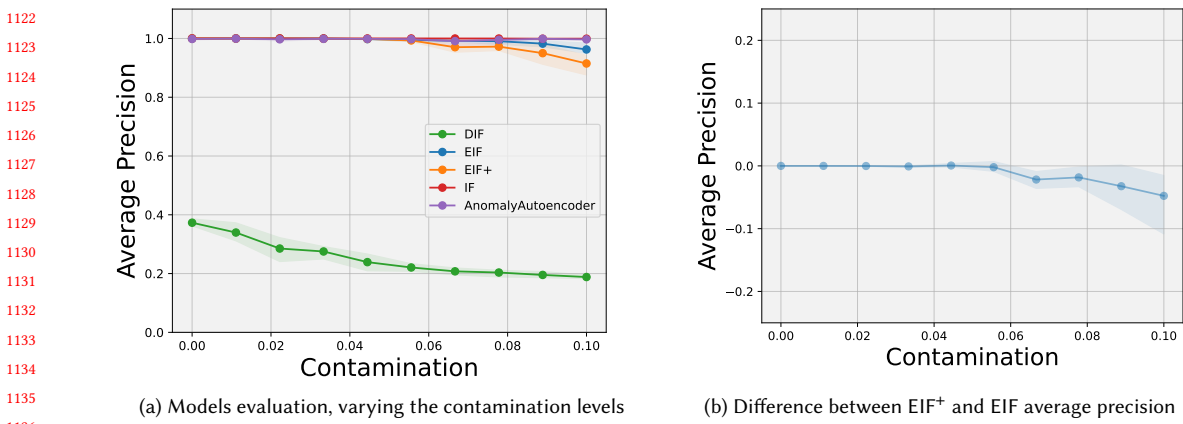
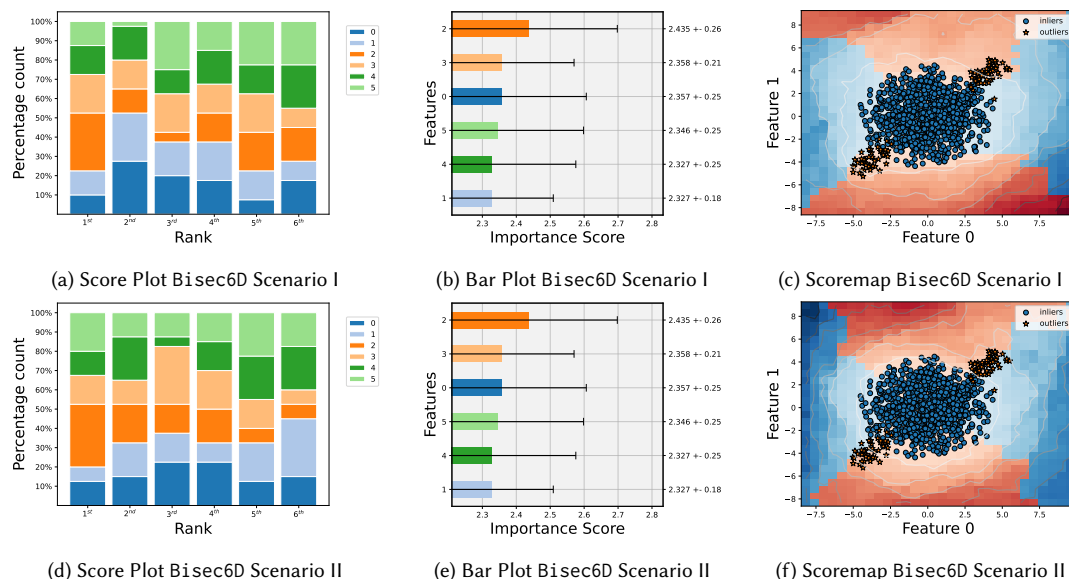


Fig. 9. Figure 9a illustrates the average precision as the contamination level in the training set increases. Figure 9b compares the performance graphs of EIF and EIF+, using the difference of their scores in various contamination levels.

important first (red line), most important first (blue line), or selected randomly (green line). The accuracy outcomes exhibit minimal variability, following a uniform pattern across all approaches.

1145 Table 6. Performances of 5 different Anomaly Detection models over Bisec6D are compared using classical Classification metrics.
 1146 Moreover, the last two columns contain the average time for a fit and predict operation. The highest metric values and the lowest
 1147 execution times are highlighted in bold

| AD Model | Scenario I | | | Scenario II | | | Time | |
|------------------|-------------|-------------|---------|-------------|-------------|-------------|-------------|--------------|
| | Avg Prec | Prec | ROC AUC | Avg Prec | Prec | ROC AUC | fit | pred |
| IF | 0.99 | 0.98 | 0.98 | 1.00 | 1.00 | 1.00 | 0.08 | 0.008 |
| EIF | 0.96 | 0.92 | 0.95 | 0.99 | 0.99 | 0.99 | 0.09 | 0.01 |
| EIF ⁺ | 0.93 | 0.81 | 0.89 | 0.99 | 1.00 | 1.00 | 0.1 | 0.01 |
| DIF | 0.19 | 0.16 | 0.53 | 0.36 | 0.32 | 0.62 | 1.62 | 1.29 |
| AutoEncoder | 0.97 | 0.95 | 0.97 | 1.00 | 1.00 | 1.00 | 3.89 | 0.09 |



1178 Fig. 10. Bar Plot, Score Plot and Scoremap for Bisect6D in the two different Scenarios, using the ExIFFI algorithm applied to the
 1179 EIF⁺ model.

1182 Interestingly, in all the plots showcased below the Average Precision metric demonstrates an increase (observed in
 1183 both the blue and red lines) when transitioning from 2 features to 1. This observation suggests that since all features
 1184 hold equal relevance for the Anomaly Detection task, the model achieves greater precision when considering a single
 1185 feature. This phenomenon occurs because all anomalies aligned with that particular feature direction are accurately
 1186 detected.

1188 Table 7 displays AUC_{FS} scores, indicating similar outcomes across different feature importance methods, except for
 1189 DIFI, which slightly underperforms compared to the others.

1192 6.2 Real-World Datasets

1194 This section outlines the outcomes of our investigations conducted on Real-World benchmark datasets, as introduced
 1195 previously. Real-world data presents a multifaceted benchmarking challenge, mainly due to the intricate distributions and

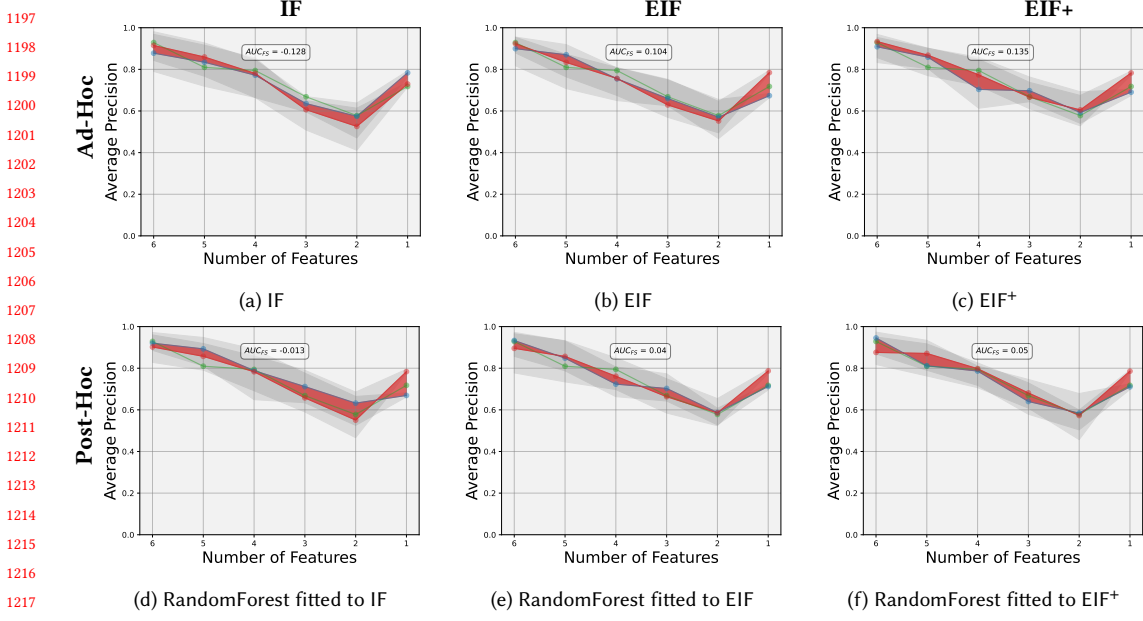


Fig. 11. Feature Selection of the different Ad-Hoc and Post-Hoc methods applied to the 3 Isolation Forest models: IF, EIF and EIF⁺. The blue line is the values of average precision, calculated with the EIF⁺ model in the Scenario II, dropping the most important feature at each step, the red line is the values of average precision dropping the least important feature at each step and the green line is the value of the feature selection dropping a random feature at each step.

Table 7. Quantitative evaluation of the effectiveness of 6 different interpretation algorithms on BiSec6D through the AUC_{FS} metric, introduced in 5.2. In the last column the average time taken by the different models to produce the importance scores is reported. The highest AUC_{FS} and lowest Importance time values are highlighted in bold.

| Interpretation | Evaluation with EIF | | Evaluation with EIF ⁺ | | Importance time |
|----------------|--------------------------|---------------------------|----------------------------------|---------------------------|-----------------|
| | Scenario I AUC_{FS} | Scenario II AUC_{FS} | Scenario I AUC_{FS} | Scenario II AUC_{FS} | |
| DIFFI | 0.026 | -0.045 | -0.027 | -0.128 | 0.55 |
| EXIFFI | 0.147 | 0.174 | -0.017 | 0.104 | 0.07 |
| EXIFFI+ | 0.121 | 0.197 | 0.054 | 0.135 | 0.07 |
| IF_RF | 0.213 | 0.224 | 0.158 | -0.013 | 0.67 |
| EIF_RF | 0.12 | 0.246 | 0.02 | 0.04 | 0.67 |
| EIF+_RF | 0.173 | 0.147 | 0.057 | 0.05 | 0.67 |

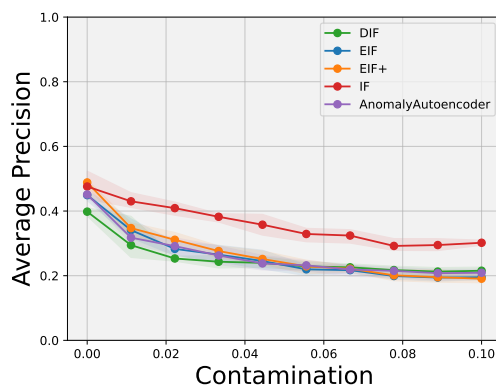
the subtle distinction between inliers and outliers. These complexities often complicate the task of reliably identifying anomalies, which in turn can affect the interpretability of results.

Our experiments, tailored to navigate these challenges, aimed to shed light on the efficacy of our models in discerning the features that affect the most the anomalies. Through careful analysis, we assessed the EIF⁺ models' performance and ExIFFI interpretability capabilities, focusing on the nuanced understanding they provide in distinguishing between normal and anomalous data points.

Specific findings from the datasets Annthyroid, Glass, and Moodify are discussed, highlighting the practical applications of our models in real-world scenarios. For a comprehensive view of all the datasets examined, refer to the extended discussions in the Appendix A.1.2, which encapsulate the broader implications of our research on real-world data analysis.

Annthyroid

6.2.1 Performance. In Figure 12, we note that the DIF, EIF, and EIF⁺ models exhibit similar performance levels, whereas the IF model overall surpasses them on this specific dataset, likely due to its structural characteristics. Interestingly, at a contamination value of 0, the EIF⁺ model slightly outperforms the others, underscoring its superior capability to generalize across unseen anomalies. This is particularly evident in Figure 12b, where the EIF⁺ model starts with negligible differences from EIF at a contamination level of 0.1, but its advantage becomes more pronounced as the contamination level decreases. This pattern suggests the EIF⁺ model's enhanced adaptability and effectiveness in handling datasets with lower contamination rates.



(a) Models evaluation, varying the contamination levels

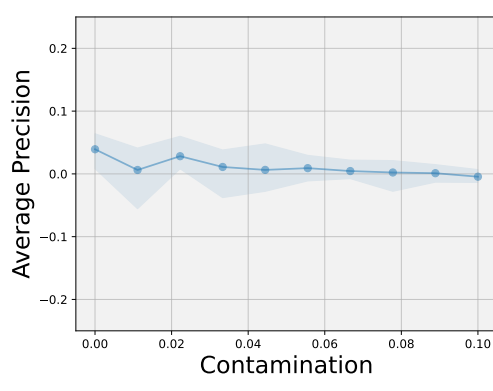
(b) Difference between EIF⁺ and EIF average precision

Fig. 12. Figure 12a illustrates the average precision as the contamination level in the training set increases. Figure 12b compares the performance graphs of EIF and EIF⁺, using the difference of their scores in various contamination levels.

The Table 8 elaborates on the numerical results depicted in the plots from Figure 12, detailing the performance improvement from Scenario I to Scenario II. The most notable enhancement is observed with the EIF⁺ model, which not only demonstrates significant performance gains but also retains the fastest computational efficiency in model fitting—being 100 times quicker than the DIF model. Additionally, it boasts the second-best timing in prediction speed. This showcases EIF⁺'s dual advantage of superior anomaly detection capability across different scenarios and exceptional computational performance, highlighting its practicality for real-world applications.

6.2.2 Importance Plots. In Figure 13, the interpretation plots for both scenarios reveal Feature 1 as the most significant, exhibiting greater robustness in Scenario II, where the model was trained solely on inliers. This robustness likely stems from enhanced precision scores. The scoremaps in Figures 13c and 13f highlight a unique distribution pattern across Features 1 and 5, suggesting a dependency between them. Notably, anomalies predominantly align along Feature 1, despite some outliers along Feature 5 that appear distanced from the normal distribution, potentially impacting

Table 8. Performances of 5 different Anomaly Detection models over Annthyroid are compared using classical Classification metrics. Moreover, the last two columns contain the average time for a fit and predict operation. The highest metric values and the lowest execution times are highlighted in bold.

| AD Model | Scenario I | | | Scenario II | | | Time | |
|-------------|-------------|-------------|-------------|-------------|-------------|-------------|-------------|-------------|
| | Avg Prec | Prec | ROC AUC | Avg Prec | Prec | ROC AUC | fit | pred |
| IF | 0.30 | 0.32 | 0.63 | 0.45 | 0.43 | 0.69 | 0.17 | 0.15 |
| EIF | 0.19 | 0.24 | 0.59 | 0.45 | 0.41 | 0.68 | 0.09 | 0.43 |
| EIF+ | 0.20 | 0.28 | 0.61 | 0.46 | 0.46 | 0.70 | 0.08 | 0.35 |
| DIF | 0.21 | 0.26 | 0.6 | 0.39 | 0.39 | 0.67 | 8.85 | 6.9 |
| AutoEncoder | 0.21 | 0.25 | 0.59 | 0.44 | 0.42 | 0.69 | 16.7 | 0.29 |

negatively the right prediction of the outliers which has a significant effect on interpretation outcomes. In Scenario II, the local scoremap more clearly demonstrates how anomalies are concentrated in areas where Feature 1 holds greater significance, offering insights into the feature’s critical role in anomaly distribution.

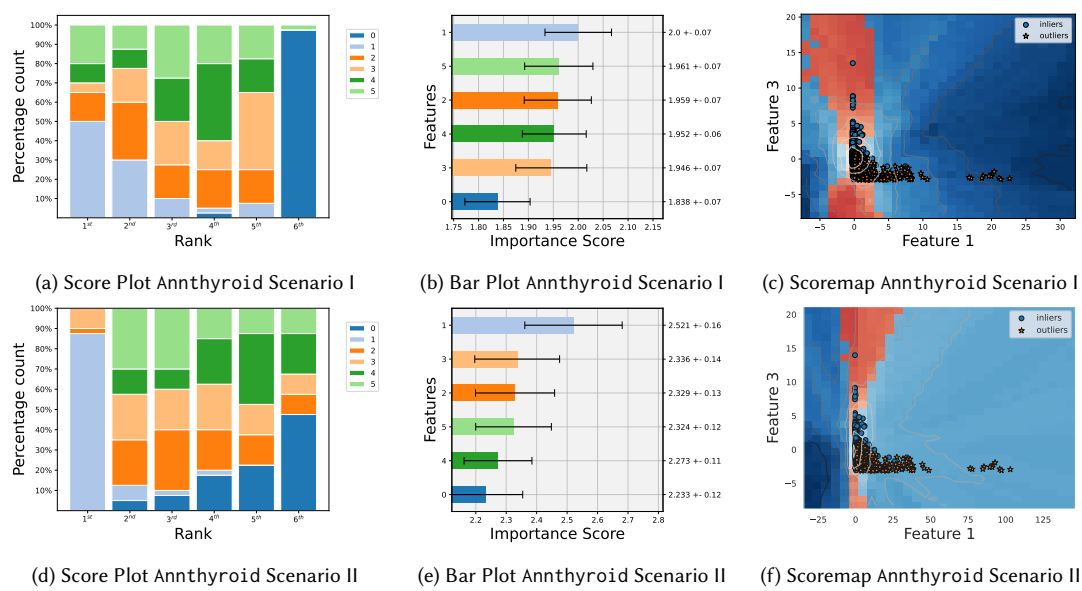


Fig. 13. Bar Plot, Score Plot and Scoremap for Annthyroid in the two different Scenarios, using the ExIFFI algorithm applied to the EIF⁺ model.

6.2.3 *Feature Selection.* Figure 13 showcases the Feature Selection plots derived from the feature rankings provided by six distinct interpretation algorithms—two for each Isolation based model, including one ad-hoc and one post-hoc interpretation via a surrogate Random Forest model. These plots depict the average precision achieved by the EIF⁺ model on the dataset, progressively excluding the least important feature as identified by each interpretation algorithm (illustrated by the red line), and excluding the most important feature at every step (shown by the blue line). The similarity in the plots, particularly within the extent of the red areas, indicates that the Feature Selection outcomes are largely equivalent across the board, with the ExIFFI + algorithm demonstrating a marginally superior performance. This

suggests a subtle advantage in feature prioritization using the ExIFFI + algorithm, though overall differences remain slight.

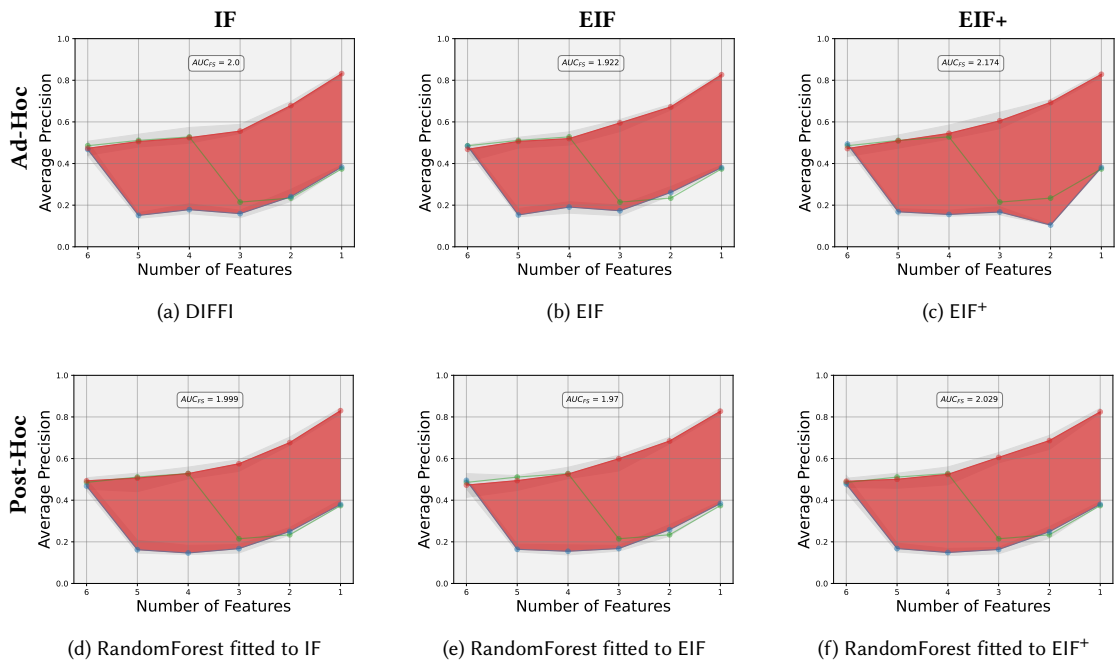


Fig. 14. Feature Selection of the different Ad-Hoc and Post-Hoc methods applied to the 3 Isolation Forest models: IF, EIF and EIF⁺. The blue line is the values of average precision, calculated with the EIF⁺ model in the Scenario II, dropping the most important feature at each step, the red line is the values of average precision dropping the least important feature at each step and the green line is the value of the feature selection dropping a random feature at each step.

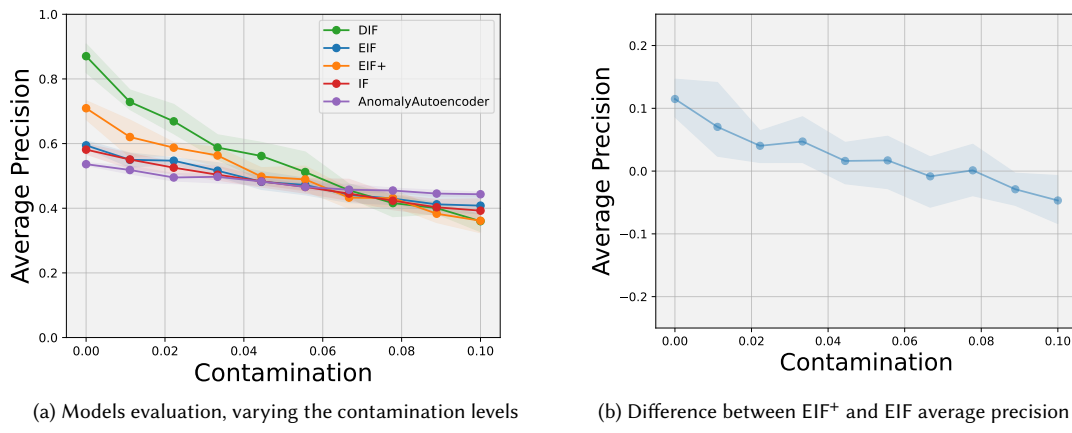
Table 9 highlights distinct performance variations between Scenario I and Scenario II, with Scenario I showing reduced effectiveness overall, particularly in post-hoc interpretation methods. This trend suggests that reliance on post-hoc interpretations might be less beneficial when the performance of anomaly detection (AD) models is low. In contrast, ad-hoc interpretation methods exhibit more consistency and slightly improved results in Scenario II, surpassing post-hoc techniques. Among these, the ExIFFI + method stands out for its superior efficiency. Moreover, the execution speed of ad-hoc interpretations notably exceeds that of post-hoc methods, emphasizing ad-hoc strategies' effectiveness and speed across different scenarios.

Glass

6.2.4 Performance. In Figure 15, we notice that the performance of all models improves as the contamination level in the training dataset decreases, with the DIF model outperforming the rest, followed by the EIF⁺. Specifically, the plot in Figure 15b highlights the EIF⁺ model's distinct advantage in achieving higher average precision at lower contamination levels, showcasing its enhanced capability to generalize effectively when trained without anomalies. This demonstrates the EIF⁺ model's proficiency in adapting to datasets with low contamination, emphasizing its strength in scenarios with unseen anomalies compared to EIF.

1405
1406
1407 Table 9. Quantitative evaluation of the effectiveness of 6 different interpretation algorithms on Annthyroid through the AUC_{FS}
1408 metric, introduced in 5.2. In the last column the average time taken by the different models to produce the importance scores is
1409 reported. The highest AUC_{FS} and lowest Importance time values are highlighted in bold.
1410
1411
1412
1413
1414
1415
1416
1417

| Interpretation | Evaluation with EIF | | Evaluation with EIF ⁺ | | Importance time |
|----------------|--------------------------|---------------------------|----------------------------------|---------------------------|-----------------|
| | Scenario I AUC_{FS} | Scenario II AUC_{FS} | Scenario I AUC_{FS} | Scenario II AUC_{FS} | |
| DIFFI | 0.963 | 2.04 | 0.91 | 2.0 | 0.57 |
| EXIFFI | 0.985 | 2.032 | 0.937 | 1.922 | 0.55 |
| EXIFFI+ | 0.983 | 2.18 | 0.975 | 2.174 | 0.59 |
| IF_RF | 0.453 | 2.055 | 0.429 | 1.999 | 2.82 |
| EIF_RF | -0.689 | 2.034 | -0.672 | 1.97 | 2.82 |
| EIF+_RF | -1.198 | 2.094 | -1.165 | 2.029 | 2.82 |



1421
1422
1423
1424
1425
1426
1427
1428
1429
1430
1431
1432
1433 Fig. 15. Figure 15a illustrates the average precision as the contamination level in the training set increases. Figure 15b compares the
1434 performance graphs of EIF and EIF⁺, using the difference of their scores in various contamination levels.
1435
1436
1437
1438
1439
1440
1441
1442
1443
1444
1445
1446
1447
1448
1449
1450
1451
1452
1453
1454
1455
1456

Table 10 illustrates that EIF⁺ maintains comparable outcomes in Scenario I and, leveraging its enhanced generalization capabilities for unseen anomalies, ranks as the second highest-performing algorithm in Scenario II. Notably, it fits 10 times faster than the DIF and predicts the entire dataset's scores 30 times more swiftly, showcasing its efficiency and efficacy in both model fitting and anomaly detection across scenarios.

6.2.5 Importance Plots. In the Figures 16a, which illustrate the importance scores for Scenario I, there's noticeable uncertainty with no clear indication of a single feature standing out as the most important. This ambiguity is highlighted by the data point distribution in Figure 16c, where we see significant variance in both the dimensions. The model appears to blend a subset of anomalies with inliers, as indicated by a broader contour plot along the feature Ba (Barium) compared to its narrower counterpart in Scenario II (Figure 16f). This difference is likely because anomalies are more distinctly clustered in a specific area of the space, suggesting they are more a subset of the data distribution rather than true anomalies. This concept was further discussed in Section 5.3.2.

1457 Table 10. Performances of 5 different Anomaly Detection models over Glass are compared using classical Classification metrics.
 1458 Moreover, the last two columns contain the average time for a fit and predict operation. The highest metric values and the lowest
 1459 execution times are highlighted in bold

| AD Model | Scenario I | | | Scenario II | | | Time | |
|------------------|-------------|-------------|-------------|-------------|-------------|------------|-------------|--------------|
| | Avg Prec | Prec | ROC AUC | Avg Prec | Prec | ROC AUC | fit | pred |
| IF | 0.36 | 0.34 | 0.62 | 0.65 | 0.68 | 0.82 | 0.07 | 0.002 |
| EIF | 0.35 | 0.27 | 0.58 | 0.57 | 0.68 | 0.82 | 0.07 | 0.01 |
| EIF ⁺ | 0.31 | 0.24 | 0.56 | 0.69 | 0.79 | 0.88 | 0.07 | 0.01 |
| DIF | 0.3 | 0.2 | 0.54 | 0.85 | 0.82 | 0.9 | 0.67 | 0.29 |
| AutoEncoder | 0.41 | 0.44 | 0.68 | 0.53 | 0.62 | 0.78 | 2.25 | 0.04 |

1460
 1461
 1462 Detailed in the Appendix A.1.2, the dataset encompasses objects made of glass, characterized by features like the
 1463 refractive index (RI) and concentrations of elements. Carletti et al. [7] pointed out that the outliers are the subclass of
 1464 headlamp glass, distinct from the window glass types of other classes. The key difference between headlamp and window
 1465 glass is the Barium due to its contribution to optical enhancements. Specifically, Barium boosts the refractive index, thus
 1466 augmenting light transmission and brightness [32] vital for automotive headlamps. Its incorporation into headlamp
 1467 glass optimizes light focus and directionality, underscoring its significance in improving headlamp functionality.

1468 The Potassium (K) it is especially used in glass types requiring increased strength or thermal resistance, such as
 1469 certain window glasses. But we can observe in the local Scoremap that the deviation from the distribution along the
 1470 variable K does not coincide with a particular distribution of anomalies.

1471 As depicted in Figures 16d and 16e Scenario II's analysis highlights Barium (Ba) as a pivotal feature, followed by
 1472 Potassium (K). This results provides an additional confirmation on the correctness of the proposed approach that aligns
 1473 with the domain knowledge on what is the most relevant attribute for the distinction between window and headlamp
 1474 glasses.

1475
 1476
 1477
 1478 6.2.6 *Feature Selection.* Figure 16 showcases the Feature Selection for the glass dataset, highlighting the superior
 1479 performance of ad-hoc interpretation algorithms over the surrogate Random Forest's feature importance method. All
 1480 models succeed in identifying key features because the performance improve the more the less important features are
 1481 dropped, improving the average precision score the more the feature are shrunked to the most important ones, reaching
 1482 a level of 0.6.

1483 In contrast, the Random Forest feature importance method not only falls short in selecting features that enhance the
 1484 average precision score—resulting in a decreased score—but also demonstrates a scenario where the blue line surpasses
 1485 the red line in the post-hoc interpretation of the EIF. This indicates that important features impacting the score were
 1486 prematurely dropped due to being assigned low importance scores by the model. So the Random Forest not only have
 1487 bad performances but in the specific case of the EIF it gave wrong scores.

1488 Table 11 reveals the performance of various interpretation algorithms across two scenarios. In Scenario I, the DIFFI
 1489 interpretation algorithm emerges as the top performer, closely followed by ExIFFI and ExIFFI +. Conversely, in Scenario
 1490 II, ExIFFI and ExIFFI + stand out, demonstrating significantly improved results, whereas the Random Forest model
 1491 consistently faces challenges in accurately interpreting feature importance. This contrast in performance between
 1492 scenarios underscores the adaptability of the DIFFI, ExIFFI, and ExIFFI + algorithms in understanding feature relevance
 1493 in complex datasets like glass, while highlighting the limitations of conventional methods like Random Forest in
 1494

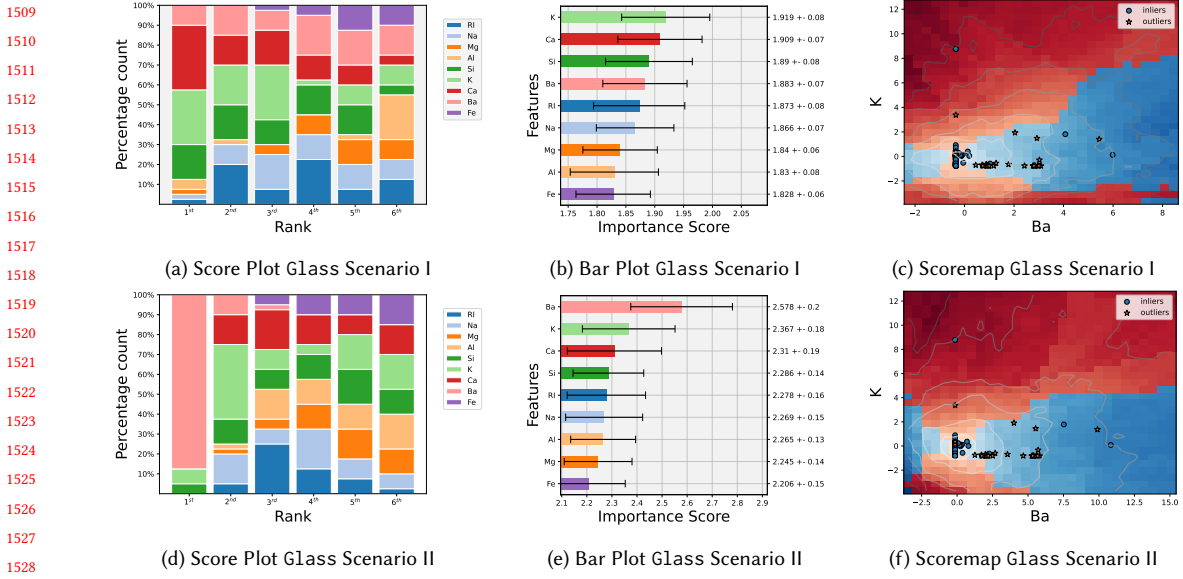


Fig. 16. Bar Plot, Score Plot and Scoremap for Glass in the two different Scenarios, using the ExIFFI algorithm applied to the EIF⁺ model.

nuanced interpretation tasks. Moreover ExIFFI, and ExIFFI + show an improved time efficiency in the computation of importance scores being almost 20 times faster than post-hoc interpretability methods like Random Forest.

Table 11. Quantitative evaluation of the effectiveness of 6 different interpretation algorithms on Glass through the AUC_{FS} metric, introduced in 5.2. In the last column the average time taken by the different models to produce the importance scores is reported. The highest AUC_{FS} and lowest Importance time values are highlighted in bold.

| Interpretation | Evaluation with EIF | | Evaluation with EIF ⁺ | | Importance time |
|----------------|--------------------------|---------------------------|----------------------------------|---------------------------|-----------------|
| | Scenario I AUC_{FS} | Scenario II AUC_{FS} | Scenario I AUC_{FS} | Scenario II AUC_{FS} | |
| DIFFI | 1.591 | 2.117 | 1.555 | 2.447 | 0.44 |
| EXIFFI | 0.465 | 2.554 | 0.564 | 2.431 | 0.01 |
| EXIFFI+ | 0.403 | 1.769 | 0.527 | 2.263 | 0.01 |
| IF_RF | -1.733 | 2.183 | -1.313 | 2.282 | 0.17 |
| EIF_RF | -1.718 | -1.634 | -1.511 | -1.64 | 0.17 |
| EIF+_RF | -1.464 | 1.944 | -1.308 | 1.632 | 0.17 |

Moodify

6.2.7 Performance. In the contamination plot 18a, it's evident that all models perform better when there are no anomalies in the training data ($\text{contamination}=0$), with the DIF model showing the most significant improvement. Although the EIF⁺ does not consistently yield high performance, it surpasses EIF in scenarios where it is trained exclusively on inliers, as anticipated. This trend is depicted in the plot comparing the performance differences between

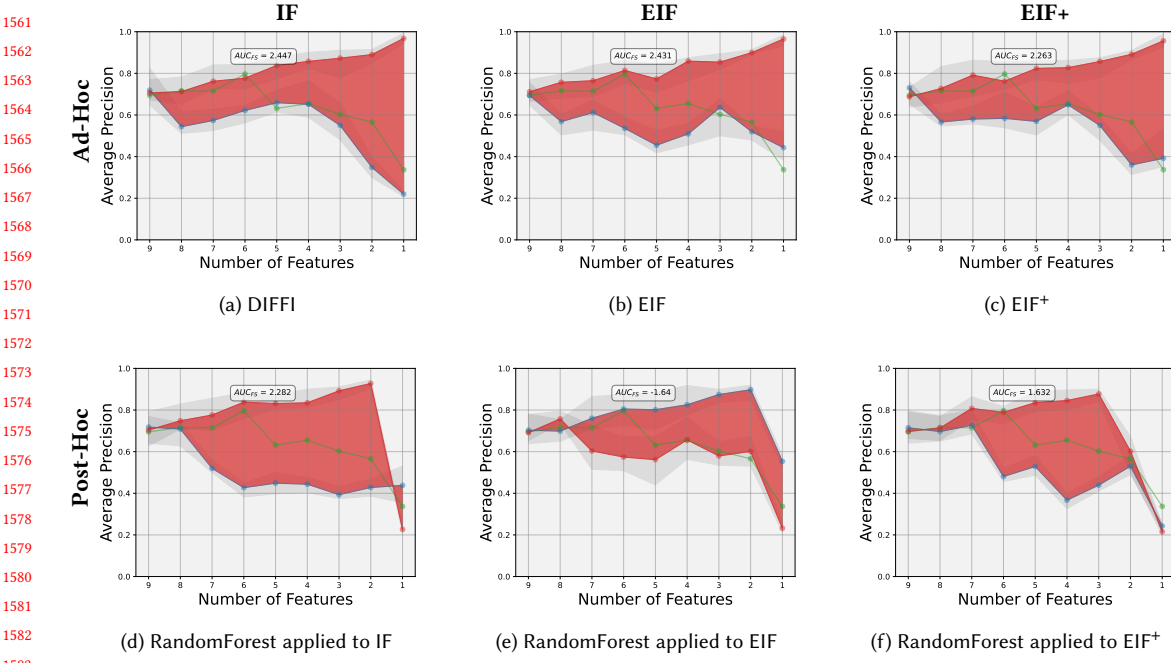


Fig. 17. Feature Selection of the different Ad-Hoc and Post-Hoc methods applied to the 3 Isolation Forest models: IF, EIF and EIF+. The blue line is the values of average precision, calculated with the EIF⁺ model in the Scenario II, dropping the most important feature at each step, the red line is the values of average precision dropping the least important feature at each step and the green line is the value of the feature selection dropping a random feature at each step.

EIF⁺ and EIF in Figure 18b, illustrating EIF⁺'s enhanced ability to adapt and identify anomalies when trained on a clean dataset.18b.

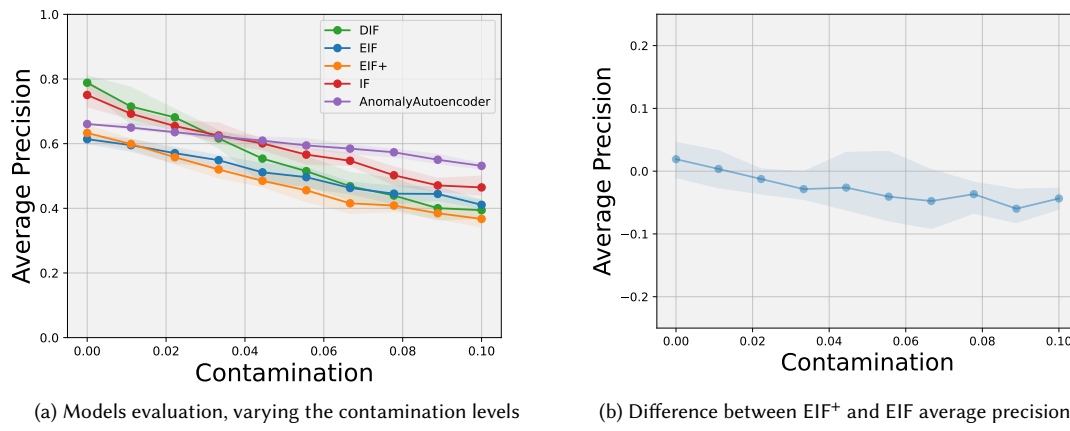


Fig. 18. Figure 18a illustrates the average precision as the contamination level in the training set increases. Figure 18b compares the performance graphs of EIF and EIF⁺, using the difference of their scores in various contamination levels.

1613 Table 12 provides detailed insights into the performance metrics of the models.

1614 Although both the DIF and the IF model achieves the highest value of Average Precision in Scenario II, as reported in
 1615 the performance table, the DIF proves to be significantly slower in the fitting and predicting operations compared to
 1616 the IF method.
 1617

1618 Consequently, the consistent results demonstrated by the IF model make it a more reliable choice in this scenario,
 1619 balancing the ability to detect anomalies with computational efficiency.
 1620

1621 The outcomes for Scenario I significantly diverge from those observed at a contamination level of 0.1, as depicted in
 1622 plot 18a. In Scenario I, the contamination level inherent to the dataset, 0.1527, is specifically considered. Notably, in this
 1623 context, the Anomaly Autoencoder exhibits very low sensitivity to changes in the training dataset's contamination
 1624 level compared to the other models.
 1625

1626 Table 12. Performances of 5 different Anomaly Detection models over Moodify are compared using classical Classification metrics.
 1627 Moreover, the last two columns contain the average time for a fit and predict operation. The highest metric values and the lowest
 1628 execution times are highlighted in bold
 1629

| AD Model | Scenario I | | | Scenario II | | | Time | |
|-------------|-------------|-------------|-------------|-------------|-------------|-------------|-------------|-------------|
| | Avg Prec | Prec | ROC AUC | Avg Prec | Prec | ROC AUC | fit | pred |
| IF | 0.35 | 0.30 | 0.59 | 0.72 | 0.73 | 0.84 | 0.11 | 0.05 |
| EIF | 0.33 | 0.37 | 0.63 | 0.65 | 0.64 | 0.79 | 0.09 | 0.27 |
| EIF+ | 0.28 | 0.27 | 0.57 | 0.66 | 0.66 | 0.80 | 0.09 | 0.25 |
| DIF | 0.26 | 0.26 | 0.56 | 0.72 | 0.73 | 0.84 | 7.76 | 7.5 |
| AutoEncoder | 0.45 | 0.53 | 0.72 | 0.65 | 0.68 | 0.81 | 16.6 | 0.26 |

1639
 1640
 1641 6.2.8 *Importance Plots*. The importance plots in Scenario I, depicted in Figures 19a, highlight four features that
 1642 significantly characterize the anomalies of the dataset, in particular the "speechliness" and the "duration", suggesting
 1643 that the dataset includes unique song types. These variations may point to specific genres such as instrumental music
 1644 or tracks of atypical lengths, like podcasts or classical music, that stand out from standard musical distributions.
 1645

1646 In contrast, Scenario II sheds light on the characteristics that set the outlier class separates from the general dataset
 1647 distribution. Specifically, the 'loudness' feature, which measures a track's overall volume in decibels (dB), as explained
 1648 in the Appendix A.1.2, is identified as particularly significant in Figure 19d. This observation is consistent with the
 1649 expectation that 'Calm' music tracks, the ones labelled as outliers, exhibit lower dB levels. The local scoremap presented
 1650 in Figure 19 provides further insight, demonstrating how 'Calm' tracks distinctly deviate based on this feature, thus
 1651 reinforcing the importance of 'loudness' in distinguishing these outliers within the dataset.
 1652

1653
 1654 6.2.9 *Feature Selection*. During the Feature Selection process, it becomes evident that the DIFFI algorithm struggles to
 1655 accurately identify the most critical features, leading to bad performance when the feature selection evaluate the model
 1656 using the most important features according to this interpretation method and , thus, yielding to a negative value of the
 1657 AUC_{FS} metric. Conversely, utilizing Random Forest as a surrogate model for interpreting the IF model's results yields
 1658 better performance, showcasing its effectiveness in feature importance evaluation.
 1659

1660 Furthermore, both the EIF and EIF⁺ models, when analyzed through ad-hoc and post-hoc interpretation methods,
 1661 achieve high scores. They demonstrate a similar trend of improved average precision as the dataset is condensed to its
 1662 most significant dimensions. This indicates that both interpretation algorithms, regardless of the interpretation method
 1663

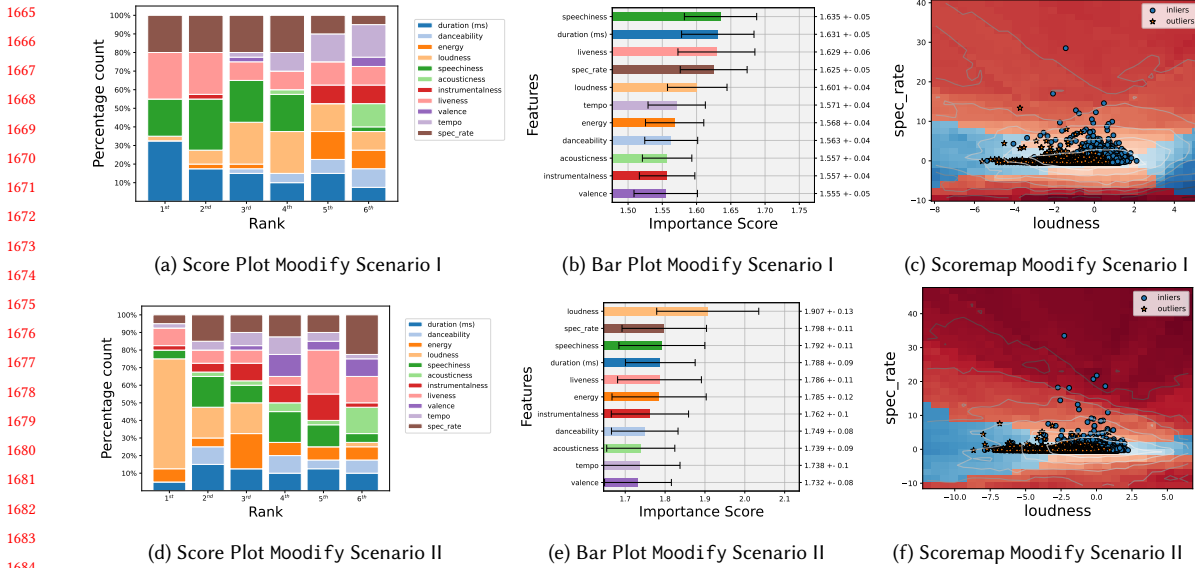


Fig. 19. Bar Plot, Score Plot and Scoremap for Moodify in the two different Scenarios, using the ExIFFI algorithm applied to the EIF⁺ model.

applied, are adept at distilling essential information, thereby enhancing their predictive accuracy when focusing on the most important features.

Table 13 showcases the AUC_{FS} scores derived from various interpretation methods. In Scenario I, interpretations appear to fail, likely because the model fails to accurately pinpoint the given anomalies, but rather represent other kinds of deviation from the normal distribution of the dataset. Conversely, when models are trained exclusively with inliers, there's a notable improvement in results. Particularly, the ExIFFI and post-hoc algorithms excel, demonstrating robust performance. A critical observation is the computational efficiency of the ExIFFI, which is 10 times faster than that of post-hoc models. This highlights the ExIFFI's advantage in scenarios with limited computational resources, emphasizing its efficacy and speed in model interpretation tasks.

Table 13. Quantitative evaluation of the effectiveness of 6 different interpretation algorithms on Moodify through the AUC_{FS} metric, introduced in 5.2. In the last column the average time taken by the different models to produce the importance scores is reported. The highest AUC_{FS} and lowest Importance time values are highlighted in bold.

| Interpretation | Evaluation with EIF | | Evaluation with EIF ⁺ | | Importance time |
|----------------|--------------------------|---------------------------|----------------------------------|---------------------------|-----------------|
| | Scenario I AUC_{FS} | Scenario II AUC_{FS} | Scenario I AUC_{FS} | Scenario II AUC_{FS} | |
| DIFFI | -1.484 | -3.66 | -1.118 | -3.368 | 0.57 |
| EXIFFI | -1.787 | -0.351 | -1.37 | -0.202 | 0.94 |
| EXIFFI+ | -1.51 | -0.239 | -0.991 | -0.041 | 0.99 |
| IF_RF | -0.785 | 2.077 | -0.723 | 2.483 | 8.05 |
| EIF_RF | -0.848 | 1.631 | -0.717 | 2.174 | 8.05 |
| EIF+_RF | -1.882 | 1.476 | -1.433 | 2.086 | 8.05 |

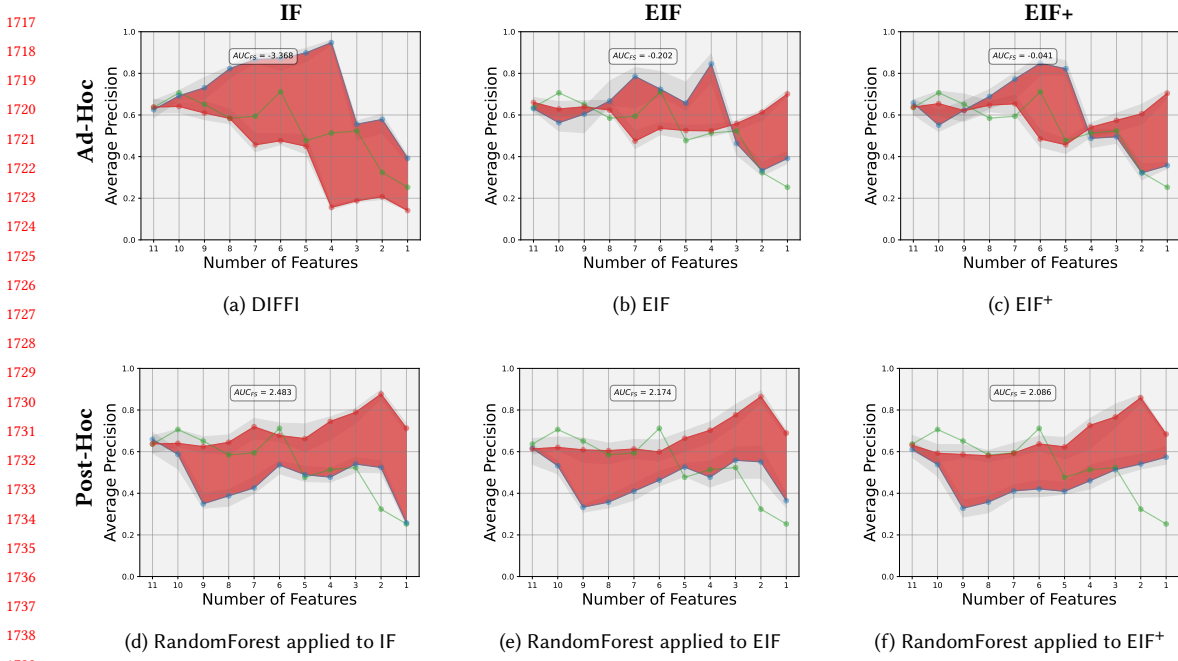


Fig. 20. Feature Selection of the different Ad-Hoc and Post-Hoc methods applied to the 3 Isolation Forest models: IF, EIF and EIF⁺. The blue line is the values of average precision, calculated with the EIF⁺ model in the Scenario II, dropping the most important feature at each step, the red line is the values of average precision dropping the least important feature at each step and the green line is the value of the feature selection dropping a random feature at each step.

6.3 EIF⁺: effect of parameter η

Section 3.2 introduces EIF⁺, an enhancement of EIF that selects hyperplanes not uniformly but via a normal distribution, concentrating them around the dataset's mean. This strategy allows EIF⁺ to partition the space more effectively, even outside the dataset's distribution, creating empty branches but enhancing AD. The spread of hyperplanes, dictated by the standard deviation scaled by η , offers improved control and sensitivity to data distribution changes, especially for new anomalies.

Setting η at 1.5 significantly boosts EIF⁺'s performance over EIF, especially in inlier-only scenarios, showcasing its advanced AD. This study examines how varying η impacts EIF⁺'s accuracy across different data distributions, revealing η 's critical role in enhancing the model's generalization and adaptability to detect anomalies effectively.

Figures 21 illustrate the model's resilience with η values of 1 or higher, where performance remains robust. However, when η ranges from 0.5 to 1, a noticeable decline in performance and increased variance are observed. Specifically, the Glass dataset demonstrates a slight reduction in effectiveness as η escalates, potentially due to its distinct structure. Unlike the datasets depicted in Figures 13f and 19f, the Glass dataset features a denser inlier concentration, as shown in Figure 16f, which may influence the observed performance trends with varying η .

6.4 Time Scaling Experiments

In this section, we compare the computational efficiency of different algorithms, evaluating the time required for model fitting, making predictions, and interpreting results. Our examination, depicted in Figures 22, presents how these

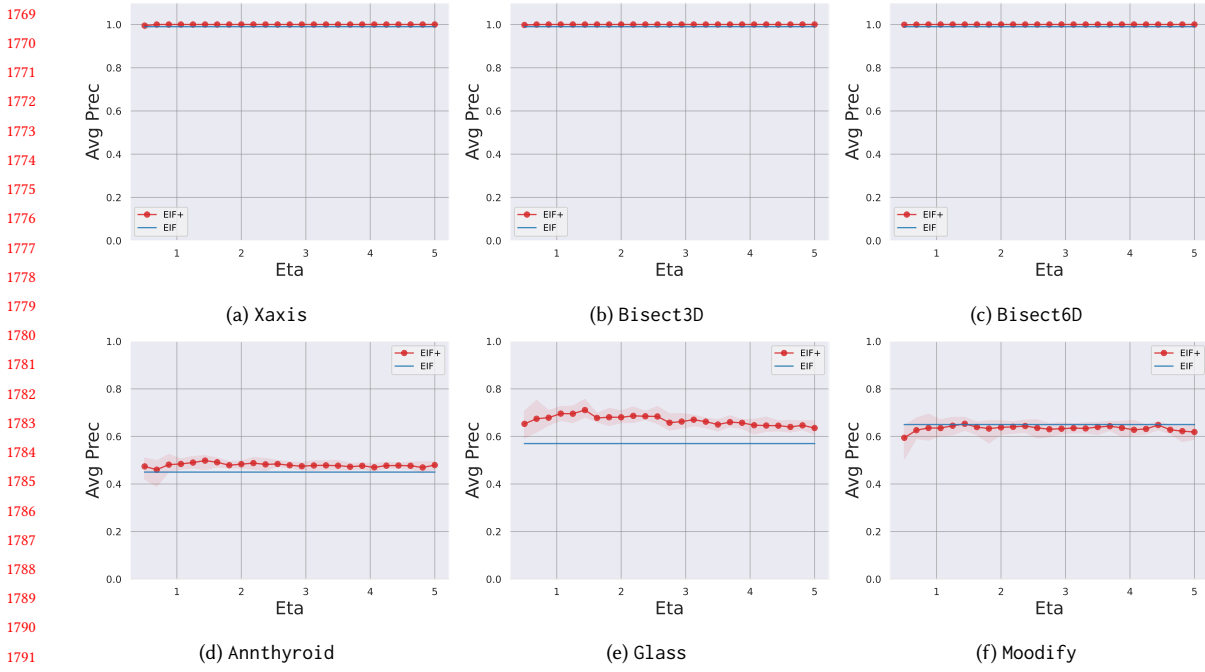


Fig. 21. Exploration of how average precision changes with variations in the η parameter.

durations adjust with dataset size increases—both by sample number and feature count, on a logarithmic scale. This investigation is crucial for understanding each algorithm’s practical use in varying scenarios, such as industrial-sized datasets, where the sample size and the feature space are generally larger than the ones encountered in the benchmark datasets used for evaluation in 5. Figures 22a, 22d details fitting times varying the sample size and number of features respectively, Figures 22b, 22e outline prediction times, and Figures 22c, 22f the time to determine importance scores, providing insight into the scalability and efficiency of these computational processes.

Analyzing computational efficiency, our observations reveal significant differences in the fitting, prediction, and interpretation speeds of various algorithms, as depicted in Figures 22a, 22d, 22b, 22e, and 22c, 22f. Specifically, the fitting time, as shown in Figure 22a, demonstrates exponential increases for both the DIF and Anomaly Autoencoder models. The Anomaly Autoencoder exhibits a steeper rise due to weight optimization requirements, contrasting with DIF, which utilizes deep neural networks with random weights for nonlinear input data transformation, hence avoiding lengthy NN training periods. For what concerns the experiment in which the time effectiveness is tested varying the number of features in the dataset, Anomaly Autoencoder can still be considered the most time consuming method while the trend of DIF is closer to the ones of the Isolation based methods (i.e. EIF, EIF⁺, IF), as shown in 22d.

The prediction time analysis, referenced in Figure 22b, highlights DIF as the most time-intensive model. This is attributed to DIF’s necessity to aggregate predictions across an ensemble of neural networks and representation spaces, significantly extending the prediction process. In 22e , instead, while DIF is still the slowest model , the Anomaly Autoencoder and IF models prediction time can be considered independent on the number of features but only dependent

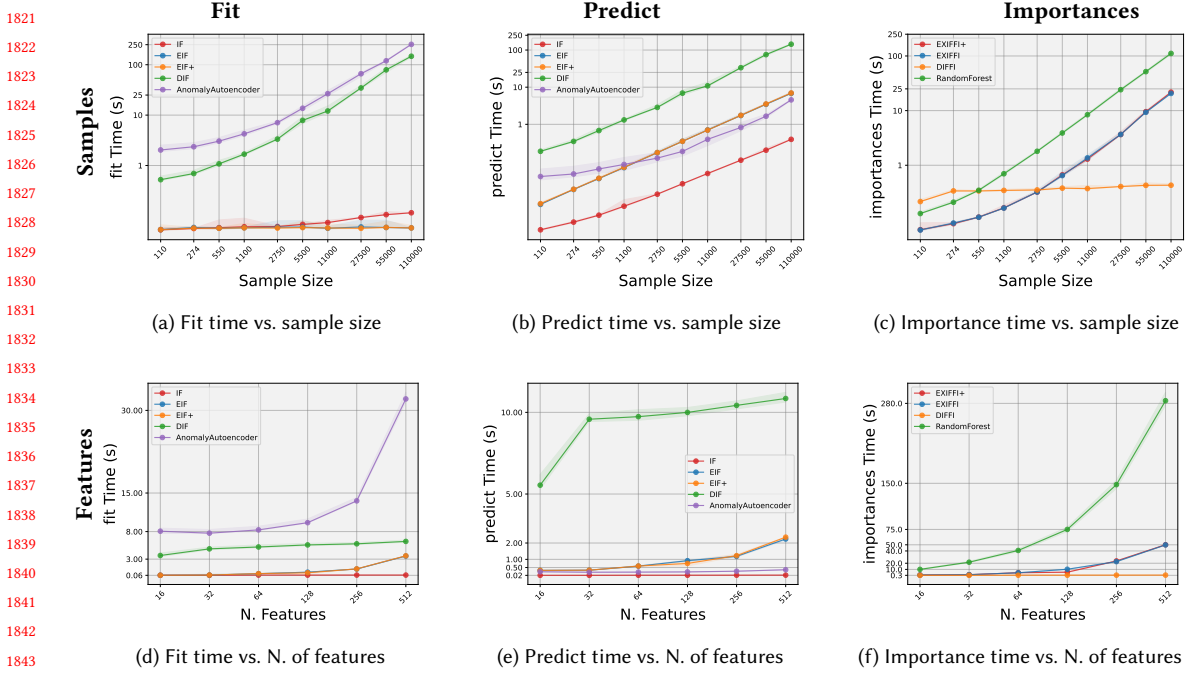


Fig. 22. Time Scaling experiments display the execution times trend of various AD and XAD algorithms varying the sample size (fixing the number of features to 6) and the cardinality of the feature space (fixing the sample size to 5000).

on the sample size. Finally, EIF and EIF⁺ depict an increasing trend with, however, much smaller values than the ones of DIF.

In the case of the interpretation, Figure 22c identifies DIFFI as the fastest algorithm for calculating importance scores. EIF and EIF⁺ experience a marked increase in computation time for this task beyond 11,000 samples. Nonetheless, their performance remains markedly better compared to the RandomForest post-hoc interpretability method, which suffers from exponential growth in execution time with larger sample and feature sizes. This analysis illustrates the efficiency and adaptability of EIF⁺ in providing rapid interpretation across varying dataset scales.

6.5 Complete Performance Report Table

Table 14 examines the performance achieved by different AD models across various datasets. The analysis focuses on Average Precision (Avg Prec), Precision (Prec), and ROC-AUC score metrics, under the two different scenarios; with outliers in the training dataset (S1) and without outliers (S2).

In S1, models are benchmarked under standard conditions, where EIF showcases superior Avg Prec, Prec, and ROC AUC scores across most datasets compared to the initial Isolation Forest (IF). This improvement underscores EIF's enhanced anomaly detection capability, particularly in handling complex data structures. However, the EIF⁺ model does not consistently outperform EIF within this scenario, indicating its modifications do not significantly impact performance under standard test conditions. S2's findings mark a distinct improvement in EIF⁺'s performance over EIF, notably in real-world datasets. In fact EIF⁺ achieves parity or surpasses EIF in Avg Prec and Prec metrics in all the dataset but Shuttle, demonstrating its refined ability to detect anomalies. This enhanced performance is attributable

Table 14. Consolidated Precision Report Across Datasets

| Scenario | Model | Measure | Synthetic | | | Real World | | | | | | | | | | | |
|----------|------------------|----------|-----------|-------|---------|------------|-------------|-------------|-------------|-------------|-------------|-------------|-------------|-------------|-------------|-------------|-------------|
| | | | Xaxis | Bisec | Bisec3D | Bisec6D | Anthyroid | Breastw | Cardio | Diabetes | Glass | Tonosphere | Moodify | Pendigits | Pima | Shuttle | Wine |
| S1 | IF | Avg Prec | 0.09 | 0.75 | 0.95 | 0.99 | 0.30 | 0.96 | 0.53 | 0.46 | 0.36 | 0.79 | 0.35 | 0.28 | 0.51 | 0.98 | 0.26 |
| | | Prec | 0.11 | 0.74 | 0.85 | 0.98 | 0.32 | 0.90 | 0.44 | 0.46 | 0.34 | 0.65 | 0.30 | 0.31 | 0.52 | 0.96 | 0.20 |
| | | ROC AUC | 0.51 | 0.85 | 0.91 | 0.98 | 0.63 | 0.90 | 0.69 | 0.70 | 0.62 | 0.73 | 0.59 | 0.64 | 0.63 | 0.97 | 0.56 |
| | EIF | Avg Prec | 0.97 | 0.97 | 0.96 | 0.96 | 0.19 | 0.91 | 0.55 | 0.47 | 0.35 | 0.82 | 0.33 | 0.23 | 0.49 | 0.90 | 0.21 |
| | | Prec | 0.89 | 0.91 | 0.89 | 0.92 | 0.24 | 0.86 | 0.59 | 0.48 | 0.27 | 0.69 | 0.37 | 0.24 | 0.49 | 0.87 | 0.20 |
| | | ROC AUC | 0.93 | 0.95 | 0.93 | 0.95 | 0.59 | 0.86 | 0.77 | 0.71 | 0.58 | 0.76 | 0.63 | 0.61 | 0.61 | 0.93 | 0.56 |
| | EIF ⁺ | Avg Prec | 0.91 | 0.94 | 0.93 | 0.93 | 0.20 | 0.88 | 0.50 | 0.44 | 0.31 | 0.84 | 0.28 | 0.21 | 0.49 | 0.70 | 0.17 |
| | | Prec | 0.89 | 0.83 | 0.71 | 0.81 | 0.28 | 0.85 | 0.52 | 0.49 | 0.24 | 0.72 | 0.27 | 0.41 | 0.50 | 0.71 | 0.00 |
| | | ROC AUC | 0.93 | 0.90 | 0.84 | 0.89 | 0.61 | 0.84 | 0.73 | 0.72 | 0.56 | 0.78 | 0.57 | 0.69 | 0.61 | 0.84 | 0.45 |
| S2 | DIF | Avg Prec | 0.06 | 0.16 | 0.30 | 0.19 | 0.21 | 0.44 | 0.58 | 0.10 | 0.30 | 0.87 | 0.26 | 0.34 | 0.41 | 0.54 | 0.07 |
| | | Prec | 0.06 | 0.20 | 0.28 | 0.16 | 0.26 | 0.49 | 0.52 | 0.90 | 0.20 | 0.76 | 0.26 | 0.39 | 0.41 | 0.60 | 0.00 |
| | | ROC AUC | 0.48 | 0.56 | 0.60 | 0.53 | 0.60 | 0.46 | 0.73 | 0.49 | 0.54 | 0.81 | 0.56 | 0.68 | 0.54 | 0.78 | 0.45 |
| | AE | Avg Prec | 0.52 | 0.89 | 0.97 | 0.97 | 0.21 | 0.61 | 0.62 | 0.45 | 0.41 | 0.76 | 0.45 | 0.22 | 0.43 | 0.90 | 0.14 |
| | | Prec | 0.46 | 0.82 | 0.92 | 0.95 | 0.25 | 0.44 | 0.62 | 0.47 | 0.44 | 0.60 | 0.53 | 0.33 | 0.44 | 0.95 | 0.10 |
| | | ROC AUC | 0.70 | 0.90 | 0.95 | 0.97 | 0.59 | 0.41 | 0.79 | 0.70 | 0.68 | 0.68 | 0.72 | 0.65 | 0.57 | 0.97 | 0.51 |
| | IF | Avg Prec | 0.10 | 0.99 | 1.00 | 1.00 | 0.45 | 0.99 | 0.68 | 0.26 | 0.65 | 0.89 | 0.72 | 0.37 | 0.58 | 0.98 | 0.61 |
| | | Prec | 0.00 | 0.95 | 1.00 | 1.00 | 0.43 | 0.94 | 0.60 | 0.31 | 0.68 | 0.79 | 0.73 | 0.42 | 0.55 | 0.97 | 0.50 |
| | | ROC AUC | 0.45 | 0.97 | 1.00 | 1.00 | 0.69 | 0.94 | 0.78 | 0.62 | 0.82 | 0.83 | 0.84 | 0.70 | 0.66 | 0.98 | 0.72 |
| S2 | EIF | Avg Prec | 0.99 | 0.99 | 0.99 | 0.99 | 0.45 | 0.98 | 0.74 | 0.55 | 0.57 | 0.90 | 0.65 | 0.27 | 0.54 | 0.97 | 0.57 |
| | | Prec | 1.00 | 1.00 | 1.00 | 0.99 | 0.41 | 0.93 | 0.72 | 0.61 | 0.68 | 0.82 | 0.64 | 0.36 | 0.57 | 0.95 | 0.60 |
| | | ROC AUC | 1.00 | 1.00 | 1.00 | 0.99 | 0.68 | 0.93 | 0.84 | 0.78 | 0.82 | 0.86 | 0.79 | 0.67 | 0.67 | 0.97 | 0.78 |
| | EIF ⁺ | Avg Prec | 0.99 | 1.00 | 0.99 | 0.99 | 0.46 | 0.99 | 0.76 | 0.61 | 0.69 | 0.96 | 0.66 | 0.36 | 0.58 | 0.91 | 0.79 |
| | | Prec | 1.00 | 1.00 | 0.99 | 1.00 | 0.46 | 0.95 | 0.73 | 0.56 | 0.79 | 0.87 | 0.66 | 0.45 | 0.57 | 0.96 | 0.70 |
| | | ROC AUC | 1.00 | 1.00 | 0.99 | 1.00 | 0.70 | 0.95 | 0.85 | 0.76 | 0.88 | 0.90 | 0.80 | 0.72 | 0.67 | 0.97 | 0.83 |
| | DIF | Avg Prec | 0.97 | 0.85 | 0.79 | 0.36 | 0.39 | 0.60 | 0.79 | 0.13 | 0.85 | 0.96 | 0.72 | 0.46 | 0.49 | 0.99 | 0.72 |
| | | Prec | 0.90 | 0.78 | 0.72 | 0.32 | 0.39 | 0.66 | 0.70 | 0.17 | 0.82 | 0.89 | 0.73 | 0.53 | 0.46 | 0.97 | 0.70 |
| | | ROC AUC | 0.94 | 0.87 | 0.84 | 0.62 | 0.67 | 0.64 | 0.83 | 0.54 | 0.90 | 0.90 | 0.84 | 0.76 | 0.59 | 0.98 | 0.83 |
| | AE | Avg Prec | 1.00 | 1.00 | 1.00 | 1.00 | 0.44 | 0.98 | 0.83 | 0.50 | 0.53 | 0.87 | 0.65 | 0.24 | 0.50 | 0.90 | 0.45 |
| | | Prec | 1.00 | 1.00 | 1.00 | 1.00 | 0.42 | 0.94 | 0.70 | 0.52 | 0.62 | 0.75 | 0.68 | 0.33 | 0.54 | 0.94 | 0.50 |
| | | ROC AUC | 1.00 | 1.00 | 1.00 | 1.00 | 0.69 | 0.93 | 0.76 | 0.73 | 0.78 | 0.80 | 0.81 | 0.66 | 0.64 | 0.97 | 0.72 |

Scenario 1 (S1) and Scenario 2 (S2) performance metrics for various Anomaly Detection models across different datasets, excluding Recall metrics. Avg Prec stands for Average Precision.

to EIF⁺'s algorithmic adjustments, optimized to grasp the unseen outliers within complex data distributions more effectively than EIF. Moreover EIF⁺ demonstrate enhanced performances by figuring as the most performing model in 6 out of 11 real world datasets and reaching perfect performances in synthetic ones.

The detailed analysis affirms EIF⁺'s superior performance in S2, attributed to algorithmic advancements in generalizing over unseen data that refine detection accuracy compared to the EIF model, that even in this analysis maintain its superiority compared to other models such as DIF or AutoEncoders in detecting anomalies.

6.6 Complete Importance Score Table

Table 15. Consolidated AUC_{FS} Across Datasets

| Scenario | Evaluation | Model | Synthetic | | | | Real World | | | | | | | | | | | |
|----------|------------------|----------|-------------|-------------|-------------|-------------|-------------|-------------|-------------|-------------|-------------|-------------|-------------|-------------|-------------|-------------|-------------|--|
| | | | Xaxis | Bisec | Bisec3D | Bisec6D | Anmthyroid | Breastw | Cardio | Diabetes | Glass | Tonosphere | Moodify | Pendigits | Pima | Shuttle | Wine | |
| S1 | EIF | DIFFI | 4.73 | 4.12 | 3.42 | 0.02 | 0.96 | 0.11 | 4.65 | -0.36 | 1.59 | 2.36 | -1.48 | 0.11 | -0.48 | -0.51 | 0.17 | |
| | | ExIFFI | 4.72 | 4.14 | 3.41 | 0.14 | 0.98 | 0.04 | 5.41 | 0.96 | 0.46 | 1.82 | -1.78 | 1.58 | -0.31 | -1.43 | 0.45 | |
| | | ExIFFI + | 4.70 | 4.05 | 3.43 | 0.12 | 0.98 | 0.07 | 4.42 | 1.05 | 0.40 | 0.61 | -1.51 | 1.86 | -0.3 | 0.45 | 0.12 | |
| | | IF_RF | -2.82 | 4.07 | 3.44 | 0.21 | 0.45 | -0.14 | 1.48 | -0.3 | -1.73 | -1.91 | -0.78 | 1.48 | -0.36 | 0.44 | -3.09 | |
| | | EIF_RF | 4.71 | 4.05 | 3.41 | 0.12 | -0.68 | -0.18 | 1.35 | 0.49 | -1.71 | -1.97 | -0.84 | -0.72 | -0.44 | 1.69 | -2.41 | |
| | | EIF+_RF | 4.70 | 4.05 | 3.41 | 0.17 | -1.19 | -0.16 | 0.32 | 0.46 | -1.46 | -1.87 | -1.88 | -1.4 | -0.28 | 1.90 | -2.81 | |
| | | DIFFI | 4.54 | 4.16 | 3.32 | -0.02 | 0.91 | 0.08 | 4.39 | -0.34 | 1.55 | -1.13 | -1.11 | 0.23 | -0.49 | -0.69 | 0.43 | |
| | EIF ⁺ | ExIFFI | 4.57 | 4.0 | 3.44 | -0.02 | 0.93 | 0.02 | 5.12 | 0.82 | 0.56 | 1.61 | -1.37 | 1.76 | -0.32 | 1.22 | 0.45 | |
| | | ExIFFI + | 4.52 | 3.98 | 3.41 | 0.05 | 0.97 | 0.08 | 4.25 | 0.74 | 0.52 | 0.45 | -0.99 | 1.92 | -0.27 | 0.73 | 0.18 | |
| | | IF_RF | -2.73 | 4.05 | 3.42 | 0.15 | 0.42 | -0.14 | 1.28 | -0.3 | -1.31 | 1.76 | -0.72 | 1.37 | -0.3 | 0.36 | -2.33 | |
| | | EIF_RF | 4.53 | 4.01 | 3.35 | 0.02 | -0.67 | -0.16 | 1.35 | 0.38 | -1.51 | -1.85 | -0.71 | -0.36 | -0.41 | 1.73 | -1.57 | |
| | | EIF+_RF | 4.52 | 4.99 | 3.37 | 0.05 | -1.16 | -0.14 | 0.36 | 0.40 | -1.3 | -1.56 | -1.43 | -0.97 | -0.28 | 1.62 | -2.05 | |
| | | DIFFI | 2.83 | 2.92 | 2.79 | -0.04 | 2.04 | 0.06 | 4.76 | -1.45 | 2.11 | -1.33 | -3.66 | -0.38 | 0.25 | -1.48 | -3.79 | |
| | | ExIFFI | 4.7 | 3.84 | 3.41 | 0.17 | 2.03 | 0.06 | 8.28 | 0.35 | 2.55 | 4.31 | -0.35 | 1.88 | -0.21 | 0.76 | 7.12 | |
| S2 | EIF | ExIFFI + | 4.72 | 3.83 | 3.43 | 0.19 | 2.18 | 0.02 | 8.6 | 0.82 | 1.76 | 2.26 | -0.23 | 1.22 | -0.03 | 0.01 | 9.0 | |
| | | IF_RF | -2.82 | 3.82 | 3.48 | 0.22 | 2.05 | 0.09 | 7.69 | -0.05 | 2.18 | -1.23 | 2.07 | 1.28 | 0.19 | 0.90 | 4.41 | |
| | | EIF_RF | 4.7 | 3.83 | 3.45 | 0.24 | 2.03 | 0.1 | 7.78 | 0.31 | -1.63 | 1.33 | 1.63 | -0.84 | 0.12 | 2.74 | 3.94 | |
| | | EIF+_RF | 4.72 | 3.83 | 3.4 | 0.14 | 2.09 | 0.1 | 8.24 | 0.33 | 1.94 | 3.58 | 1.47 | -0.24 | 0.06 | 2.13 | 4.87 | |
| | | DIFFI | 2.72 | 2.92 | 2.83 | -0.12 | 2.0 | 0.06 | 4.33 | -1.48 | 2.44 | 1.92 | -3.36 | -0.76 | 0.3 | -1.45 | -3.49 | |
| | | ExIFFI | 4.60 | 3.84 | 3.45 | 0.1 | 1.92 | 0.08 | 8.38 | 0.31 | 2.43 | 2.84 | -0.20 | 2.23 | -0.2 | 0.31 | 8.12 | |
| | | ExIFFI + | 4.58 | 3.82 | 3.43 | 0.13 | 2.17 | 0.06 | 8.73 | 1.17 | 2.26 | 1.41 | -0.04 | 1.32 | -0.02 | -0.13 | 9.25 | |
| | EIF ⁺ | IF_RF | -2.67 | 3.82 | 3.39 | 0.19 | 1.99 | 0.06 | 7.88 | -0.12 | 2.28 | -1.08 | 2.48 | 1.38 | 0.21 | 0.64 | 4.53 | |
| | | EIF_RF | 4.51 | 3.84 | 3.46 | 0.04 | 1.97 | 0.09 | 7.85 | 0.35 | -1.64 | 0.69 | 2.17 | -1.28 | 0.17 | 2.11 | 4.36 | |
| | | EIF+_RF | 4.53 | 3.83 | 3.47 | 0.05 | 2.02 | 0.07 | 8.3 | 0.29 | 1.63 | 2.17 | 2.08 | -0.74 | 0.14 | 2.11 | 5.64 | |

AUC_{FS} metric values for different interpretation algorithms with Average Precision evaluated with EIF and EIF⁺ in Scenario I (S1) and Scenario II (S2) across different datasets. The highest value in S2 are highlighted in bold.

Table 15 collects the values of the newly introduced AUC_{FS} metric across all the 15 benchmark datasets used for the evaluation of the proposed ExIFFI interpretation model. As already discussed in 5 ExIFFI is compared to another ad-hoc interpretability algorithm (i.e. DIFFI) and to a post-hoc interpretability approach based on the feature importance computation provided by the Random Forest surrogate model.

Observing the presented values it is possible to conclude that for what concerns Synthetic datasets the values of the metric are quite high for all the models, except for the case of Bisec6D dataset where the feature importance assignment task is quite challenging as described in 6.1.6.

Regarding the Real World datasets the peculiar manner in which inliers and outliers are defined renders the assessment of interpretability performance of the models under consideration challenging. This fact holds true in particular for the Breastw, Pima, Shuttle and Moodify datasets which are in fact characterized by the presence of similar AUC_{FS} values, most of which are negative.

With regard to the remaining 7 datasets, focusing on the evaluation with EIF⁺, that proved to be the optimal model for the Anomaly Detection task, it is possible to confirm the superiority of the proposed approaches ExIFFI and ExIFFI + which showcase the highest AUC_{FS} value in 5 out of 7 datasets in Scenario I and in 6 out of 7 datasets in Scenario II.

In fact, the AUC_{FS} metric values are highly correlated to the efficacy of the specific interpretation model on a certain dataset and scenario (i.e. Scenario I or Scenario II). As a consequence, ExIFFI and ExIFFI + being the optimal

1977 interpretation methods in quantitative terms, in particular in Scenario II, aligns with the results presented in 6.5
 1978 regarding the enhanced precision of EIF⁺ in detecting anomalous samples.

1979
 1980 Concluding, this analysis confirms the effectiveness of using the proposed EIF⁺ and ExIFFI methods in a combined
 1981 way in order to achieve at the same time optimal anomaly detection and interpretability results.

1982 7 CONCLUSIONS

1983 This paper has explored the critical domain of unsupervised AD, a pivotal task for identifying irregular patterns or
 1984 behaviors. While the task of identifying anomalies is foundational, our work underscores that it's often insufficient
 1985 for real-world applications. Users' need to comprehend the rationale behind model predictions, facilitating root cause
 1986 analysis and engendering trust in the model, is paramount.

1987
 1988 Our primary contribution lies in the introduction of ExIFFI, an interpretability approach that is inspired by DIFFI
 1989 (a model-specific tool designed to explain Isolation Forest predictions) and aims at providing both local and global
 1990 interpretability for the Extended Isolation Forest (EIF).

1991 Furthermore, this work presents EIF⁺, a variant of EIF tailored to improve generalization performance. We provide a
 1992 comprehensive comparative analysis among Isolation-based and deep learning based AD approaches, which, to our
 1993 knowledge, represents the most exhaustive study available in the literature.

1994 Our experimental results corroborate the utility of ExIFFI. Controlled experiments on synthetic data underscore the
 1995 robustness of our approach. However, when dealing with real-world datasets, limitations tied to the nature of labeled
 1996 anomalies often diverge from the isolation assumption required by tree-based models for their effectiveness. In such
 1997 cases, evaluating the quality of interpretations becomes challenging. This motivated further experiments where models
 1998 are trained on inliers only, revealing the value of ExIFFI when classification performance improves.

1999 Moreover, the *AUC_{FS}* metric, based on the Unsupervised Feature Selection proxy task, was presented in order
 2000 introduce a quantitative measure to compare the effectiveness of diverse interpretation algorithms.

2001 Finally, the applicability of the two novel methods introduced (i.e. EIF⁺ and ExIFFI) on large-scale dataset, as the
 2002 ones that may be encountered on an industrial setting, was assessed through ad-hoc Time Scaling experiments whose
 2003 outcomes are reported in Section 6.4.

2004 Moving forward, avenues for future research should explore innovative ways to leverage the information encoded
 2005 in splitting nodes, especially when uncertainty arises due to multiple variables competing for the role of the most
 2006 relevant feature. Additionally, an intriguing research direction could delve into a more comprehensive assessment of
 2007 using ExIFFI for feature selection in unsupervised AD settings. While our study has demonstrated its potential in this
 2008 context, dedicated research endeavors are warranted to fully explore its capabilities. In conclusion, a possible direction
 2009 for future research endeavors to explore the feasibility of deploying EIF⁺ and ExIFFI methodologies within authentic
 2010 industrial contexts, where demand for such models is steadily escalating.

2011 REFERENCES

- [1] Stefan Aeberhard and M. Forina. 1991. Wine. UCI Machine Learning Repository. DOI: <https://doi.org/10.24432/C5PC7J>.
- [2] André Altmann, Laura Tolosí, Oliver Sander, and Thomas Lengauer. 2010. Permutation importance: a corrected feature importance measure. *Bioinformatics* 26, 10 (2010), 1340–1347.
- [3] Roel Bouman, Zaharah Bukhsh, and Tom Heskes. 2023. Unsupervised anomaly detection algorithms on real-world data: how many do we need? *arXiv preprint arXiv:2305.00735* (2023).
- [4] Lucas C. Brito, Gian Antonio Susto, Jorge N. Brito, and Marcus A.V. Duarte. 2022. An explainable artificial intelligence approach for unsupervised fault detection and diagnosis in rotating machinery. *Mechanical Systems and Signal Processing* 163 (2022), 108105. <https://doi.org/10.1016/j.ymssp.2021.108105>

- [5] D. Campos and J. Bernardes. 2010. Cardiotocography. UCI Machine Learning Repository. DOI: <https://doi.org/10.24432/C51S4N>.
- [6] Mattia Carletti, Marco Maggipinto, Alessandro Beghi, Gian Antonio Susto, Natalie Gentner, Yao Yang, and Andreas Kyek. 2020. Interpretable Anomaly Detection for Knowledge Discovery in Semiconductor Manufacturing. In *2020 Winter Simulation Conference (WSC)*. 1875–1885. <https://doi.org/10.1109/WSC48552.2020.9384026>
- [7] Mattia Carletti, Chiara Masiero, Alessandro Beghi, and Gian Antonio Susto. 2019. Explainable machine learning in industry 4.0: Evaluating feature importance in anomaly detection to enable root cause analysis. In *2019 IEEE international conference on systems, man and cybernetics (SMC)*. IEEE, 21–26.
- [8] Mattia Carletti, Matteo Terzi, and Gian Antonio Susto. 2023. Interpretable Anomaly Detection with DIFFI: Depth-based Isolation Forest Feature Importance.
- [9] Aggarwal Charu C. 2015. Outlier Analysis. , 98–101 pages.
- [10] European Commission. 2020. *On Artificial Intelligence—A European Approach to Excellence and Trust*. https://ec.europa.eu/info/publications/white-paper-artificial-intelligence-european-approach-excellence-and-trust_en
- [11] Roberto Confalonieri, Ludovik Coba, Benedikt Wagner, and Tarek R Besold. 2021. A historical perspective of explainable Artificial Intelligence. *Wiley Interdisciplinary Reviews: Data Mining and Knowledge Discovery* 11, 1 (2021), e1391.
- [12] Finale Doshi-Velez and Been Kim. 2017. Towards a rigorous science of interpretable machine learning. *arXiv preprint arXiv:1702.08608* (2017).
- [13] B. German. 1987. Glass Identification. UCI Machine Learning Repository. DOI: <https://doi.org/10.24432/C5WW2P>.
- [14] Leilani H Gilpin, David Bau, Ben Z Yuan, Ayesha Bajwa, Michael Specter, and Lalana Kagal. 2018. Explaining explanations: An overview of interpretability of machine learning. In *2018 IEEE 5th International Conference on data science and advanced analytics (DSAA)*. IEEE, 80–89.
- [15] Sahand Hariri, Matias Carrasco Kind, and Robert J. Brunner. 2021. Extended Isolation Forest. *IEEE Transactions on Knowledge and Data Engineering* 33, 4 (2021), 1479–1489. <https://doi.org/10.1109/TKDE.2019.2947676>
- [16] Douglas M Hawkins. 1980. *Identification of outliers*. Vol. 11. Springer.
- [17] Essam H Houssein, Marwa M Emam, Abdelmejid A Ali, and Ponnuthurai Nagarathnam Suganthan. 2021. Deep and machine learning techniques for medical imaging-based breast cancer: A comprehensive review. *Expert Systems with Applications* 167 (2021), 114161.
- [18] Nirmal Sobha Kartha, Clément Gautrais, and Vincent Verheyen. 2021. Why Are You Weird? Infusing Interpretability in Isolation Forest for Anomaly Detection. *arXiv:2112.06858 [cs.LG]*
- [19] Ahmad F Klaib, Nawaf O Alsrehin, Wasen Y Melhem, Haneen O Bashtawi, and Aws A Magableh. 2021. Eye tracking algorithms, techniques, tools, and applications with an emphasis on machine learning and Internet of Things technologies. *Expert Systems with Applications* 166 (2021), 114037.
- [20] Manfred Krafft, Laszlo Sajtos, and Michael Haenlein. 2020. Challenges and opportunities for marketing scholars in times of the fourth industrial revolution. *Journal of Interactive Marketing* 51, 1 (2020), 1–8.
- [21] Miron B Kursa and Witold R Rudnicki. 2010. Feature selection with the Boruta package. *Journal of statistical software* 36 (2010), 1–13.
- [22] Julien Lesouple, Cédric Baudoin, Marc Spigai, and Jean-Yves Tourneret. 2021. Generalized isolation forest for anomaly detection. *Pattern Recognition Letters* 149 (2021), 109–119. <https://doi.org/10.1016/j.patrec.2021.05.022>
- [23] Zheng Li, Yue Zhao, Xiyang Hu, Nicola Botta, Cezar Ionescu, and George H. Chen. 2023. ECOD: Unsupervised Outlier Detection Using Empirical Cumulative Distribution Functions. *IEEE Transactions on Knowledge and Data Engineering* 35, 12 (Dec. 2023), 12181–12193. <https://doi.org/10.1109/tkde.2022.3159580>
- [24] Zhong Li, Yuxuan Zhu, and Matthijs Van Leeuwen. 2023. A Survey on Explainable Anomaly Detection. *ACM Trans. Knowl. Discov. Data* 18, 1, Article 23 (sep 2023), 54 pages. <https://doi.org/10.1145/3609333>
- [25] Pantelis Linardatos, Vasilis Papastefanopoulos, and Sotiris Kotsiantis. 2020. Explainable ai: A review of machine learning interpretability methods. *Entropy* 23, 1 (2020), 18.
- [26] Fei Tony Liu, Kai Ming Ting, and Zhi-Hua Zhou. 2008. Isolation Forest. In *2008 Eighth IEEE International Conference on Data Mining*. 413–422. <https://doi.org/10.1109/ICDM.2008.17>
- [27] Scott M Lundberg, Gabriel G Erion, and Su-In Lee. 2018. Consistent individualized feature attribution for tree ensembles. *arXiv preprint arXiv:1802.03888* (2018).
- [28] Scott M Lundberg and Su-In Lee. 2017. A Unified Approach to Interpreting Model Predictions. In *Advances in Neural Information Processing Systems* 30, I. Guyon, U. V. Luxburg, S. Bengio, H. Wallach, R. Fergus, S. Vishwanathan, and R. Garnett (Eds.). Curran Associates, Inc., 4765–4774.
- [29] Scott M Lundberg and Su-In Lee. 2017. A Unified Approach to Interpreting Model Predictions. In *Advances in Neural Information Processing Systems*, I. Guyon, U. Von Luxburg, S. Bengio, H. Wallach, R. Fergus, S. Vishwanathan, and R. Garnett (Eds.), Vol. 30. Curran Associates, Inc. https://proceedings.neurips.cc/paper_files/paper/2017/file/8a20a8621978632d76c43dfd28b67767-Paper.pdf
- [30] Tim Miller. 2019. Explanation in artificial intelligence: Insights from the social sciences. *Artificial Intelligence* 267 (2019), 1–38. <https://doi.org/10.1016/j.artint.2018.07.007>
- [31] Christoph Molnar. 2020. *Interpretable machine learning*. Lulu. com.
- [32] Hounaïda Mrabet, Ismail Khattech, Souhir Bouzidi, Lilia Kechiche, A. Jbeli, Nuha Al Harbi, Chaker Bouzidi, Francisco Muñoz, and Rolindes Balda. 2024. Influence of barium substitution on the physical, thermal, optical and luminescence properties of Sm³⁺-doped metaphosphate glasses for reddish orange light applications. *RSC Adv.* 14 (2024), 2070–2079. Issue 3. <https://doi.org/10.1039/D3RA08015C>
- [33] C.L. Blake D.J. Newman and C.J. Merz. -. Statlog (Shuttle). UCI Machine Learning Repository. DOI: <https://doi.org/10.24432/C5WS31>.

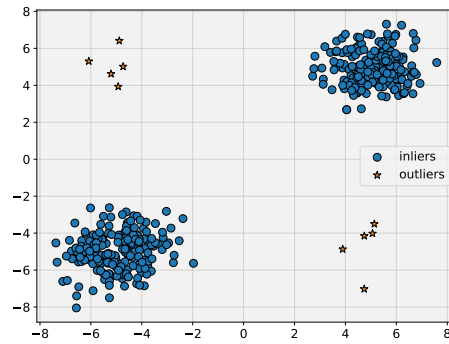
- 2081 [34] David F. N. Oliveira, Lucio F. Vismari, Alexandre M. Nascimento, Jorge R. de Almeida, Paulo S. Cugnasca, João B. Camargo, Leandro Almeida,
 2082 Rafael Gripp, and Marcelo Neves. 2022. A New Interpretable Unsupervised Anomaly Detection Method Based on Residual Explanation. *IEEE Access*
 2083 10 (2022), 1401–1409. <https://doi.org/10.1109/ACCESS.2021.3137633>
- 2084 [35] B.R. Preiss. 2000. *Data Structures and Algorithms with Object-Oriented Design Patterns in Java*. Wiley. <https://books.google.it/books?id=ywpRAAAAMAAJ>
- 2085 [36] Ross Quinlan. 1987. Thyroid Disease. UCI Machine Learning Repository. DOI: <https://doi.org/10.24432/C5D010>.
- 2086 [37] Shebuti Rayana. 2016. ODDS Library. <https://odds.cs.stonybrook.edu>
- 2087 [38] Lukas Ruff, Jacob R. Kauffmann, Robert A. Vandermeulen, Grégoire Montavon, Wojciech Samek, Marius Kloft, Thomas G. Dietterich, and Klaus-
 2088 Robert Müller. 2021. A Unifying Review of Deep and Shallow Anomaly Detection. *Proc. IEEE* 109, 5 (2021), 756–795. <https://doi.org/10.1109/JPROC.2021.3052449>
- 2089 [39] V. Sigillito, S. Wing, L. Hutton, , and K. Baker. 1989. Ionosphere. UCI Machine Learning Repository. DOI: <https://doi.org/10.24432/C5W01B>.
- 2090 [40] Timo Speith. 2022. A review of taxonomies of explainable artificial intelligence (XAI) methods. In *2022 ACM Conference on Fairness, Accountability,
 2091 and Transparency*, 2239–2250.
- 2092 [41] Hugues Turbé, Mina Bjelogrlic, Christian Lovis, and Gianmarco Mengaldo. 2023. Evaluation of post-hoc interpretability methods in time-series
 2093 classification. *Nature Machine Intelligence* 5, 3 (2023), 250–260.
- 2094 [42] Maksymilian Wojtas and Ke Chen. 2020. Feature importance ranking for deep learning. *Advances in neural information processing systems* 33 (2020),
 2095 5105–5114.
- 2096 [43] William Wolberg. 1992. Breast Cancer Wisconsin (Original). UCI Machine Learning Repository. DOI: <https://doi.org/10.24432/C5HP4Z>.
- 2097 [44] Hongzuo Xu, Guansong Pang, Yijie Wang, and Yongjun Wang. 2023. Deep isolation forest for anomaly detection. *IEEE Transactions on Knowledge
 2098 and Data Engineering* (2023).
- 2099 [45] Min Xu, Jeanne M David, Suk Hi Kim, et al. 2018. The fourth industrial revolution: Opportunities and challenges. *International journal of financial
 2100 research* 9, 2 (2018), 90–95.
- 2101
- 2102

A APPENDICES

A.1 Datasets

2106 *A.1.1 Synthetic datasets.* We considered the following synthetic datasets:

- 2107 • The Bimodal dataset was exploited also by other researchers like Hariti et. al [15], making it a well-suited
 2108 synthetic example. The resulting point distribution of the Bimodal dataset is depicted in the scatter plot in
 2109 Figure 23. The contamination factor used for the Bimodal dataset is 2.5%.
- 2110



2111 Fig. 23. Scatter Plot of the **bimodal** Dataset

2112 In particular, the two clusters of inliers are positioned along the bisector line while the outliers are placed along
 2113 the anti-bisector line. As it can be noticed from a detailed observation of the scatter plot, there is a significant
 2114 discrepancy in terms of quantity between inliers and outliers. In fact, the dataset was manipulated in order to
 2115

2133 ensure the imbalance between normal and anomalous points to replicate a common scenario in the context of
 2134 Anomaly Detection.
 2135

- 2136 • The datasets referred to as **Xaxis** and **Yaxis** originate from the research paper authored by Carletti et al. [8].
 2137 In this particular scenario, inlier points are randomly sampled from a six-dimensional sphere centered at the
 2138 origin with a radius of 5.

2139 To generate the outlier data, a specific feature is chosen to be associated with anomalous values. In this instance,
 2140 feature 0 is selected for the **Xaxis** dataset, and feature 1 is chosen for the **Yaxis** dataset. All other features
 2141 consist of random noise values drawn from a standard normal distribution, denoted as $X \sim N(0, 1)$.

2142 Subsequently, outlier points are sampled along these specific features, maintaining a predefined proportion
 2143 relative to the inliers. In this specific case, there is one outlier for every 10 inliers.

- 2144 • The **Bisec** dataset closely resembles the **Xaxis** and **Yaxis** datasets. In this dataset, the inliers are distributed fol-
 2145 lowing a normal distribution pattern within a six-dimensional sphere. Conversely, the anomalies are positioned
 2146 along the bisector line of the Feature 0 and Feature 1 subspace, equidistant from the origin as the anomalies in
 2147 the **Xaxis** and **Yaxis** datasets.

2148 As the names suggest, **Bisec3D** and **Bisec6D** datasets are constructed similarly to the **Bisec** dataset. However,
 2149 in **Bisec3D**, the anomalies are placed along the bisector line of the subspace defined by Feature 0, Feature 1,
 2150 and Feature 2. In **Bisec6D**, the anomalies are positioned along the bisector line spanning all six dimensions of
 2151 the dataset. The proportion of the outliers remains 1-10 as in the **Xaxis** and **Yaxis** datasets.

2152 A.1.2 Real-world Datasets. This is the list of considered real-world datasets:

- 2153 • **Annthyroid**: The **Annthyroid** dataset [36] is part of the UCI Machine Learning Repository. It is a three-class
 2154 Classification dataset. The aim of the classification task associated with this dataset is to detect whether a patient
 2155 is hypothyroid (i.e. the patient has an underactive thyroid) or not. For this scope, the three classes used refer to
 2156 the functioning conditions of the thyroid that can be *normal* (not hypothyroid), *hyperfunctioning* (overactive
 2157 thyroid) and *subnormal*. The dataset originally contained 15 categorical and 6 numerical attributes. In order to
 2158 adapt it to an Anomaly Detection task only the numerical attributes were considered and the *hyperfunctioning*
 2159 and *subnormal* function classes were considered as part of the outliers while the *normal* functioning samples
 2160 are used to build the inlier class. The six numerical features represent, respectively, the following quantities:
 2161 TSH, T3, TT4, T4U, and FTI.
 - 2162 – **TSH (Thyroid-Stimulating Hormone)**: TSH is an hormone produced by the pituitary gland. An underac-
 2163 tive thyroid (hypothyroidism) is associated with high levels of TSH while low levels of TSH are associated
 2164 with an overactive thyroid (hyperthyroidism).
 - 2165 – **T3 (Triiodothyronine)**: T3 is one of the thyroid hormones. It plays a crucial role in regulating the
 2166 metabolism. It is important to measure the levels of this hormone, specifically in cases of hyperthyroidism.
 - 2167 – **TT4 (Total Thyroxine)**: This quantity represents the total amount of the T4 thyroid hormone in the
 2168 blood. T4 levels are associated to the overall thyroid hormone production.
 - 2169 – **T4U (Thyroxine-Binding Globulin)**: T4U measures the level of thyroxine-binding globulin, a protein
 2170 binding to thyroid hormones in the blood. T4U levels are connected to the thyroid hormone availability in
 2171 the body.

- 2185 – **FTI (Free Thyroxine Index):** Taking into account the T4 and T4U levels, the FTI provides an estimate of
 2186 the amount of free thyroxine (T4) in the blood. It is used to asses the free, active thyroid hormone levels in
 2187 the body.
- 2188 • **Breast:** The Breast dataset [43] is a Binary Classification dataset where the target is the presence of breast
 2189 cancer or not in a patient. The peculiarity of the samples contained in this dataset is that they are formed by
 2190 categorical features. Normally, the Anomaly Detection models described in this paper are not built to deal
 2191 with categorical features but in this particular case the high number of levels (e.g. The age variable has nine
 2192 levels: 10-19, 20-29, ...; the tumor-size feature has levels equal to 0-4,5-9,10-14, ...) characterizing the Breast
 2193 dataset's attributes makes it possible to consider them as numerical features. A noteworthy consequence to
 2194 consider is that when the samples of the Breast dataset are represented in a scatter plot, as it happens with
 2195 the Local Importance Scoremap in Figure 35c, they appear to have a grid-like shape. The dataset is composed
 2196 of samples coming from the clinical cases of Dr. Wolberg collected in a time span going from January 1989 to
 2197 November 1991. The dataset is composed by 9 features representing the following quantities: Clump Thickness,
 2198 Uniformity of Cell Size, Uniformity of Cell Shape, Marginal Adhesion, Single Epithelial Cell Size, Bare Nuclei,
 2199 Bland Chromatin, Normal Nucleoli and Mitoses.
 2200
- 2201 • **Cardio:** The Cardio [5] dataset is part of the UCI Machine Learning Repository and its complete name is
 2202 Cardiotocography since it contains measurements of fetal heart rate (FHR) and uterine contraction (UC) on
 2203 cardiotocograms ⁴. This dataset contains 3 classes that were assigned by expert obstetricians: *normal*, *suspect*,
 2204 and *pathologic*. In order to use this dataset for Anomaly Detection the suspect class was discarded and the
 2205 pathologic class was downsampled to 176 points to maintain unbalance with respect to the normal class. There
 2206 are 21 features.
 2207
- 2208 • **Glass:** The Glass dataset [13] is originally used for multi-class classification to distinguish 7 different types of
 2209 glasses. There are 9 features: the first one is the Refractive Index while the others measure the concentration of
 2210 Magnesium (Mg), Silicon (Si), Calcium (Ca), Iron (Fe), Sodium (Na), Aluminum (Al), Potassium (K) and Barium
 2211 (Ba) in the glass samples. The seven original glass groups were divided into two: Groups 1,2,3 and 4 represent
 2212 Window Glasses while the remaining ones are non-window glasses: containers glass, tableware glass and
 2213 headlamp glass. Among the non-window glasses, headlamp glasses were considered as outliers while Window
 2214 Glasses are labeled as inliers in order to convert this dataset to be used for Anomaly Detection. According
 2215 to some prior knowledge on the subject the Barium (Ba) and Potassium (K) concentration should be decisive
 2216 in distinguishing between headlamp and window glasses. In fact Barium is considered the crucial element to
 2217 perform the distinction between headlamp and window glasses since it is usually added to the category of
 2218 headlamp glasses in order to improve their optical properties. Another potential key attribute is Potassium (K)
 2219 that is frequently exploited to enhance strength and thermal resistance of window glasses. For the interested
 2220 reader a more detailed on this topic is provided in Section 6.2.5.
 2221
- 2222 • **Ionosphere:** The Ionosphere dataset [39] contains measurements collected by a radar in Goose Bay, Labrador.
 2223 The measurement system consisted of 16 high-frequency antennas with a transmitted power in the order of
 2224 6.4 kilowatts. The targets to measure were free electrons in the Ionosphere. Originally this is built as a Binary
 2225 Classification dataset where the two classes are *good* if the captured electrons show some kind of structure in
 2226

2227 ⁴A cardiotogram is a medical test monitoring fetal hearth rate and uterine contractions during pregnancy. It is used to assess the health status of the fetus
 2228 and the progress of labor during pregnancy and childbirth

2229 ⁵The complete list of features names can be found at: <https://archive.ics.uci.edu/dataset/193/cardiotocography>

the ionosphere and *bad* otherwise. The signal is processed with an autocorrelation function depending on the time of a pulse and the pulse number. There are 17 pulse numbers and each of them is identified by a pair of features for a total of 34 features.

- **Pima:** The Pima dataset ⁶ comes from the National Institute of Diabetes, Digestive and Kidney Diseases. It is a Binary Classification dataset whose aim is to predict whether a patient has diabetes or not. This dataset is the result of the application of some constraints to a larger dataset. In Pima, in fact, the data considered are obtained from female patients of at least 21 years of age coming from the Pima Indian heritage. The dataset contains 8 features indicating some typical diagnostic measurements: Number of pregnancies, Plasma Glucose Concentration, Diastolic Blood Pressure, Triceps skin thickness, 2-hour serum if insulin, BMI (Body Mass Index), Diabetes Pedigree function, and Age.
- **Pendigits:** The Pendigits dataset collects data regarding handwritten digits produced by Forty-four human writers. The task associated with this dataset is the one of recognizing the correct written digit. The dataset is composed of 16 features and the number of objects per class (i.e. per digit) was reduced by a factor of 10 % to increase the unbalance between classes in order to adapt the dataset as a benchmark for the evaluation of Anomaly Detection models.
- **Shuttle:** The Shuttle dataset [33] describes radiator positions in a NASA space shuttle. The samples are characterized by 9 attributes. Originally, the dataset is used for Multi-Class Classification with the target variable containing seven possible classes, which are: Radiator Flow, Fpv Close, Fpv Open, High, Bypass, Bpv Close, and Bpv Open. Besides the normal Radiator Flow class about 20% of the data points describe anomalous situations. To reduce the amount of anomalies the Radiator Flow class is used to form the inlier class while a stratified sampling procedure was applied to classes 2,3,5,6 and 7. Finally, data coming from class 4 were discarded.
- **Wine:** The Wine dataset [1] is part of the UCI Machine Learning repository and it was originally created as a 3-class classification dataset. In fact, it contains data resulting from a chemical analysis of wines grown in the same region of Italy but obtained from 3 different cultivars. So the aim of a Classification model applied to this dataset would be to correctly predict the original culture of wine given its chemical properties. As it is usually done in these cases the dataset was adapted to test Anomaly Detection models considering the data from two cultures as inliers and the ones beholding to the last culture as the outliers. The dataset is composed by 13 features representing the following quantities: Alcohol, Malic Acid, Ash, Alcalinity of ash, Magnesium, Total phenols, Flavanoids, Nonflavanoid phenols, Proanthocyanins, Color Intensity, Hue, OD280/OD315 ⁷ of diluted wines, and Proline.
- **Diabetes:** The Diabetes dataset ⁸ is a Binary Classification dataset with medical data about patients used to predict whether they have diabetes or not. There are 4 categorical and 4 numerical variables. In order to use the ExIFFI model only the numerical variables were considered:
 - Age: The age ranges between 0 and 80 and it can be an important factor since Diabetes is usually diagnosed in older adults.
 - BMI (Body Mass Index): Measure of body fat based on weight and height. High BMI values are linked to a higher risk of diabetes.

⁶<https://www.kaggle.com/datasets/uciml/pima-indians-diabetes-database>

⁷These codes refers to two measurements of the optical density of a wine sample performed at two different wavelengths: 280 nm and 315 nm. These measurements are typically exploited to assess the protein content and the stability of wine

⁸<https://www.kaggle.com/datasets/iammustafatz/diabetes-prediction-dataset>

- 2289 – HbA1c-Level: The Hemoglobin A1c Level it's a measure of a person's average blood sugar level over the
 2290 past 2-3 months. A high level of HbA1c is usually associated with high diabetes risk.
 2291 – blood-glucose-level: The amount of glucose in the bloodstream at a given time. High glucose levels are a
 2292 key factor to detect Diabetes.

2293 Finally, the target variable is a binary variable indicating the presence or absence of diabetes in the patient.
 2294 Following the usual protocol for Real World Datasets, the inlier group will be represented by healthy patients
 2295 while the ones affected by diabetes will be placed in the outlier group.

- 2296 • Moodify: Moodify is a recommendation app ⁹ that classifies Spotify songs according to the emotions transmitted
 2297 to the users. The system is trained on the Moodify dataset ¹⁰ which contains features regarding the main
 2298 characteristics of about 278.000 songs and the target is a 4 levels categorical variable with the following coding:
 2299 (1) *Sad*
 2300 (2) *Happy*
 2301 (3) *Energetic*
 2302 (4) *Calm*

2303 The label with the lowest frequency (15%) in the dataset is *Calm* so that was used to create the outliers group
 2304 while the inlier group is formed by the songs that belong to the other three classes.

2305 The dataset is composed of 11 numerical features describing different musical attributes of a song. Except for
 2306 the Loudness variable, which expresses the overall loudness of the track in decibels (dB), all the features have
 2307 values contained in the [0,1] interval. The variable names are the following: Acousticness, Danceability, Energy,
 2308 Instrumentalness, Liveness, Loudness, Speechiness, Valence, and Tempo. Other variables are Duration (ms) and
 2309 spec-rate.

2310 **A.1.3 Draw-backs of Isolation Forest.** Next, we delve deeper into the artifacts of the IF and how the EIF is able to
 2311 avoid them. The primary distinction among the mentioned models lies in their approach to determining splitting
 2312 hyperplanes. In the case of the IF, it operates under the constraint of splitting the feature space along a single dimension.
 2313 Consequently, the constructed splitting hyperplane is invariably orthogonal to one dimension while remaining parallel
 2314 to the others.

2315 The EIF model instead relaxes this constraint, it allows multiple splits in the feature space along different dimensions,
 2316 thus the splitting hyperplane can be oriented differently in each isolation tree. This relaxation helps to provide a more
 2317 expressive way to capture complex data distributions while maintaining performances. Moreover, as Hariri et al. pointed
 2318 out in [15], the EIF avoids the creation of regions where the anomaly score is lower only due to the imposed constraints.
 2319 In Figure 24 we can observe that the effect of the constraint is twofold: (i) it generates bundles in the hyperplanes
 2320 orthogonal to the main directions, and (ii) it creates "artifacts", i.e. low anomaly score zones in their intersections, as we
 2321 can observe in the Scoremap 24a.

2322 As we progressively relax the IF constraint on splitting directions, these artifacts tend to disappear. We simulated the
 2323 evolution of the anomaly score surface by allowing the hyperplane to split along a new feature in each step. Figure
 2324 vividly demonstrates the gradual elimination of artifact-prone regions.

2325
 2326
 2327
 2328
 2329
 2330
 2331
 2332
 2333
 2334
 2335
 2336
 2337
 2338 ⁹More details on the Moodify project can be found at: <https://github.com/orzana1/Moodify>

2339 ¹⁰<https://www.kaggle.com/datasets/abdullahorzan/moodify-dataset>

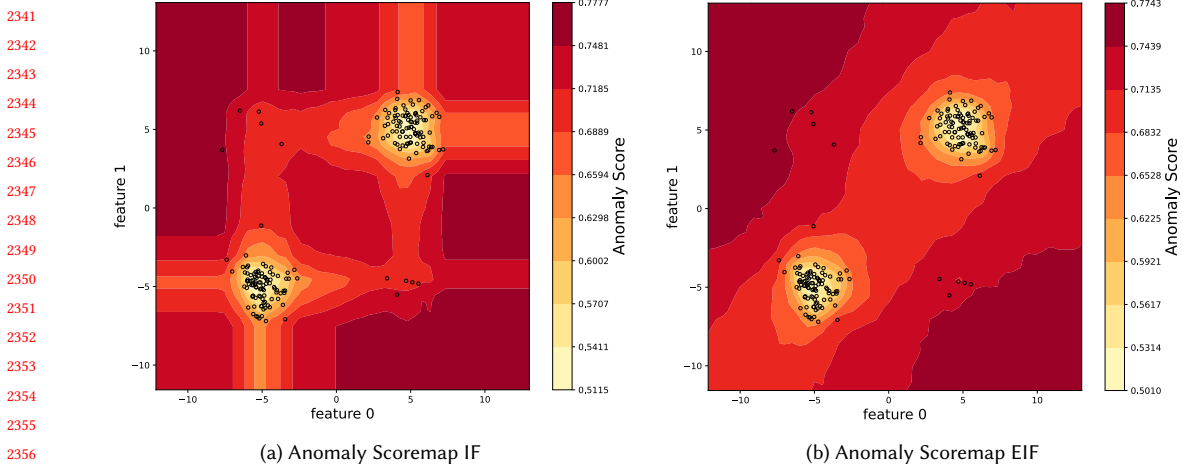


Fig. 24. Scoremap showing the differences between IF and EIF in the two dimensional space dataset Bimodal described in Section 5.3.1. Figure inspired from [15].

A.2 Non Depth-Based importance

In general, it is accurate to assert that the amount of feature importance attributed by a particular node k to a given sample x , provided that the node effectively separates the samples, should be greater if the node is closer to the root of the tree, and the importance score should decrease as the node becomes deeper within the tree. This principle is derived from the same concept used to determine anomaly scores, which are higher for samples that on average are in leafs closer to the root of the tree.

Two distinct approaches exist for assigning importance scores to nodes the one used in the ExIFFI algorithm and the one of which is proposed by the DIFFI algorithm. The DIFFI algorithm importance scores are assigned to nodes based on a weighting scheme that inversely relates the score to the depth of the node. This approach is parameterized to ensure that scores decrease as nodes become deeper within the tree.

The ExIFFI algorithm is an alternative approach for assigning importance scores to nodes in a decision tree, which differs from the DIFFI algorithm by not using the inverse of the depth to decrease the score as the node becomes deeper in the tree. This stems from the fact that the maximum acceptable score for a node is directly linked to the number of elements it must partition. As the depth of the node increases, this number inevitably decreases. Therefore, we assert that it is redundant and potentially misleading to incorporate an additional parameter to weigh the importance score.

The underlying idea is that as the node becomes deeper in the tree, it is responsible for splitting fewer and fewer elements, and therefore, it should not be penalized by reducing its importance score because the structure of the algorithm itself decreases the importance on average after every step deeper in the tree. In contrast, a node that splits many elements closer to the root of the tree may be more important because it has a greater impact on the separation of the data, but its importance should not be guaranteed by an external factor.

The EXIFFI algorithm adjusts the maximum score acceptable for a node based on the number of elements it needs to split, which allows for a fair comparison of the importance of nodes across different depths in the tree. This approach can help to avoid overestimating the importance of nodes that are close to the root and underestimating the importance of nodes that are deeper in the tree, risk that the DIFFI algorithm does not take into account.

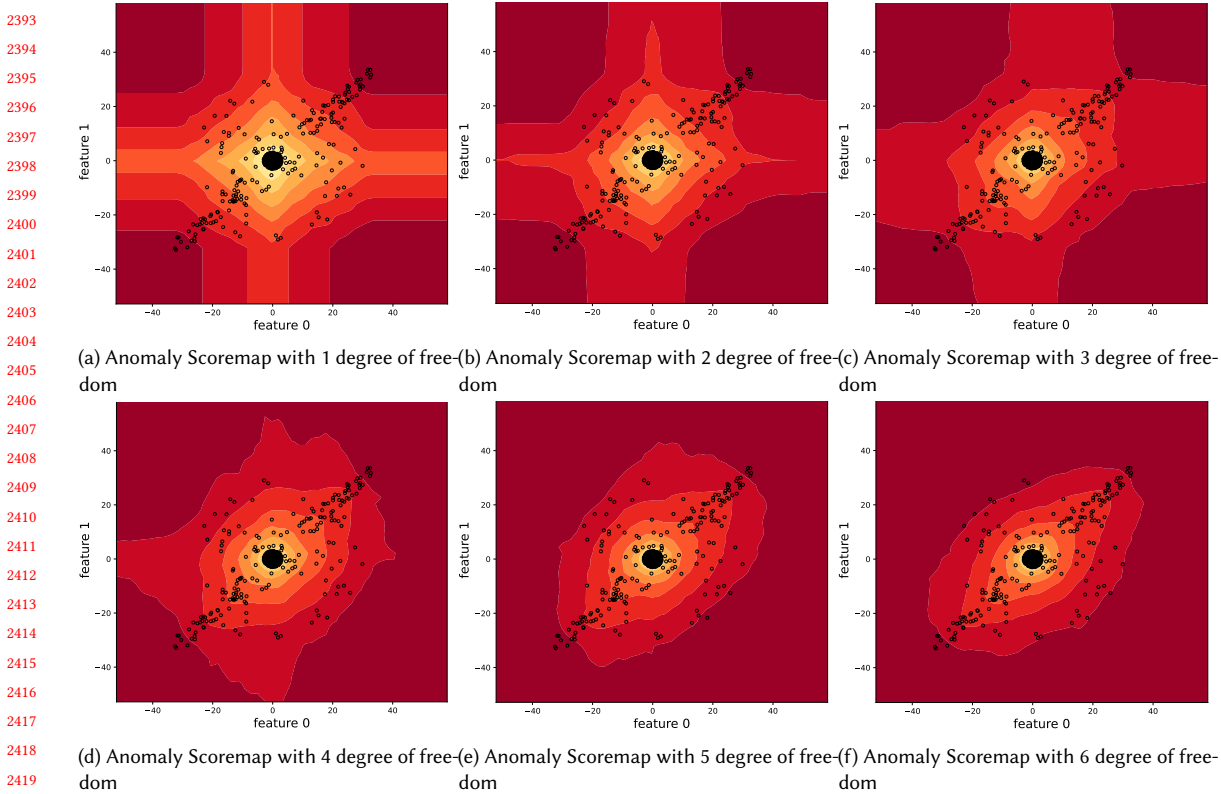


Fig. 25. Scoremap resulting from adding one degree of freedom per time while searching for splitting hyperplanes. In this way we move from the classic IF 25a to the EIF 25f. The experiment is performed on the six dimensional space dataset Bisect described in Section 5.3.1.

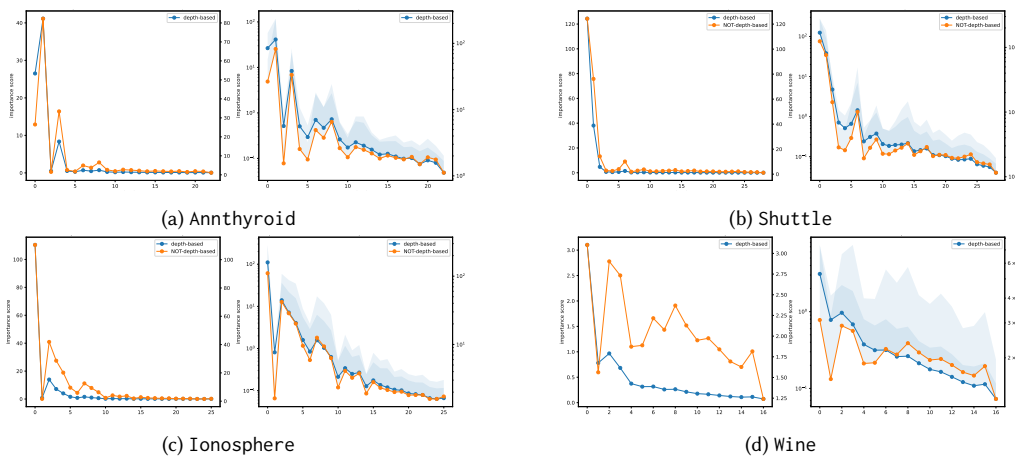


Fig. 26. Analysis of the average scores of the nodes related to their depth.

We conducted an analysis of the ExIFFI algorithm with and without the depth parameter, in order to identify differences in the evolution of the score at different depths of the trees. To achieve this, we plotted the average score of the nodes at various levels of depth in the forests, as shown in Figure 26.

The results of this analysis indicate that the score generally decreases without the use of a depth parameter. Although the ExIFFI algorithm without the depth parameter produced higher scores, the overall shape of the graph is still descending as nodes are evaluated deeper in the tree. This suggests that the ExIFFI algorithm is effective in assigning importance scores to nodes, even when the depth parameter is not utilized.

In summary, our analysis suggests that the ExIFFI algorithm is a robust method for assigning importance scores to nodes in decision trees, with or without the use of a depth parameter.

A.3 Complete Local Scoremaps

A useful instrument for the selection of the best pair of features to include in the Local Scoremap is represented by the so-called Complete Local Scoremap.

In scenarios in which a comprehensive analysis is sought, a more exhaustive study would involve the inspection of Local Importance Scoremaps covering all conceivable pairs of features. By systematically aggregating the acquired scoremaps into a composite "matrix of plots" a lucid comprehension of the hierarchy among the most and least influential features can be derived.

Furthermore, this additional graphical instrument allows for conducting a profound and detailed graphical analysis of the dataset and its features in order to achieve a qualitative comprehension of the model's output other than just considering the mere Feature importance scores.

For sake of readability, only the Complete Local Scoremap of the Diabetes dataset is presented here (Figure 27). The Complete Scoremaps of the remaining datasets are contained in the GitHub Repository of this study¹¹.

A.4 Synthetic Experiments

Yaxis

Prior to the analysis of the experiment results on the Yaxis dataset it is worth noticing how this dataset was produced with the same process used to obtain the Xaxis dataset with the only difference that anomalies were distributed along Feature 1 instead of Feature 0. As a consequence the outcomes of the experiments are expected to be very similar, if not coincident, with the ones obtained on Xaxis and described in 6.1 except for the Importance plots, that will be illustrated in A.4.2, where the most relevant feature is expected to be Feature 1, instead of Feature 0.

A.4.1 Performance. Similarly to what was observed for the Xaxis dataset in Figure 28a it is possible to notice how EIF and EIF⁺ obtain a perfect Average Precision score of 1 for almost all the contamination values considered and their performances are corresponding as depicted in Figure 28b. Additionally the IF model struggles to detect anomalies in a dataset were the drawbacks of the Isolation Forest model are exposed and the deep learning based approaches considered (i.e. DIF and Autoencoder) are able to achieve similar performances to EIF and EIF⁺ only for minimal values of the contamination level.

A Performance Report of the various AD models explored in this study is reported in Table 16 highlighting the difference between Scenario I and Scenario II. The results are very close to the ones presented in 6.1 with EIF and EIF⁺ being clearly the optimal models both in terms of evaluation metrics and time efficiency.

¹¹The GitHub Repository can be found at: <https://github.com/alessioarcudi/ExIFFI>

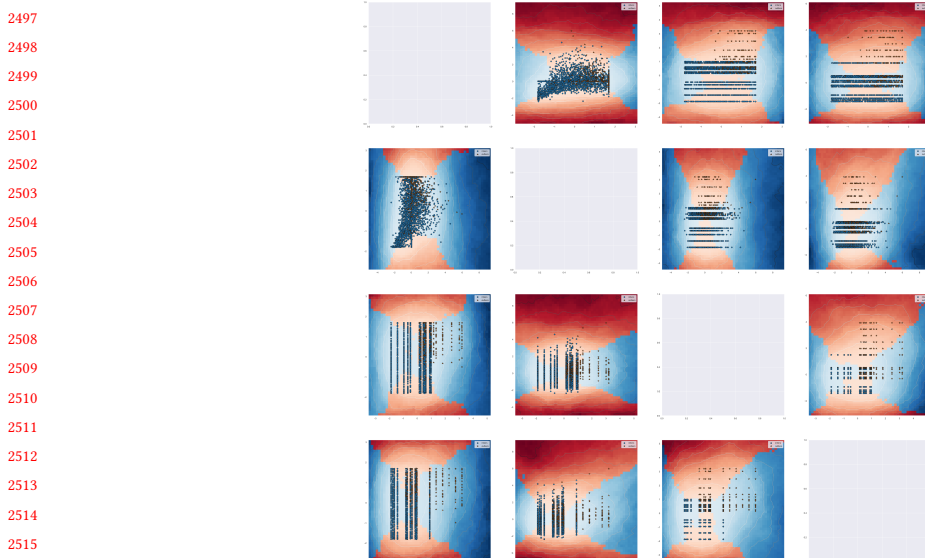
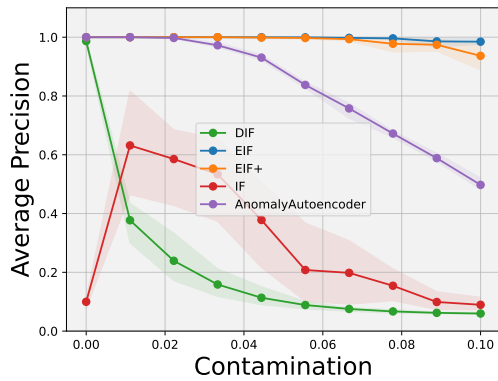


Fig. 27. Complete Local Scoremap for the Diabetes dataset



(a) Models evaluation, varying the contamination levels

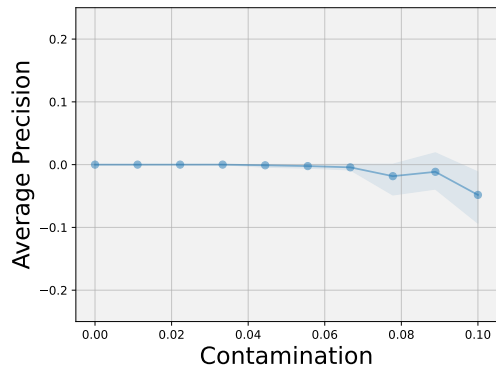
(b) Difference between EIF⁺ and EIF average precision

Fig. 28. Figure 28a illustrates the average precision as the contamination level in the training set increases. Figure 28b compares the performance graphs of EIF and EIF⁺, using the difference of their scores in various contamination levels.

A.4.2 Importance Plots. An evaluation of the proposed interpretation model ExIFFI + is presented in Figure 29. As expected the results are symmetrical to the ones obtained in Xaxis with Feature 1 being the most relevant feature in both Scenario I and II and the dominance of this variable can also be observed in the Local Scoremaps depicted in Figures 29c and 29f.

A.4.3 Feature Selection. Also in the Feature Selection Plots, portrayed in Figure 30, a clear resemblance with the plots displayed in Figure 5 can be observed. Also for Yaxis the newly introduced ad-hoc interpretability methods ExIFFI and

Table 16. Yaxis Precision Report

| AD Model | Scenario I | | | | Scenario II | | | | Time | |
|-------------|-------------|-------------|-------------|-------------|-------------|-------------|-------------|-------------|-------------|--------------|
| | Avg Prec | Prec | Rec | ROC AUC | Avg Prec | Prec | Rec | ROC AUC | fit | pred |
| IF | 0.1 | 0.07 | 0.07 | 0.48 | 0.12 | 0.1 | 0.1 | 0.5 | 0.06 | 0.006 |
| EIF | 0.97 | 0.85 | 0.85 | 0.91 | 0.99 | 1.0 | 1.0 | 1.0 | 0.05 | 0.07 |
| EIF+ | 0.94 | 0.9 | 0.9 | 0.94 | 0.99 | 0.99 | 0.99 | 0.99 | 0.05 | 0.07 |
| DIF | 0.05 | 0.01 | 0.01 | 0.45 | 0.99 | 0.97 | 0.97 | 0.98 | 1.65 | 1.33 |
| AutoEncoder | 0.54 | 0.49 | 0.49 | 0.71 | 1.0 | 1.0 | 1.0 | 1.0 | 4.07 | 0.07 |

Table 17. Performances of 5 different Anomaly Detection models over Yaxis are compared using classical Classification metrics. Moreover the last two columns contain the average time for a fit and predict operation. The highest metric values and the lowest execution times are highlighted in bold.

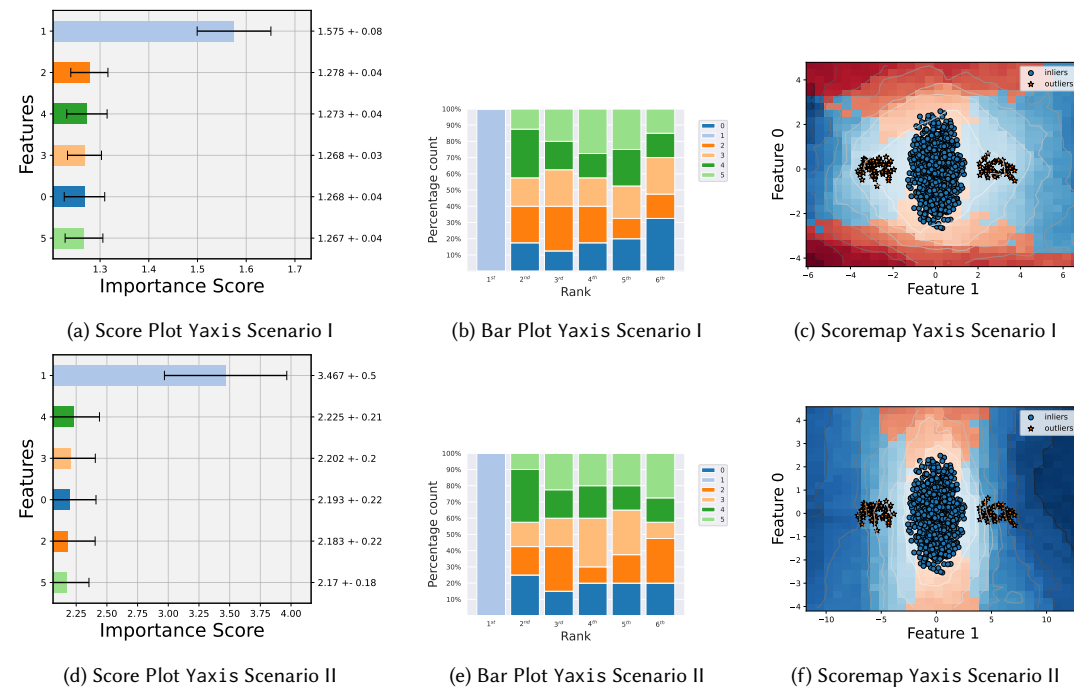


Fig. 29. Bar Plot, Score Plot and Scoremap of the dataset Yaxis in the two different Scenarios, using the ExIFFI algorithm applied to the EIF+ model.

ExIFFI + produce better looking plots than the ones produced by DIFFI and, in particular, by post-hoc interpretability methods based on the Random Forest surrogate model.

The outcomes just commented after a detailed observation of the Feature Selection plots are reflected on the AUC_{FS} values collected, for all the possible combinations of evaluation and interpretation methods, in Table 18. The best values are associated to ExIFFI and ExIFFI + models which are also the best performing ones in terms of computational efficiency.

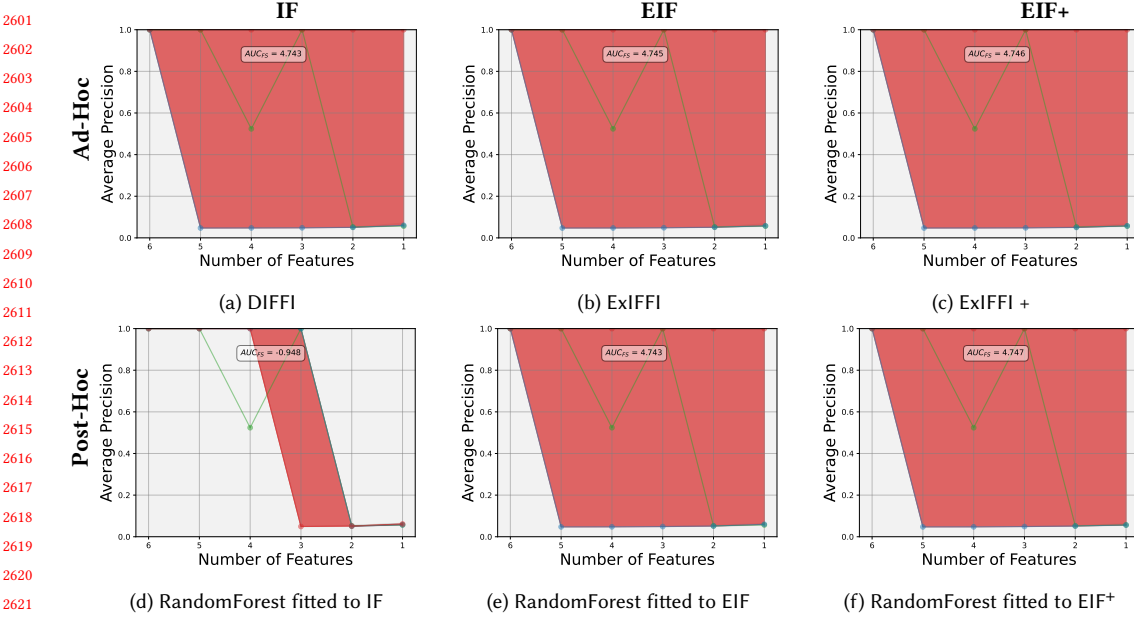


Fig. 30. Feature Selection of the different Ad-Hoc and Post-Hoc methods applied to the 3 Isolation Forest models: IF, EIF and EIF⁺. The blue line is the values of average precision, calculated with the EIF⁺ model in the Scenario II, dropping the most important feature at each step, the red line is the values of average precision dropping the least important feature at each step and the green line is the value of the feature selection dropping a random feature at each step.

Table 18. Feature Selection Scores Xaxis

| Interpretation | Evaluation with EIF | | Evaluation with EIF ⁺ | | Importance time |
|----------------|---------------------------------|----------------------------------|----------------------------------|----------------------------------|-----------------|
| | Scenario I AUC _{FS} | Scenario II AUC _{FS} | Scenario I AUC _{FS} | Scenario II AUC _{FS} | |
| DIFFI | 4.726 | 4.74 | 4.567 | 4.743 | 0.36 |
| EXIFFI | 4.723 | 4.735 | 4.508 | 4.745 | 0.16 |
| EXIFFI+ | 4.726 | 4.733 | 4.51 | 4.746 | 0.16 |
| IF_RF | -2.838 | -0.952 | -2.704 | -0.948 | 0.67 |
| EIF_RF | 4.738 | 4.729 | 4.531 | 4.743 | 0.67 |
| EIF+_RF | 4.729 | 4.741 | 4.542 | 4.747 | 0.67 |

Table 19. Quantitative evaluation of the effectiveness of 6 different interpretation algorithms on Yaxis through the AUC_{FS} metric, introduced in 5.2. In the last column the average time taken by the different models to produce the importance scores is reported. The highest AUC_{FS} and lowest Importance time values are highlighted in bold.

Bisec

A.4.4 Performance. Figure 31a reports the Average Precision of various AD models in relation to different percentages of outliers inserted in the training set and taking part to the fitting process of the models. Similarly to what can be observed in the Bisec3D dataset, described in 6.1.3, the entity of the models shows comparable results except for the DIF model where the Average Precision suffers a significant drop as outliers are progressively included as training

samples. The EIF and EIF⁺ models emerge as the ones with the highest metric values and their performances are comparable as shown in Figure 31b.

2656

2657

2658

2659

2660

2661

2662

2663

2664

2665

2666

2667

2668

2669

2670

2671

2672

2673

2674

2675

2676

2677

2678

2679

2680

2681

2682

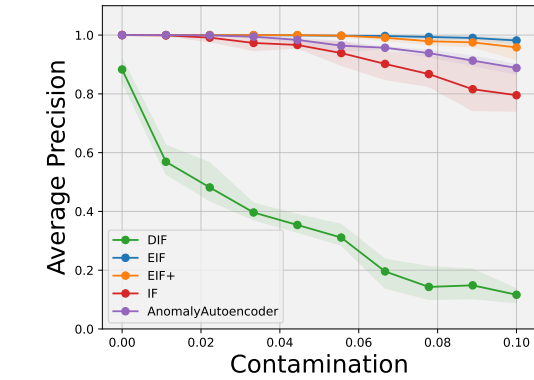
2683

2684

2685

2686

2687



(a) Models evaluation, varying the contamination levels

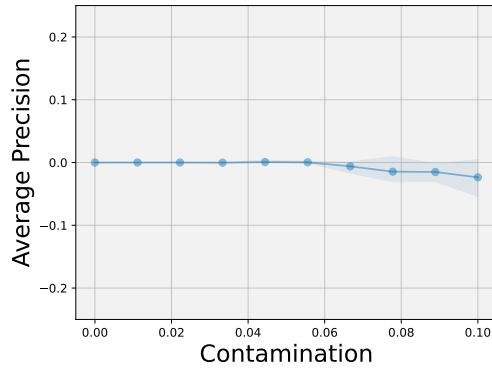
(b) Difference between EIF⁺ and EIF average precision

Fig. 31. Figure 31a illustrates the average precision as the contamination level in the training set increases. Figure 31b compares the performance graphs of EIF and EIF⁺, using the difference of their scores in various contamination levels.

Table 20 offers a more detailed overview of the performances of the Anomaly Detection models considered focusing on the comparison between Scenario I (i.e. all the outliers inserted in the training set) and Scenario II (i.e. training set composed of only inliers). After a careful analysis of the values reported on the table it is possible to conclude about the superiority of the EIF and EIF⁺ models, that achieve excellent results both in terms of precision of detecting anomalies and time efficiency.

Table 20. Performances of 5 different Anomaly Detection models over Bisec are compared using classical Classification metrics. Moreover the last two columns contain the average time for a fit and predict operation. The highest metric values and the lowest execution times are highlighted in bold

| AD Model | Scenario I | | | | Scenario II | | | | Time | |
|-------------|------------|------|------|---------|-------------|------------|------------|------------|-------------|--------------|
| | Avg Prec | Prec | Rec | ROC AUC | Avg Prec | Prec | Rec | ROC AUC | fit | pred |
| IF | 0.75 | 0.74 | 0.74 | 0.85 | 0.99 | 0.95 | 0.95 | 0.97 | 0.05 | 0.006 |
| EIF | 0.97 | 0.91 | 0.91 | 0.95 | 0.99 | 1.0 | 1.0 | 1.0 | 0.05 | 0.06 |
| EIF+ | 0.94 | 0.83 | 0.83 | 0.9 | 1.0 | 1.0 | 1.0 | 1.0 | 0.05 | 0.07 |
| DIF | 0.16 | 0.2 | 0.2 | 0.56 | 0.85 | 0.78 | 0.78 | 0.87 | 1.54 | 1.21 |
| AutoEncoder | 0.89 | 0.82 | 0.82 | 0.9 | 1.0 | 1.0 | 1.0 | 1.0 | 3.77 | 0.06 |

A.4.5 Importance Plots. The newly introduced ExIFFI + interpretation model is evaluated through the plots presented in Figure 32. As expected, considering how this synthetic dataset was constructed, it is possible to select two relevant features (i.e. Feature 0 and 1) with similar importance scores that stand out with the respect to the ones of other variables contained in the dataset, as represented in Figures 32a and 32d. The Local Scoremaps, displayed in Figures 32c and 32f, provides a better visual explanation on how the anomalies and importance scores are distributed in the feature space.

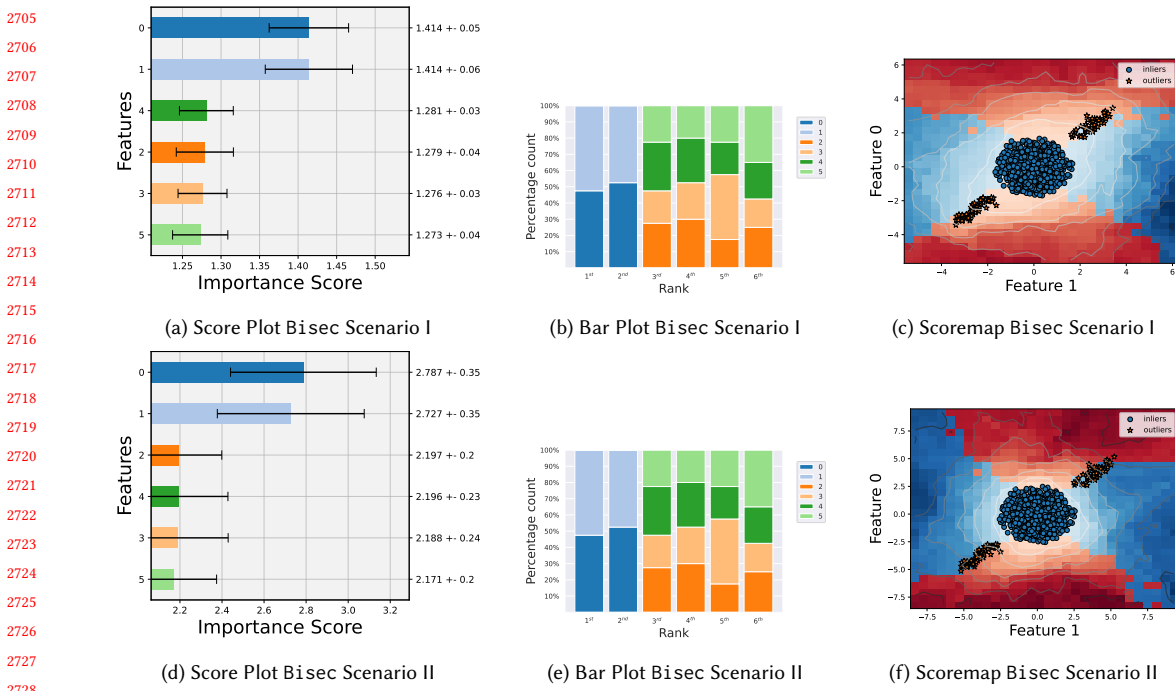


Fig. 32. Bar Plot, Score Plot and Scoremap for Bisec in the two different Scenarios, using the ExIFFI algorithm applied to the EIF⁺ model.

A.4.6 Feature Selection. The plots obtained as a result of the application of the Unsupervised Feature Selection proxy task, represented in Figure 33, present a similar behavior. For what concerns the Feature Selection approach in which at every step the least important feature is excluded (i.e. red line) the Average Precision obtains constantly a perfect score of 1. On the other hand, if attributes are removed starting from the most relevant one the precision drop significantly after both Feature 0 and Feature 1 are excluded. This outcome testifies the importance of these two feature since the performance of the model are dramatically worse once these variables are not taken into account.

Various interpretation algorithms are quantitatively compared through the usage of the AUC_{FS} metric, whose values are reported in Table 21. Because of the similarity across the plots observed in A.4.6 the values of AUC_{FS} are comparable, thus all the models are valid choices. If a selection has to be made in order to use one of the cited models in a practical application the choice would fall on the proposed ExIFFI and ExIFFI + that achieve a significant speed up in the computation of the importance scores with the respect to the other models.

A.5 Real World Experiments

Breastw

A.5.1 Performance. Figure 34a portrays the trend of the Average Precision metric as the contamination of the training set enlarges from 0 to 10 % on the different AD methods discussed in Section 5.1. It can be noticed how all the models perform more or less perfectly (i.e. with a score of 1) independently on the amount of anomalous samples seen at training time except for the DIF model that shows low precision values, around 0.6.

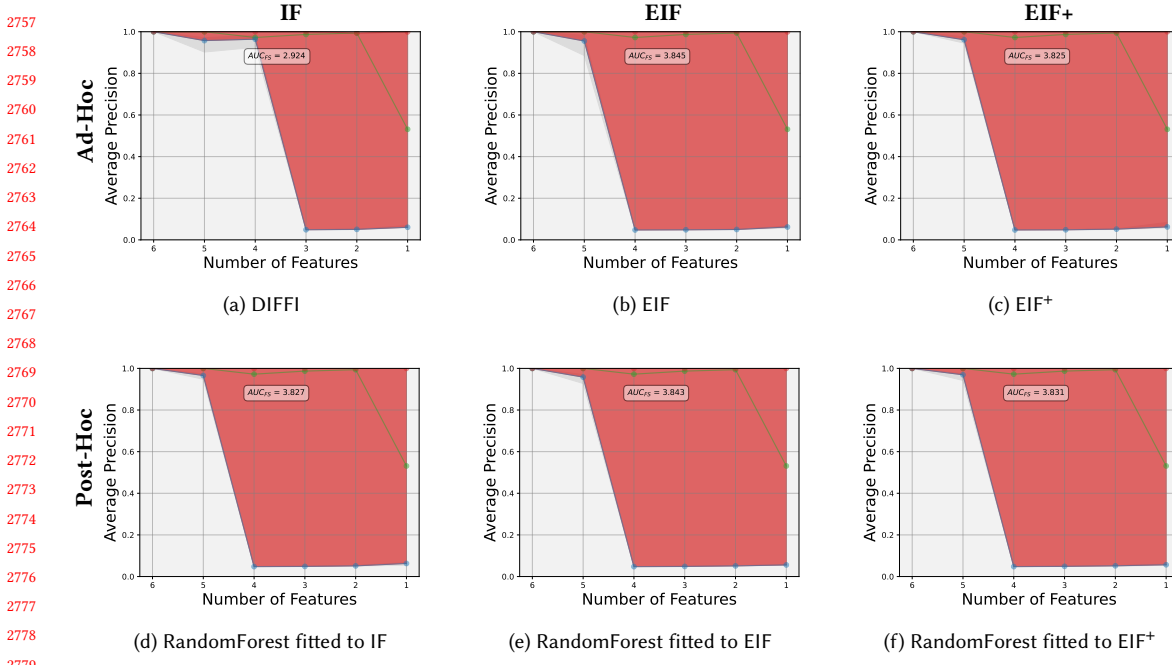


Fig. 33. Feature Selection of the different Ad-Hoc and Post-Hoc methods applied to the 3 Isolation Forest models: IF, EIF and EIF⁺. The blue line is the values of average precision, calculated with the EIF⁺ model in the Scenario II, dropping the most important feature at each step, the red line is the values of average precision dropping the least important feature at each step and the green line is the value of the feature selection dropping a random feature at each step.

Table 21. Quantitative evaluation of the effectiveness of 6 different interpretation algorithms on Biseq through the AUC_{FS} metric, introduced in 5.2. In the last column the average time taken by the different models to produce the importance scores is reported. The highest AUC_{FS} and lowest Importance time values are highlighted in bold.

| Interpretation | Evaluation with EIF | | Evaluation with EIF ⁺ | | Importance time |
|----------------|--------------------------|---------------------------|----------------------------------|---------------------------|-----------------|
| | Scenario I AUC_{FS} | Scenario II AUC_{FS} | Scenario I AUC_{FS} | Scenario II AUC_{FS} | |
| DIFFI | 4.121 | 2.925 | 4.166 | 2.924 | 0.34 |
| EXIFFI | 4.148 | 3.846 | 4.003 | 3.845 | 0.16 |
| EXIFFI+ | 4.05 | 3.832 | 3.985 | 3.825 | 0.16 |
| IF_RF | 4.072 | 3.82 | 4.05 | 3.827 | 0.66 |
| EIF_RF | 4.058 | 3.833 | 4.018 | 3.843 | 0.66 |
| EIF+_RF | 4.053 | 3.835 | 4.998 | 3.831 | 0.66 |

In Table 22 it is possible to compare in detail different typical metrics used to assess the overall performances of AD models. In particular dividing the evaluation between Scenario I and Scenario II it is possible to observe how these two training strategies may or may not affect the model's performances. With regard to the Breastw dataset one can discern that there is a clear difference between the two scenarios only for the Autoencoder model (that is in fact the only model not showing a perfectly constant trend in the Contamination Plot of Figure 34a) while the other models manifest only minor changes passing from Scenario I to Scenario II. Finally in the context of time efficiency a significant

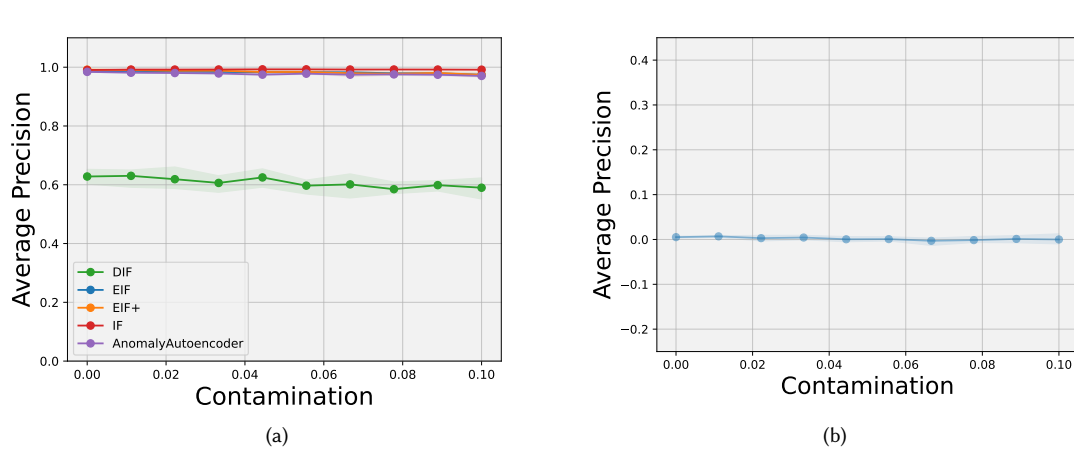


Fig. 34. Fig. 34a Represent the average precision the more the level of contamination of the train set is increased. The Fig. 34b Give show specifically the graphs of the EIF and EIF⁺

gap can be observed between isolation-based approaches (i.e. IF, EIF and EIF⁺) and AD methods based on deep learning models (i.e. DIF and Autoencoder).

Table 22. Performances of 5 different Anomaly Detection models over Breastw are compared using classical Classification metrics. Moreover, the last two columns contain the average time for a fit and predict operation. The highest metric values and the lowest execution times are highlighted in bold

| AD Model | Scenario I | | | Scenario II | | | Time | |
|------------------|-------------|------------|------------|-------------|-------------|-------------|-------------|---------------|
| | Avg Prec | Prec | ROC AUC | Avg Prec | Prec | ROC AUC | fit | pred |
| IF | 0.96 | 0.9 | 0.9 | 0.99 | 0.94 | 0.94 | 0.11 | 0.005 |
| EIF | 0.91 | 0.86 | 0.86 | 0.98 | 0.93 | 0.93 | 0.12 | 0.0007 |
| EIF ⁺ | 0.88 | 0.85 | 0.84 | 0.99 | 0.95 | 0.95 | 0.12 | 0.0006 |
| DIF | 0.44 | 0.49 | 0.46 | 0.6 | 0.66 | 0.64 | 0.74 | 0.58 |
| AutoEncoder | 0.61 | 0.44 | 0.41 | 0.98 | 0.94 | 0.93 | 2.56 | 0.05 |

A.5.2 Importance Plots. The peculiar grid-like distribution of samples within the Breastw dataset, as exhibited in the Figure 35c, possess the consequence of generating interpretation results in the Bar and Score plots not aligned with the typical outcomes described in the other real world datasets included in this study. Indeed discerning the distribution of relevance scores between different attributes is easier in Scenario I where Feature 8 clearly emerges as the crucial feature (Figure 35a while in Scenario II the latter, still considered the most prominent as shown in Figure 35d, is associated with a lower margin on the other features. Figures 35c and 35f illustrate the Local Scoremap that are not particularly effective in showing the distribution of anomalies as points easy to isolate from others because of the grid-like distribution of samples.

A.5.3 Feature Selection. The series of plots contained in Figure 36 confirms the uncertainty in distributing the importance of different features in this particular set of data. In fact for all the interpretation algorithms evaluated there is not a significant difference in applying the Unsupervised Feature Selection proxy task in increasing (red line) or decreasing

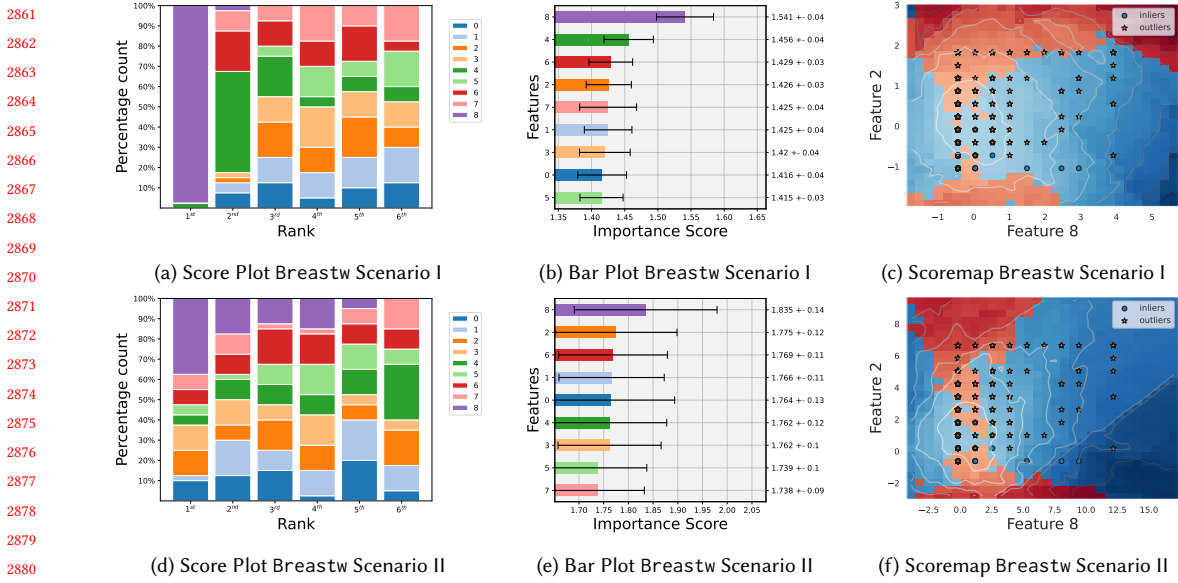


Fig. 35. Bar Plot, Score Plot and Scoremap for Breastw in the two different Scenarios, using the ExIFFI algorithm applied to the EIF⁺ model.

(blue line) order of feature relevance. Notably also the green line, representing a Feature Selection strategy in which a random feature is removed at each step, is almost overlapped to the red and blue ones meaning that there is not a single or a group of features with an importance significantly higher than the others. As a result, the quantitative measures of interpretability efficiency, represented by the AUC_{FS} metric, are all approximately equal to zero. The trend of the Average Precision metric is roughly constant at perfect scores (i.e. close to 1) until the number of features composing the input space is reduced to 3 where the Average Precision starts to decrease its magnitude. The likely implication is that while the model needs at least three features to maintain acceptable performances in detecting outliers. It is possible to conclude that the behavior depicted by plots below is very similar to the one observed for the Bisect6D synthetic dataset (Section 6.1.6), where the anomalies were distributed across all the features.

As already discussed in previous sections int the Breastw dataset the relevance is evenly shared across most of the features and consequently there it not possible to identify an interpretation method that achieves a better explanation than the others. We can indeed consider the slight differences in the AUC_{FS} values grouped in Table 23 as a result of the stochasticity inherently present in the attribution of importance scores .

Cardio

A.5.4 Performance. The plot contained in Figure 37a illustrates how the gradual addition of outliers in the training set affects the Average Precision values achieved by various AD models on the Cardio dataset. The trend is similar across all the datasets and the difference between the metrics values across the models are minor: passing from 0 to 10 % of contamination the Average Precision is associated with a decrease of about 3 percentage points. A focus on the proposed method, EIF⁺, and its counterpart, EIF, is proposed in Figure 37b and it shows how EIF⁺ starts from higher values for low contamination levels and it is overcomed by EIF as the number of anomalies included in the fitting stage

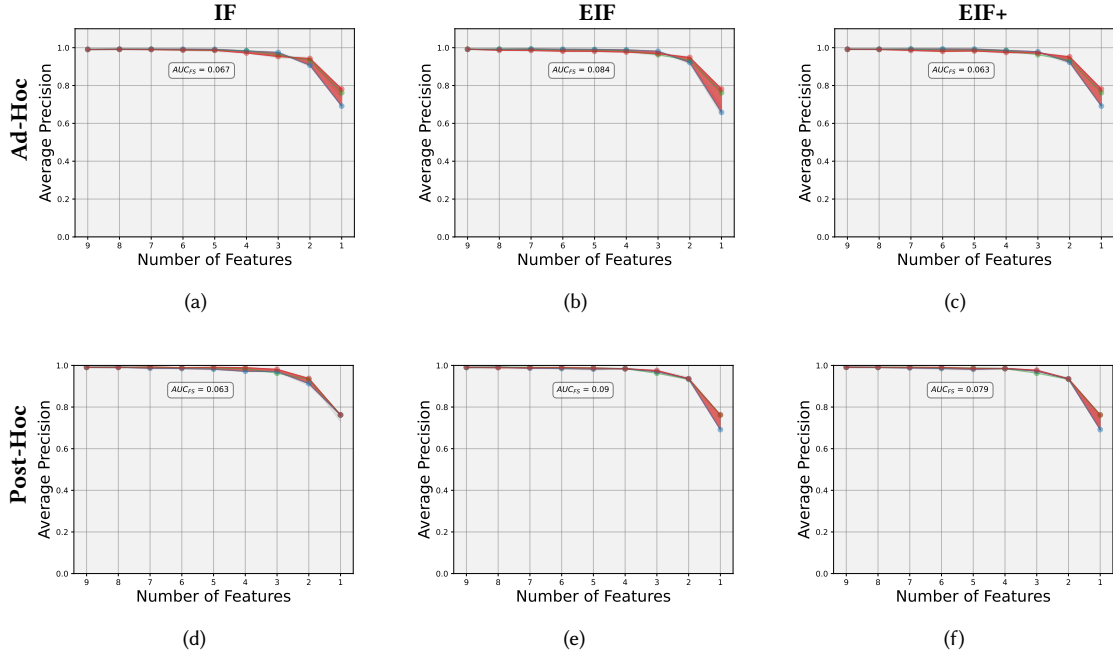


Fig. 36. Feature Selection of the different Ad-Hoc and Post-Hoc methods applied to the 3 Isolation Forest models: IF, EIF and EIF⁺. The blue line is the values of average precision, calculated with the EIF⁺ model in the Scenario II, dropping the most important feature at each step, the red line is the values of average precision dropping the least important feature at each step and the green line is the value of the feature selection dropping a random feature at each step.

Table 23. Quantitative evaluation of the effectiveness of 6 different interpretation algorithms on Breastw through the AUC_{FS} metric, introduced in 5.2. In the last column the average time taken by the different models to produce the importance scores is reported. The highest AUC_{FS} and lowest Importance time values are highlighted in bold.

| Interpretation | Evaluation with EIF | | Evaluation with EIF ⁺ | | Importance time |
|----------------|--------------------------|---------------------------|----------------------------------|---------------------------|-----------------|
| | Scenario I AUC_{FS} | Scenario II AUC_{FS} | Scenario I AUC_{FS} | Scenario II AUC_{FS} | |
| DIFFI | 0.11 | 0.064 | 0.083 | 0.067 | 0.46 |
| EXIFFI | 0.044 | 0.062 | 0.026 | 0.084 | 0.04 |
| EXIFFI+ | 0.079 | 0.027 | 0.084 | 0.063 | 0.04 |
| IF_RF | -0.148 | 0.091 | -0.142 | 0.063 | 0.19 |
| EIF_RF | -0.181 | 0.109 | -0.169 | 0.09 | 0.19 |
| EIF+_-RF | -0.164 | 0.104 | -0.145 | 0.079 | 0.19 |

raises. The following behavior with the expectations associated to the inherent structure of these two algorithms, in fact EIF⁺ is optimized in settings where there is a lack of anomalous points in the training set.

In Table 24 the AD models are evaluated through some well-known classification metrics in Scenario I and Scenario II. The decreasing trend described in Figure 37a is reflected here not only on the Average Precision metrics but also on Precision and ROC AUC score. From an overall analysis of the metrics the DIF model appears as the one with the highest values of Average Precision but at the same time it is affected by notably elevated fit and prediction times. On

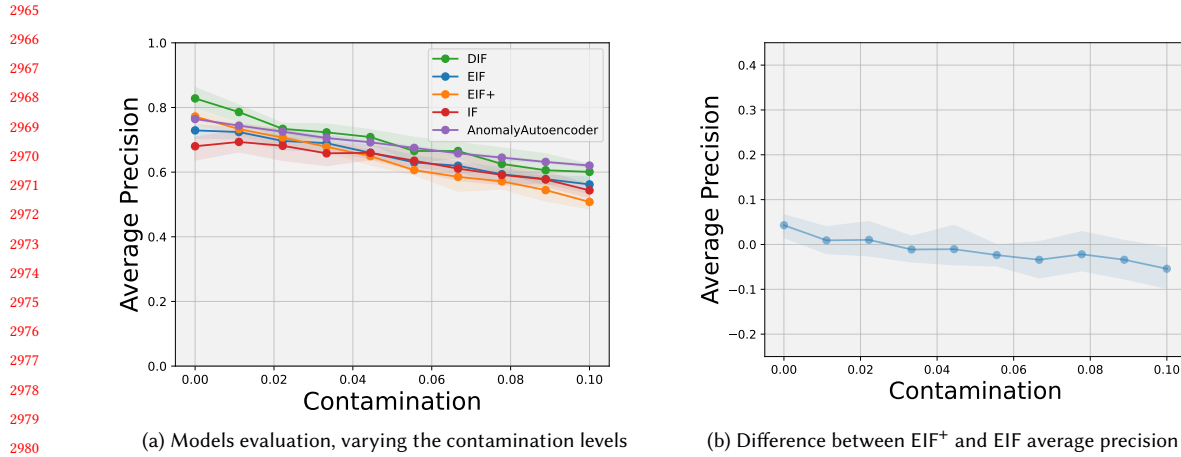


Fig. 37. Figure 37a illustrates the average precision as the contamination level in the training set increases. Figure 37b compares the performance graphs of EIF and EIF⁺, using the difference of their scores in various contamination levels.

the other acceptable metric values and execution times are showed by EIF and EIF⁺ making them more appropriate models for this task.

Table 24. Performances of 5 different Anomaly Detection models over Cardio are compared using classical Classification metrics. Moreover, the last two columns contain the average time for a fit and predict operation. The highest metric values and the lowest execution times are highlighted in bold

| AD Model | Scenario I | | | Scenario II | | | Time | |
|------------------|-------------|-------------|-------------|-------------|-------------|-------------|-------------|--------------|
| | Avg Prec | Prec | ROC AUC | Avg Prec | Prec | ROC AUC | fit | pred |
| IF | 0.53 | 0.44 | 0.69 | 0.68 | 0.6 | 0.78 | 0.12 | 0.014 |
| EIF | 0.55 | 0.59 | 0.77 | 0.74 | 0.72 | 0.84 | 0.16 | 0.001 |
| EIF ⁺ | 0.5 | 0.52 | 0.73 | 0.76 | 0.73 | 0.85 | 0.133 | 0.05 |
| DIF | 0.58 | 0.52 | 0.73 | 0.79 | 0.7 | 0.83 | 2.81 | 2.28 |
| AutoEncoder | 0.62 | 0.62 | 0.79 | 0.83 | 0.7 | 0.76 | 6.1 | 0.104 |

A.5.5 Importance Plots. Figure 38 exploits the Bar Plot, Score Plot and Local Scoremaps to compare the different explanations provided by ExIFFI + in Scenario I and Scenario II. In both training strategies Feature 6 and Feature 2 stand out as two of the most relevant features to distinguish between a normal and a pathological condition in a Cardiotogram, as explained in Appendix A.1.2. The Local Scoremaps (Figure 38c and 38f) provide a visual aid on how anomalies (represented by red stars) are indeed scattered along the directions identified by the previously cited attributes.

A.5.6 Feature Selection. The Feature Selection plots portrayed in Figure 39 represents a clear marker in support of the superiority of the proposed interpretation algorithms ExIFFI and ExIFFI +. As a matter of fact the plots related to the methods just mentioned, contained in Figure 39b and 39c, present a symmetric shape. This is the ideal shape we expected to achieve when this kind of plot for the performance evaluation and comparison of interpretation models was firstly designed. In fact, this shape proves the fact that the model was able to correctly rank all the features according to its importance scores. This happens because as features are removed in increasing order of relevance (red line) the

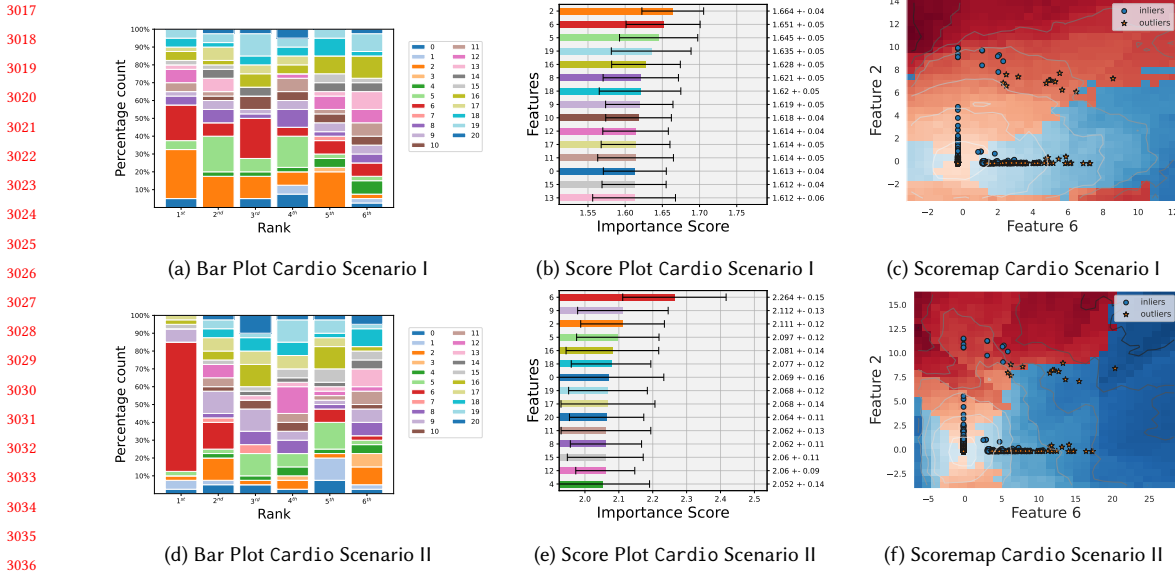


Fig. 38. Bar Plot, Score Plot and Scoremap for Cardio in the two different Scenarios, using the ExIFFI algorithm applied to the EIF⁺ model.

Average Precision displays a constantly increasing trend while a constantly decreasing trend can be observed as the most important attributes are progressively excluded from the feature space.

The direct consequence of the optimal behavior of ExIFFI and ExIFFI + is certified in Table 25 where these two models display the highest AUC_{FS} values, whether they are evaluated with EIF or EIF⁺. The metric values obtained by DIFFI and post-hoc interpretation based on Random Forest are instead inferior because, as it can be observed in Figures , the increasing trend of the red line is not perfectly mirrored by the blue one that displays a oscillating behavior. To conclude, another point in favour to the proposed approaches is the time taken to obtain the importance scores which is substantially reduced with respect to the ones of the other models considered.

Table 25. Quantitative evaluation of the effectiveness of 6 different interpretation algorithms on Cardio through the AUC_{FS} metric, introduced in 5.2. In the last column the average time taken by the different models to produce the importance scores is reported. The highest AUC_{FS} and lowest Importance time values are highlighted in bold.

| Interpretation | Evaluation with EIF | | Evaluation with EIF ⁺ | | Importance time |
|----------------|--------------------------|---------------------------|----------------------------------|---------------------------|-----------------|
| | Scenario I AUC_{FS} | Scenario II AUC_{FS} | Scenario I AUC_{FS} | Scenario II AUC_{FS} | |
| DIFFI | 4.653 | 4.768 | 4.398 | 4.333 | 0.57 |
| EXIFFI | 5.417 | 8.286 | 5.122 | 8.381 | 0.34 |
| EXIFFI+ | 4.421 | 8.609 | 4.252 | 8.73 | 0.3 |
| IF_RF | 1.483 | 7.696 | 1.282 | 7.889 | 1.8 |
| EIF_RF | 1.358 | 7.781 | 1.353 | 7.855 | 1.8 |
| EIF+_RF | 0.32 | 8.241 | 0.36 | 8.302 | 1.8 |

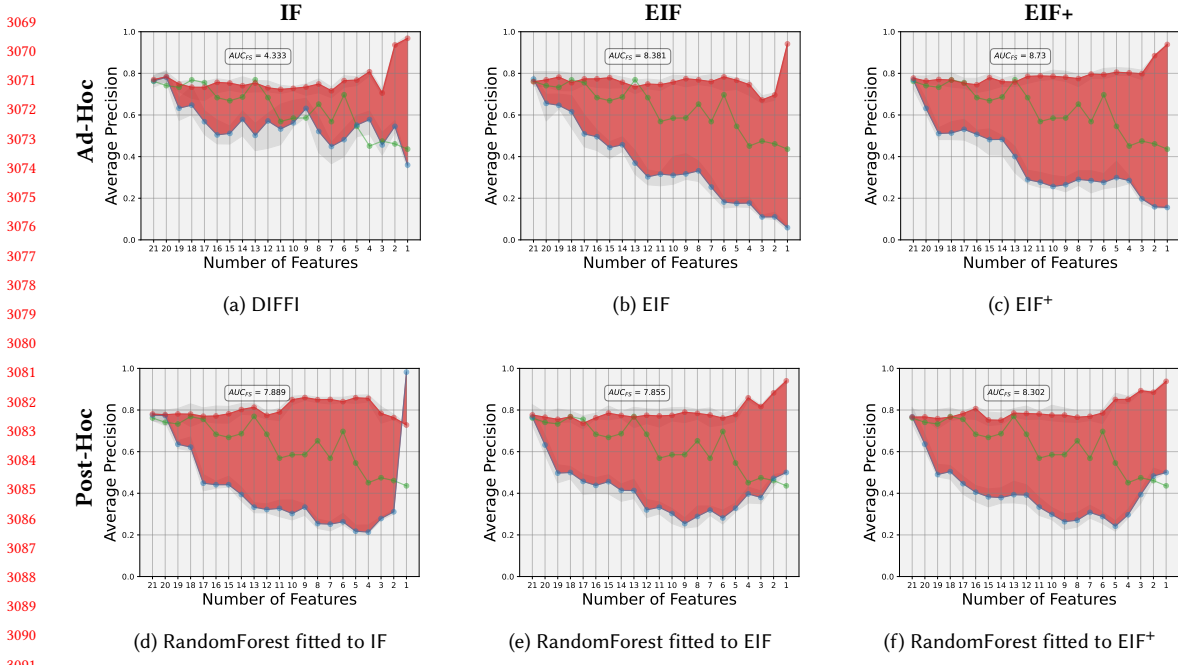
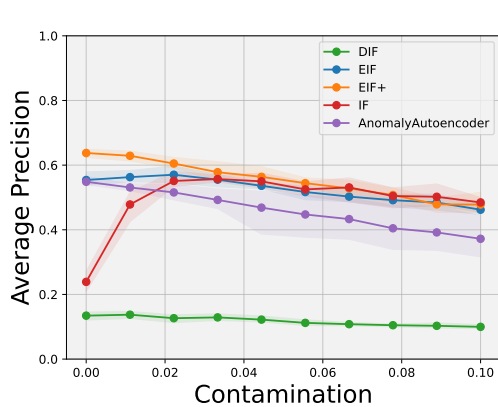


Fig. 39. Feature Selection of the different Ad-Hoc and Post-Hoc methods applied to the 3 Isolation Forest models: IF, EIF and EIF⁺. The blue line is the values of average precision, calculated with the EIF⁺ model in the Scenario II, dropping the most important feature at each step, the red line is the values of average precision dropping the least important feature at each step and the green line is the value of the feature selection dropping a random feature at each step.

3099 Diabetes

3100 **A.5.7 Performance.** The peculiarity of the Diabetes dataset, as described in A.1.2, in the context of this study is its
 3101 low dimensionality since its observations are fully described using just four features. As a consequence the behavior
 3102 of the AD models considered as abnormal samples are progressively included in the training set, displayed in Figure
 3103 40a, is diverse from the ones observed in other benchmark datasets. In particular the IF model possesses an unique
 3104 increasing Average Precision trend that saturates at a contamination level around 5 %. On the other hand the DIF model
 3105 showcases an essentially constant trend at substantially low Average Precision values if compared to the other methods.
 3106 An explanation of the underperformance of this model could be the presence of overfitting because of the usage of an
 3107 highly complex approach from a simple task as the ones of separating anomalous points from normal ones on a four
 3108 dimensional feature space. Finally, the proposed EIF⁺ model stands out as the reference model in this study, immediately
 3109 followed by EIF as highlighted in Figure 40b.

3110 Table 26 portrays the difference, in terms of the Average Precision, Precision and AUC ROC score metrics, in the two
 3111 approaches used to train, and successively test, the presented Anomaly Detection approaches: Scenario I and Scenario
 3112 II. As already made clear in Figure 40a there are some visible differences in the model performances as anomalies are
 3113 included in the training process (i.e. in the passage from Scenario II to Scenario I). The most optimal model is the
 3114 proposed EIF⁺ due to its superior metric values and its unparalleled efficiency in both the fitting and prediction stages.



(a) Models evaluation, varying the contamination levels

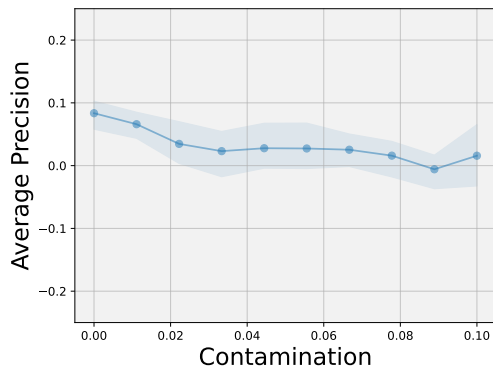
(b) Difference between EIF⁺ and EIF average precision

Fig. 40. Figure 40a illustrates the average precision as the contamination level in the training set increases. Figure 40b compares the performance graphs of EIF and EIF⁺, using the difference of their scores in various contamination levels.

Table 26. Performances of 5 different Anomaly Detection models over Diabetes are compared using classical Classification metrics. Moreover, the last two columns contain the average time for a fit and predict operation. The highest metric values and the lowest execution times are highlighted in bold

| AD Model | Scenario I | | | Scenario II | | | Time | |
|-------------|-------------|-------------|-------------|-------------|-------------|-------------|------------|--------------|
| | Avg Prec | Prec | ROC AUC | Avg Prec | Prec | ROC AUC | fit | pred |
| IF | 0.46 | 0.46 | 0.7 | 0.26 | 0.31 | 0.62 | 0.13 | 0.069 |
| EIF | 0.47 | 0.48 | 0.71 | 0.55 | 0.61 | 0.78 | 0.1 | 0.008 |
| EIF+ | 0.44 | 0.49 | 0.72 | 0.61 | 0.56 | 0.76 | 0.1 | 0.008 |
| DIF | 0.1 | 0.90 | 0.49 | 0.13 | 0.17 | 0.54 | 10.2 | 9.05 |
| AutoEncoder | 0.45 | 0.47 | 0.7 | 0.5 | 0.52 | 0.73 | 17.82 | 0.28 |

A.5.8 Importance Plots. The outcomes of the explanations granted by ExIFFI + are illustrated in Figure 41. Analyzing the Score Plots, represented in Figures 41b and 41e and the Bar Plots, represented in Figures 41a and 41d, it is clear how the two most important features are *HbA1c_level* and *blood_glucose_level*. As elucidated in A.1.2 the Hemoglobin A1c Level and the amount of glucose in the bloodstream represent crucial indicators to discriminate between patients affected or not by diabetes.

A.5.9 Feature Selection. The validity of the interpretation of the EIF⁺ model provided by the ExIFFI + model is confirmed once again in the plots represented in Figure 41 where Unsupervised Feature Selection is exploited as a proxy task for the comparison of ad-hoc and post-hoc interpretation algorithms. The plot related to the ExIFFI + model is the only one associated with a shape that certifies the correctness of the model in ranking the features according to their relevance for the Anomaly Detection task. Indeed the plot placed in Figure 42c is the unique graph where the red line always contains superior Average Precision values in comparison to the blue line. Conversely in the plots referred to other interpretation methods the metrics values oscillate without providing any clear sign of whether the feature selection approach associated with the blue or red line is superior.

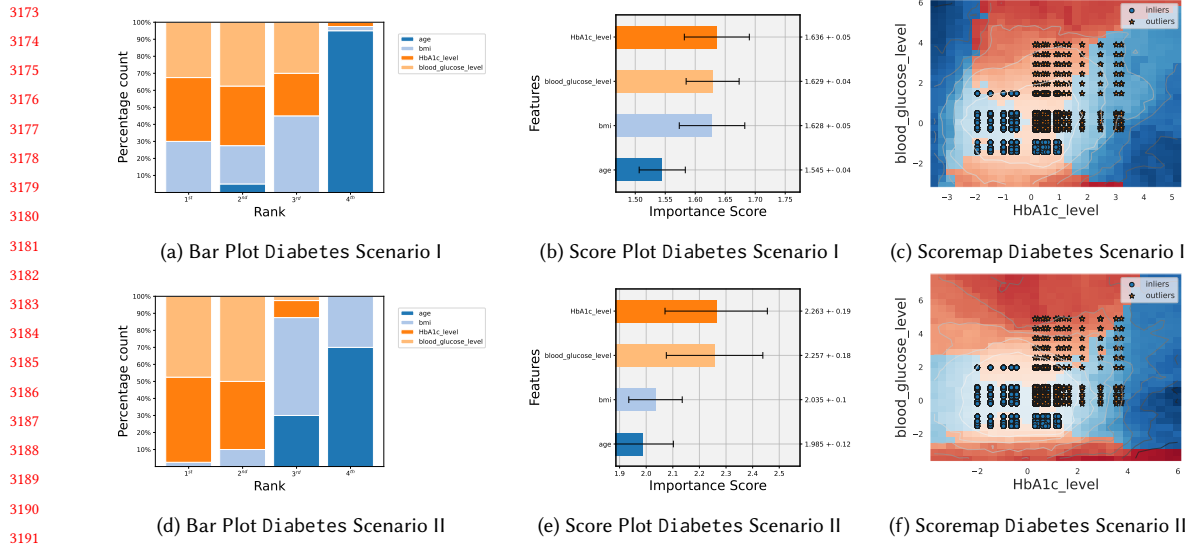


Fig. 41. Bar Plot, Score Plot and Scoremap for Diabetes in the two different Scenarios, using the ExIFFI algorithm applied to the EIF⁺ model.

In Table 27 the AUC_{FS} values, for a quantitative comparison of the effectiveness of the interpretability provided by the diverse methods analysed in this study are contained. As already observed from a careful analysis of the Feature Selection plots (Figure 42) the explanation better aligned with the ground truth is the one provided by the proposed ExIFFI + approach. On the other hand the outcomes provided by the other considered models prove to be less satisfactory, in particular the ones produced by the DIFFI interpretation algorithm which are paired with negative AUC_{FS} values, a clear prove of an erroneous ranking of attributes' relevance.

Table 27. Quantitative evaluation of the effectiveness of 6 different interpretation algorithms on Diabetes through the AUC_{FS} metric, introduced in 5.2. In the last column the average time taken by the different models to produce the importance scores is reported. The highest AUC_{FS} and lowest Importance time values are highlighted in bold.

| Interpretation | Evaluation with EIF | | Evaluation with EIF ⁺ | | Importance time |
|----------------|--------------------------|---------------------------|----------------------------------|---------------------------|-----------------|
| | Scenario I AUC_{FS} | Scenario II AUC_{FS} | Scenario I AUC_{FS} | Scenario II AUC_{FS} | |
| DIFFI | -0.363 | -1.455 | -0.345 | -1.481 | 0.63 |
| EXIFFI | 0.967 | 0.354 | 0.826 | 0.313 | 0.50 |
| EXIFFI+ | 1.058 | 0.822 | 0.747 | 1.171 | 0.52 |
| IF_RF | -0.303 | -0.059 | -0.302 | -0.123 | 2.04 |
| EIF_RF | 0.491 | 0.315 | 0.383 | 0.355 | 2.04 |
| EIF+_RF | 0.463 | 0.332 | 0.407 | 0.296 | 2.04 |

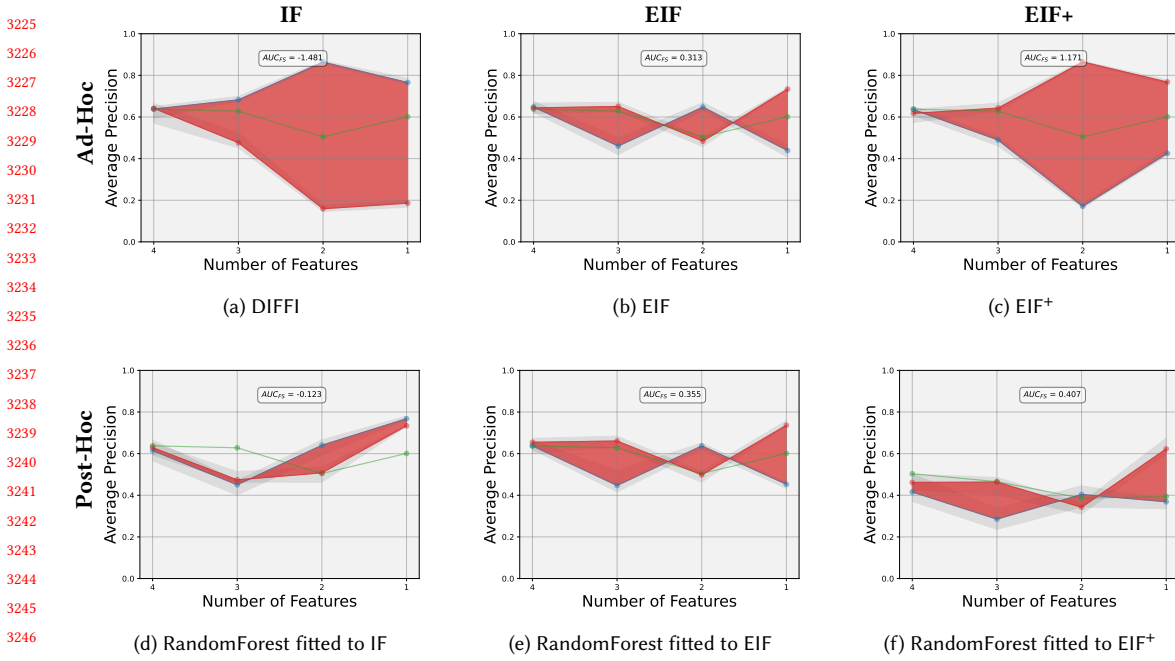


Fig. 42. Feature Selection of the different Ad-Hoc and Post-Hoc methods applied to the 3 Isolation Forest models: IF, EIF and EIF⁺. The blue line is the values of average precision, calculated with the EIF⁺ model in the Scenario II, dropping the most important feature at each step, the red line is the values of average precision dropping the least important feature at each step and the green line is the value of the feature selection dropping a random feature at each step.

Ionosphere

The Ionosphere dataset, as described in A.1.2, stands out as the dataset with the highest dimensionality (i.e. 33 features) inside the list of benchmark datasets used for the performance assessment in this study. This characteristic may have some consequences on the outcomes of the experiments described in the following sections.

A.5.10 Performance. The results of the evaluation of each Anomaly Detection model across different values of the contamination hyperparameter are portrayed in Figure 43a. The entirety of the models show how the gradual addition of anomalies in the dataset does not result in a significant effect on the Average Precision metric that, in fact, shows more or less constant values very close to a perfect score of 1. The proposed approach EIF⁺, together with the DIF model, are the ones showing the best metric values, followed by EIF, as highlighted in the comparison between EIF⁺ and EIF displayed in Figure 43b.

As a result of a careful observations of Table 28 it is possible to conclude that the optimal models for the Anomaly Detection task on the Ionosphere dataset are EIF⁺ and DIF. The performances offered by these models are in fact superior to the ones of all other methods but since EIF⁺ demonstrates significantly improved efficiency during both the fitting and prediction phases it is the best choice in this scenario.

A.5.11 Importance Plots. In Figure 44 it is possible to see how challenging the task of interpreting the relevance of the features used by an AD model can be in the case of feature spaces of high dimensionality. As it can be in fact concluded observing both the Score Plots (Figures 44b, 44e) and the Bar Plots (Figures 44a, 44d) the importance is evenly

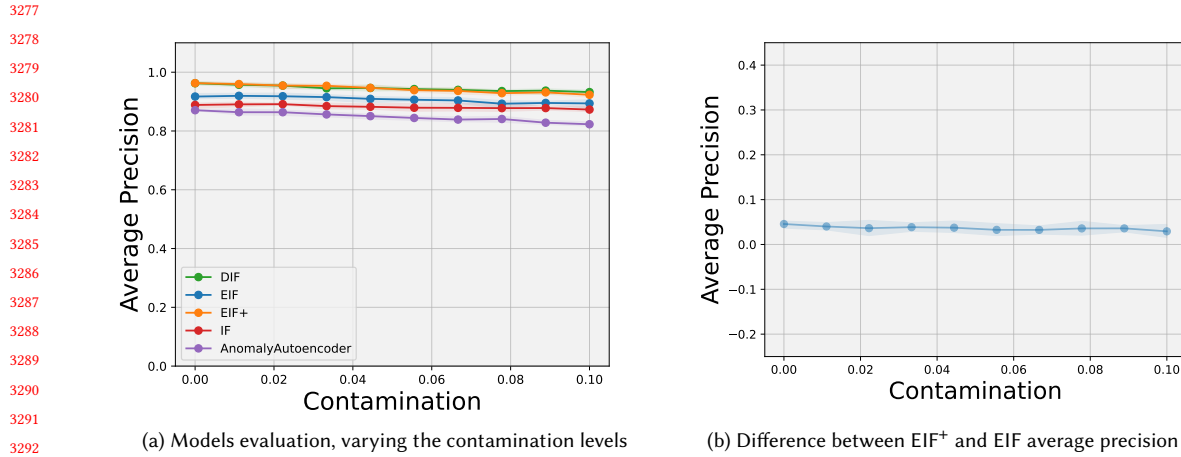


Fig. 43. Figure 43a illustrates the average precision as the contamination level in the training set increases. Figure 43b compares the performance graphs of EIF and EIF⁺, using the difference of their scores in various contamination levels.

Table 28. Performances of 5 different Anomaly Detection models over Ionosphere are compared using classical Classification metrics. Moreover, the last two columns contain the average time for a fit and predict operation. The highest metric values and the lowest execution times are highlighted in bold

| AD Model | Scenario I | | | Scenario II | | | Time | |
|------------------|-------------|-------------|-------------|-------------|-------------|------------|-------------|---------------|
| | Avg Prec | Prec | ROC AUC | Avg Prec | Prec | ROC AUC | fit | pred |
| IF | 0.79 | 0.65 | 0.73 | 0.89 | 0.79 | 0.83 | 0.05 | 0.0026 |
| EIF | 0.82 | 0.69 | 0.76 | 0.9 | 0.82 | 0.86 | 0.14 | 0.02 |
| EIF ⁺ | 0.84 | 0.72 | 0.78 | 0.96 | 0.87 | 0.9 | 0.11 | 0.02 |
| DIF | 0.87 | 0.76 | 0.81 | 0.96 | 0.89 | 0.9 | 0.72 | 0.44 |
| AutoEncoder | 0.76 | 0.6 | 0.68 | 0.87 | 0.75 | 0.8 | 2.26 | 0.09 |

shared across all features and it is daunting to find a single feature or a small subset of features whose relevance is significantly higher than the one of the remaining attributes.

A.5.12 Feature Selection. The phenomenon observable in the Feature Selection plots of the Ionosphere (Figure 42) dataset is similar to the one presented in section A.5 for the Breastw dataset. Essentially since the importance is shared across a group of features the Average Precision follows a constant trend and starts to decrease as important features are progressively removed from the group of relevant attributes.

Table 29 lists the values of the AUC_{FS} metric in Scenario I and Scenario II. The only interpretation models able to provide a feature ranking correctly aligning with the dataset's characteristics are ExIFFI + and the post-hoc Random Forest model applied to the EIF⁺ AD method. Among these two the most efficient one in terms of computational time is ExIFFI +.

Pendigits

A.5.13 Performance. Figure 46a represents the trend of the Average Precision metrics as anomalies are gradually inserted into the train process of the five Anomaly Detection models used for experimental evaluation. The models

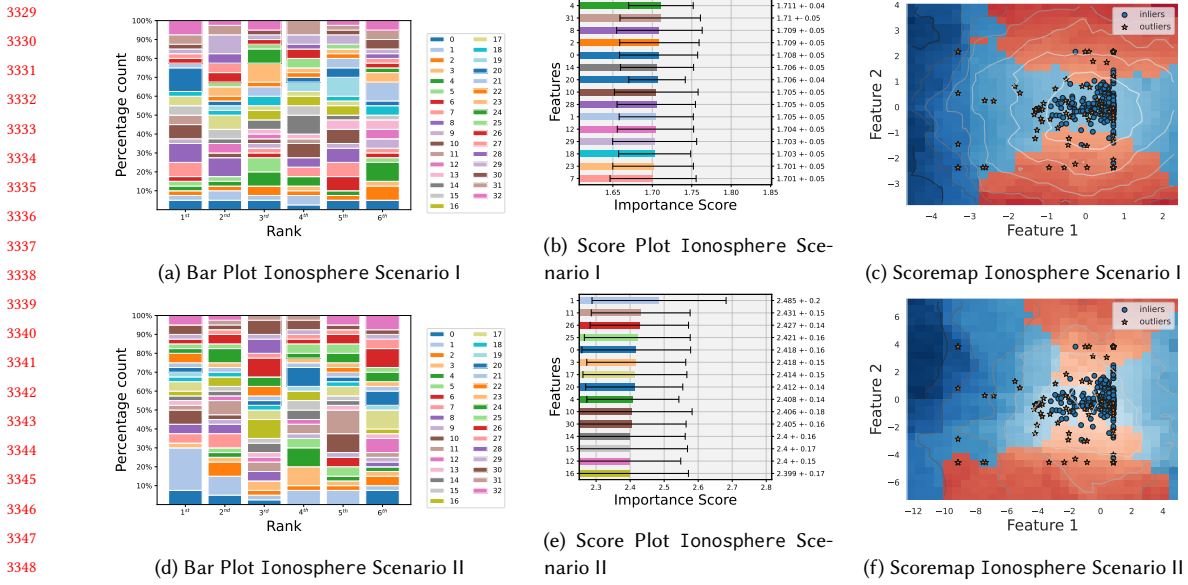


Fig. 44. Bar Plot, Score Plot and Scoremap for Ionosphere in the two different Scenarios, using the ExIFFI algorithm applied to the EIF⁺ model.

Table 29. Quantitative evaluation of the effectiveness of 6 different interpretation algorithms on Ionosphere through the AUC_{FS} metric, introduced in 5.2. In the last column the average time taken by the different models to produce the importance scores is reported. The highest AUC_{FS} and lowest Importance time values are highlighted in bold.

| Interpretation | Evaluation with EIF | | Evaluation with EIF ⁺ | | Importance time |
|----------------|--------------------------|---------------------------|----------------------------------|---------------------------|-----------------|
| | Scenario I AUC_{FS} | Scenario II AUC_{FS} | Scenario I AUC_{FS} | Scenario II AUC_{FS} | |
| DIFFI | 2.367 | -1.336 | -1.135 | 1.924 | 0.31 |
| EXIFFI | 1.828 | 4.313 | 1.615 | 2.841 | 0.16 |
| EXIFFI+ | 0.619 | 2.268 | 0.454 | 1.41 | 0.17 |
| IF_RF | -1.914 | -1.237 | 1.762 | -1.087 | 0.6 |
| EIF_RF | -1.975 | 1.337 | -1.857 | 0.695 | 0.6 |
| EIF+_RF | -1.871 | 3.586 | -1.568 | 2.171 | 0.6 |

presenting the higher precision values in presence of only inliers in the training set (i.e. Scenario II) are DIF, IF and the proposed EIF⁺, whose performances drop as the number of outliers increases and saturate to reach similar values as the other models. For what concerns the comparison between EIF and its improved version, introduced in this study, EIF⁺, depicted in Figure 46b, it is possible to notice how EIF⁺ shows better performances than EIF when the number of outliers considers for training is limited and the two models tend to become closer in terms of performances as the contamination factor increases. This behavior is a direct consequence of how the EIF⁺ approach is build to optimize the generalizability capabilities of the EIF model.

Table 30 reports a detailed evaluation of the performances of the AD models compared in the Contamination plot, focusing on the comparison between the Scenario I and Scenario II training approaches. The three models highlighted in Figure 46a (i.e. IF, DIF and EIF⁺) are the unique ones where a significant difference can be noticed switching from

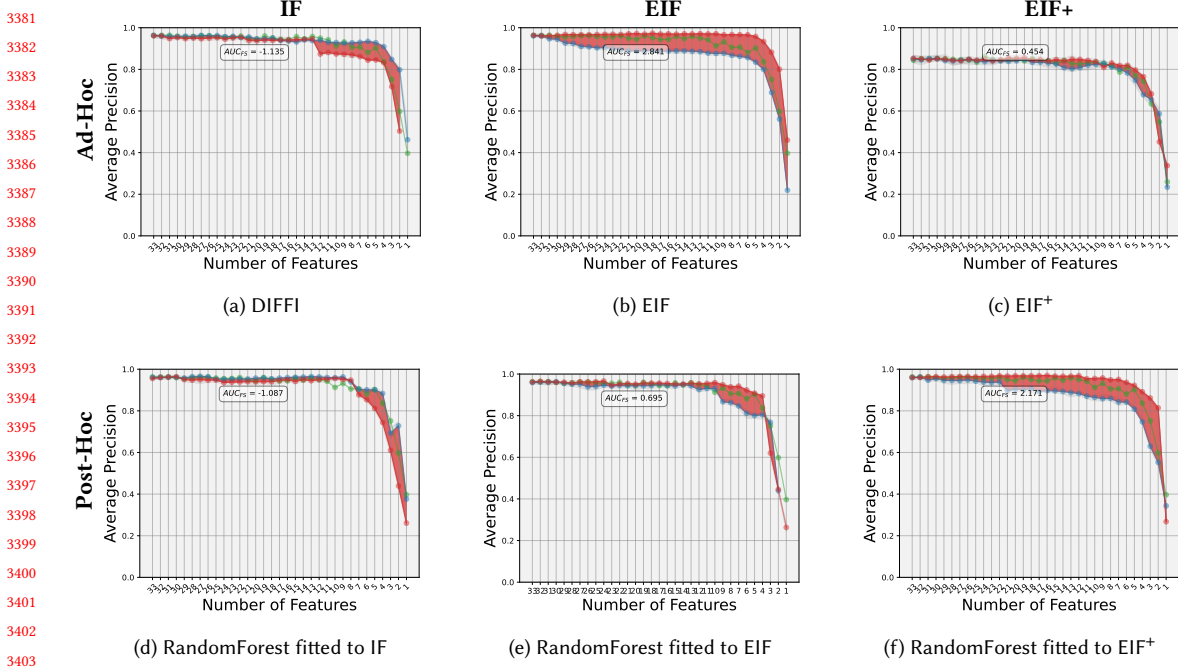


Fig. 45. Feature Selection of the different Ad-Hoc and Post-Hoc methods applied to the 3 Isolation Forest models: IF, EIF and EIF⁺. The blue line is the values of average precision, calculated with the EIF⁺ model in the Scenario II, dropping the most important feature at each step, the red line is the values of average precision dropping the least important feature at each step and the green line is the value of the feature selection dropping a random feature at each step.

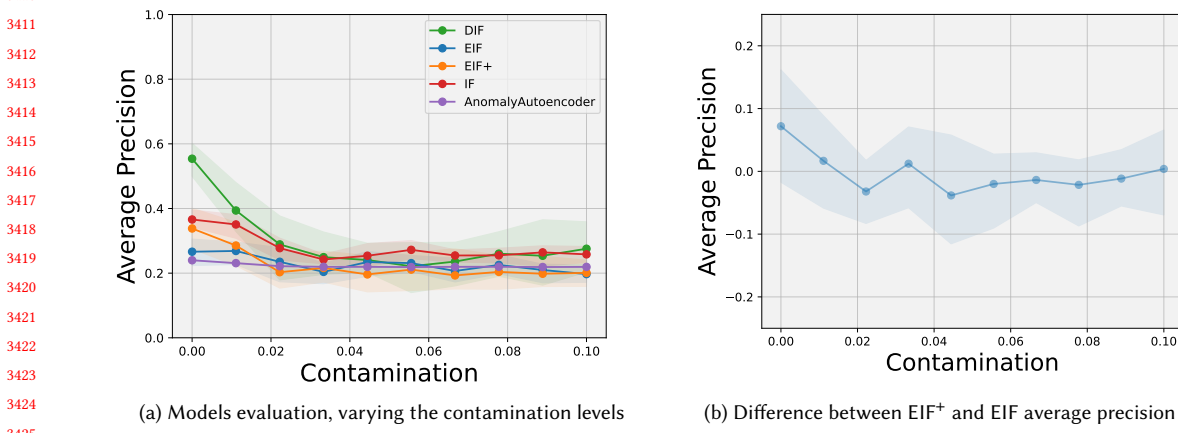


Fig. 46. Figure 46a illustrates the average precision as the contamination level in the training set increases. Figure 46b compares the performance graphs of EIF and EIF⁺, using the difference of their scores in various contamination levels.

Scenario I to Scenario II. The best model in terms of Average Precision is DIF but, at the same time, it is associated with dramatically high computational time, in terms of fit and predict, with the respect to the isolation-based AD models

Manuscript submitted to ACM

making its usage not ideal, mainly in real world applications. As a consequence EIF⁺ can be considered as the optimal choice for the Pendigits dataset.

Table 30. Performances of 5 different Anomaly Detection models over Pendigits are compared using classical Classification metrics. Moreover, the last two columns contain the average time for a fit and predict operation. The highest metric values and the lowest execution times are highlighted in bold.

| AD Model | Scenario I | | | Scenario II | | | Time | |
|-------------|-------------|-------------|-------------|-------------|-------------|-------------|-------------|-------------|
| | Avg | Prec | ROC AUC | Avg | Prec | ROC AUC | fit | pred |
| IF | 0.28 | 0.31 | 0.64 | 0.37 | 0.42 | 0.7 | 0.07 | 0.03 |
| EIF | 0.23 | 0.24 | 0.61 | 0.27 | 0.36 | 0.67 | 0.07 | 0.44 |
| EIF+ | 0.21 | 0.41 | 0.69 | 0.36 | 0.45 | 0.72 | 0.07 | 0.45 |
| DIF | 0.34 | 0.39 | 0.68 | 0.46 | 0.53 | 0.76 | 10.2 | 8.36 |
| AutoEncoder | 0.22 | 0.33 | 0.65 | 0.24 | 0.33 | 0.66 | 19.0 | 0.32 |

A.5.14 Importance Plots. Similarly to what can be observed in the Ionosphere dataset, Figure 47 portraits how it is challenging to identify a single dominant feature in terms of importance. As a consequence it can be concluded the probably there is a small group of features along which anomalies are distributed. Observing the Score Plots (Figures 47b, 47e) and the Bar Plots (Figures 47a, 47d) it can be noticed how Features 1, 3 and 5 may be included in this group of relevant attributes since they appear in the top 3 ranking in both Scenario I and Scenario II.

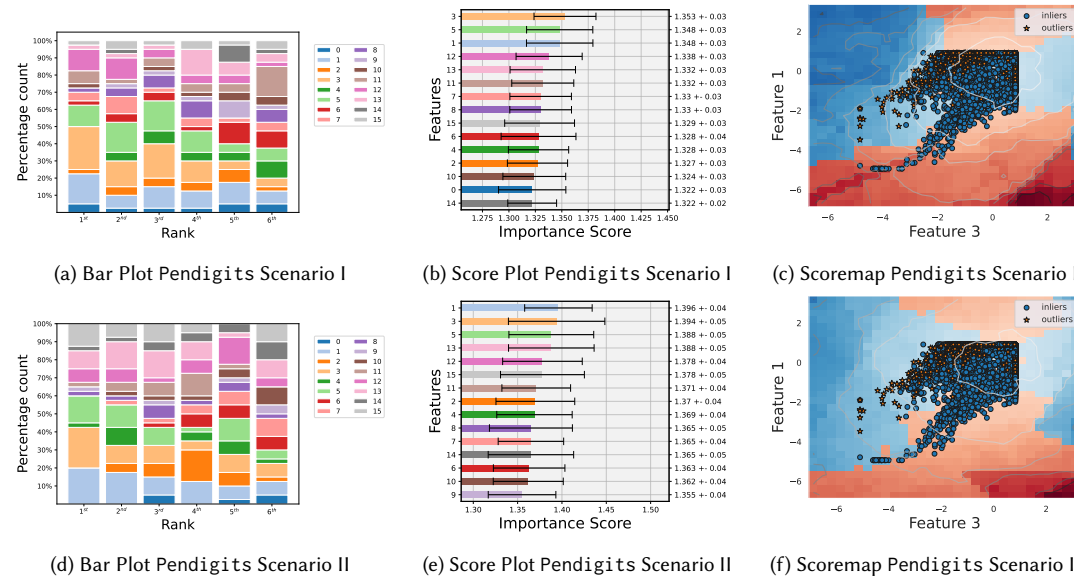
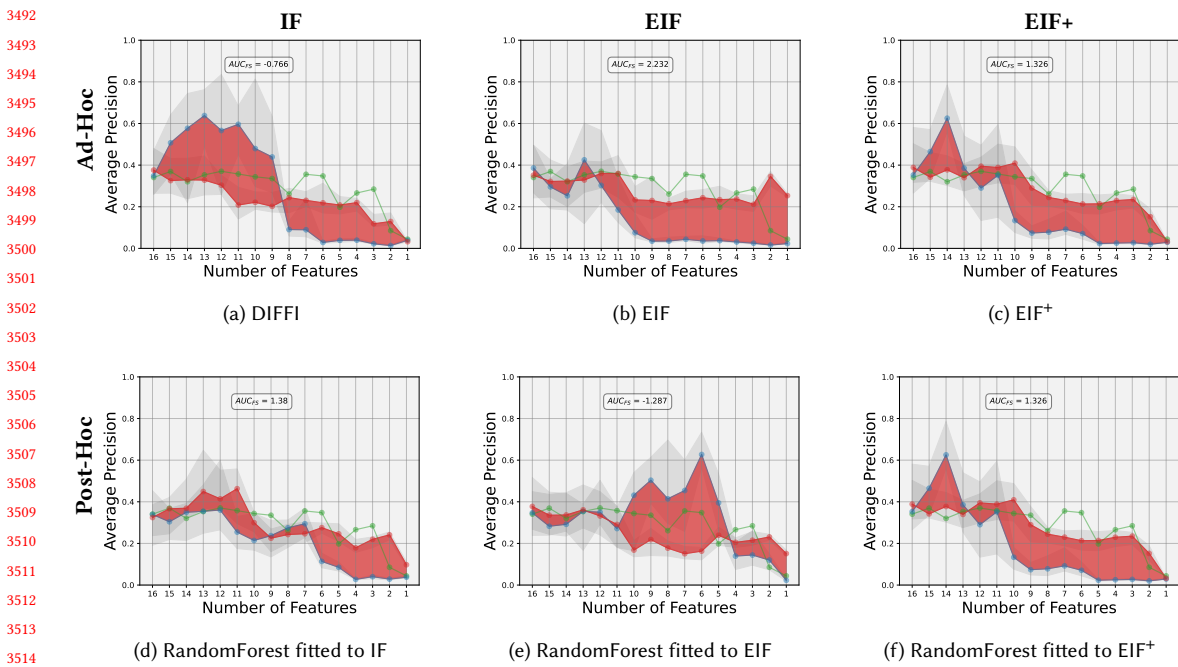


Fig. 47. Bar Plot, Score Plot and Scoremap for Pendigits in the two different Scenarios, using the ExIFFI algorithm applied to the EIF⁺ model.

3485 **A.5.15 Feature Selection.** A confirmation of the conclusions reached from the analysis conducted in A.5.14 can be
 3486 achieved looking at the Feature Selection plots organized in Figure 48. In particular in Figure 48c it is possible to
 3487 highlight how the Average Precision gradually decreases reducing the number of input features from 3 to 1, meaning
 3488 that dropping one of features 1,3 or 5 the model loses crucial information for the detection of anomalous points and
 3489 thus its detecting performance experience a considerable drop.
 3490



3504 Fig. 48. Feature Selection of the different Ad-Hoc and Post-Hoc methods applied to the 3 Isolation Forest models: IF, EIF and EIF⁺.
 3505 The blue line is the values of average precision, calculated with the EIF⁺ model in the Scenario II, dropping the most important feature
 3506 at each step, the red line is the values of average precision dropping the least important feature at each step and the green line is the
 3507 value of the feature selection dropping a random feature at each step.
 3508

3513 To conclude the experimental evaluation of the Pendigits dataset it is possible to analyse Table 31, where a
 3514 quantitative evaluation of the effectiveness of the different interpretation methods proposed is carried on. The model
 3515 that correctly captures the ranking of features according to their relevance is ExIFFI, followed by ExIFFI + as it is
 3516 testified by the high values of the AUC_{FS} metric. On the other hand explanations based on post-hoc methods using
 3517 Random Forest as a surrogate model prove to wrongly interpret the importance of features and are consequently
 3518 associated to negative values of AUC_{FS} . Finally it is also worth noticing how the interpretation methods deriving from
 3519 Isolation-based AD methods (i.e. DIFFI, ExIFFI and ExIFFI +) showcase much more efficient time performances in the
 3520 computation of the importance scores with the respect to the post-hoc methods.
 3521

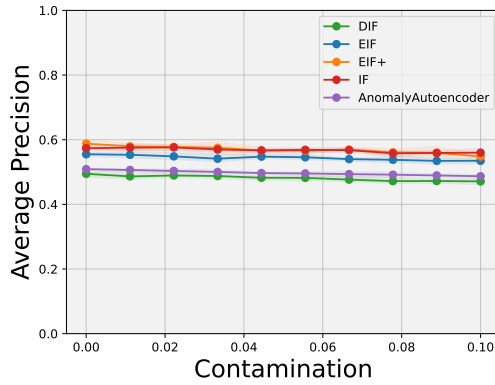
Pima

3532 **A.5.16 Performance.** The Contamination plot for the Pima dataset is reported in Figure 49a. It depicts how the Average
 3533 Precision metric of the AD models considered is not affected by the amount of outliers included in the training set. The
 3534 Manuscript submitted to ACM
 3535

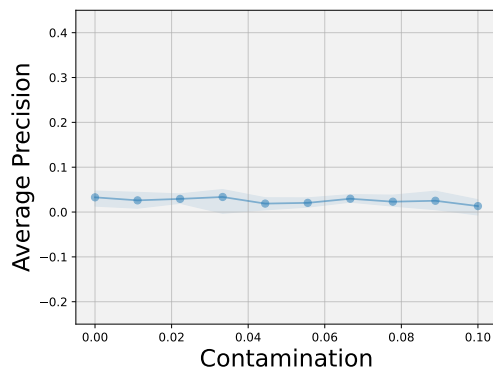
Table 31. Quantitative evaluation of the effectiveness of 6 different interpretation algorithms on Pendigits through the AUC_{FS} metric, introduced in 5.2. In the last column the average time taken by the different models to produce the importance scores is reported. The highest AUC_{FS} and lowest Importance time values are highlighted in bold.

| Interpretation | Evaluation with EIF | | Evaluation with EIF ⁺ | | Importance time |
|----------------|--------------------------|---------------------------|----------------------------------|---------------------------|-----------------|
| | Scenario I AUC_{FS} | Scenario II AUC_{FS} | Scenario I AUC_{FS} | Scenario II AUC_{FS} | |
| DIFFI | 0.118 | -0.384 | 0.233 | -0.766 | 0.37 |
| EXIFFI | 1.588 | 1.887 | 1.767 | 2.232 | 1.25 |
| EXIFFI+ | 1.868 | 1.227 | 1.921 | 1.326 | 1.22 |
| IF_RF | 1.484 | 1.281 | 1.377 | 1.38 | 8.9 |
| EIF_RF | -0.728 | -0.842 | -0.368 | -1.287 | 8.9 |
| EIF+_RF | -1.402 | -0.249 | -0.971 | -0.748 | 8.9 |

Isolation-based models (i.e. IF, EIF and EIF⁺) emerge as the ones with the better performances though the margin on the deep learning based methods (i.e. DIF and Autoencoder) is minimal.



(a) Models evaluation, varying the contamination levels



(b) Difference between EIF⁺ and EIF average precision

Fig. 49. Figure 49a illustrates the average precision as the contamination level in the training set increases. Figure 49b compares the performance graphs of EIF and EIF⁺, using the difference of their scores in various contamination levels.

Table 32 includes additional metrics other than Average Precision and focuses on the cases in which the training set's contamination is null (i.e. Scenario II) and equal to the total number of outliers in the dataset (i.e. Scenario I). As already described in A.5.16 the difference between the two previously depicted scenarios is minimal and the proposed EIF⁺ once again proves to be the optimal model also on the Pima dataset.

A.5.17 Importance Plots. In Figure 50 the outcomes produced by the ExIFFI + model in interpreting the EIF⁺ model are reported. Prior to commenting the feature ranking produced by the Score and Bar Plots it is crucial to notice how the outliers are overlapped with the normal points in the Pima dataset as it can be realized looking at the Local scoremaps contained in Figures 50c and 50f. This observation is explanatory for the peculiar phenomenon encountered in the Contamination plot, in fact since outliers are mostly overlapped to normal points including them or not into the training set will not affect the Average Precision metric.

Table 32. Performances of 5 different Anomaly Detection models over Pima are compared using classical Classification metrics. Moreover, the last two columns contain the average time for a fit and predict operation. The highest metric values and the lowest execution times are highlighted in bold

| AD Model | Scenario I | | | Scenario II | | | Time | |
|-------------|-------------|-------------|-------------|-------------|-------------|-------------|-------------|--------------|
| | Avg Prec | Prec | ROC AUC | Avg Prec | Prec | ROC AUC | fit | pred |
| IF | 0.51 | 0.52 | 0.63 | 0.58 | 0.55 | 0.66 | 0.11 | 0.008 |
| EIF | 0.49 | 0.49 | 0.61 | 0.54 | 0.57 | 0.67 | 0.07 | 0.03 |
| EIF+ | 0.49 | 0.5 | 0.61 | 0.58 | 0.57 | 0.67 | 0.08 | 0.03 |
| DIF | 0.41 | 0.41 | 0.54 | 0.49 | 0.46 | 0.59 | 1.17 | 1.00 |
| AutoEncoder | 0.43 | 0.44 | 0.57 | 0.5 | 0.54 | 0.64 | 3.11 | 0.06 |

The superimposition of anomalies and normal observations is verified because, as described in 6.2, the real world benchmark datasets normally used in the literature to assess the performances of Anomaly Detection models are nothing more than an adaptation of Binary or Multi Class Classification datasets to the task of identifying outliers. As a consequence the data points that are labeled as anomalous (i.e. the data samples beholding to the least represented class) in some cases may not truly deviate from the inliers distributions as they should as anomalous points. As a consequence AD models based on the concept of isolating anomalies from inliers (such as EIF⁺) may not be effective to solve the Anomaly Detection task on this dataset and the interpretations furnished by ExIFFI + may be misleading and not aligned with the ground truth. In any case, according to the Score Plots produced (and represented in Figure 50b and 50e) the most important features, both in Scenario I and Scenatio II, are *BloodPressure*, *BMI* and *Insulin*.

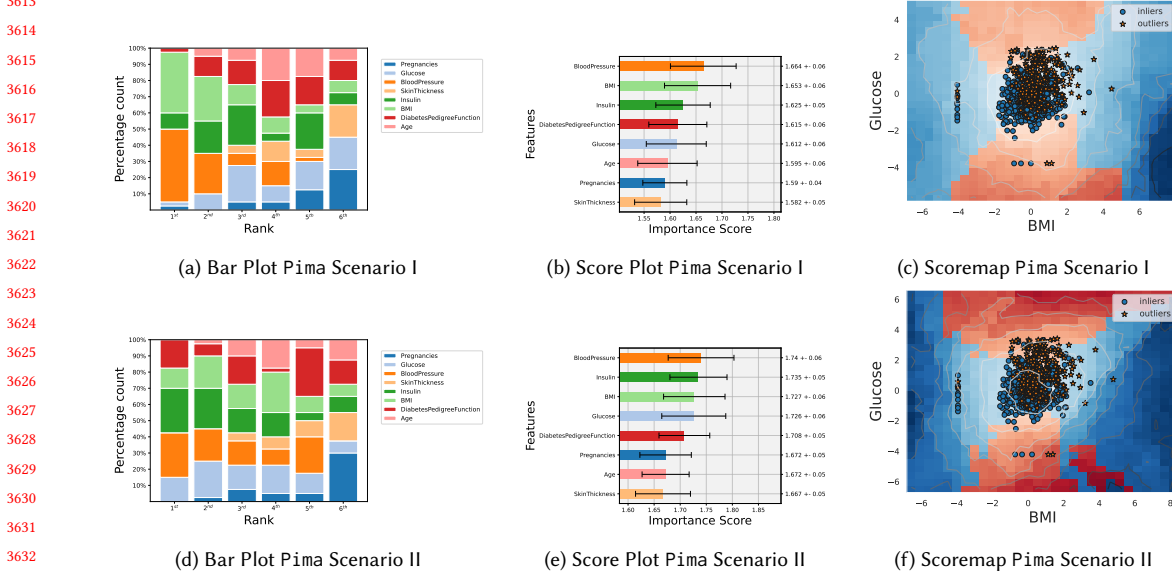


Fig. 50. Bar Plot, Score Plot and Scoremap for Pima in the two different Scenarios, using the ExIFFI algorithm applied to the EIF⁺ model.

A.5.18 Feature Selection. As a consequence of the peculiar distribution of anomalies in the Pima dataset, the results produced by the application of the Unsupervised Feature Selection proxy task (Figure 50 do not show interesting shapes

since in most of the cases the Average Precision stays constant, both in the red and blue line, across all the different subset of features considered.

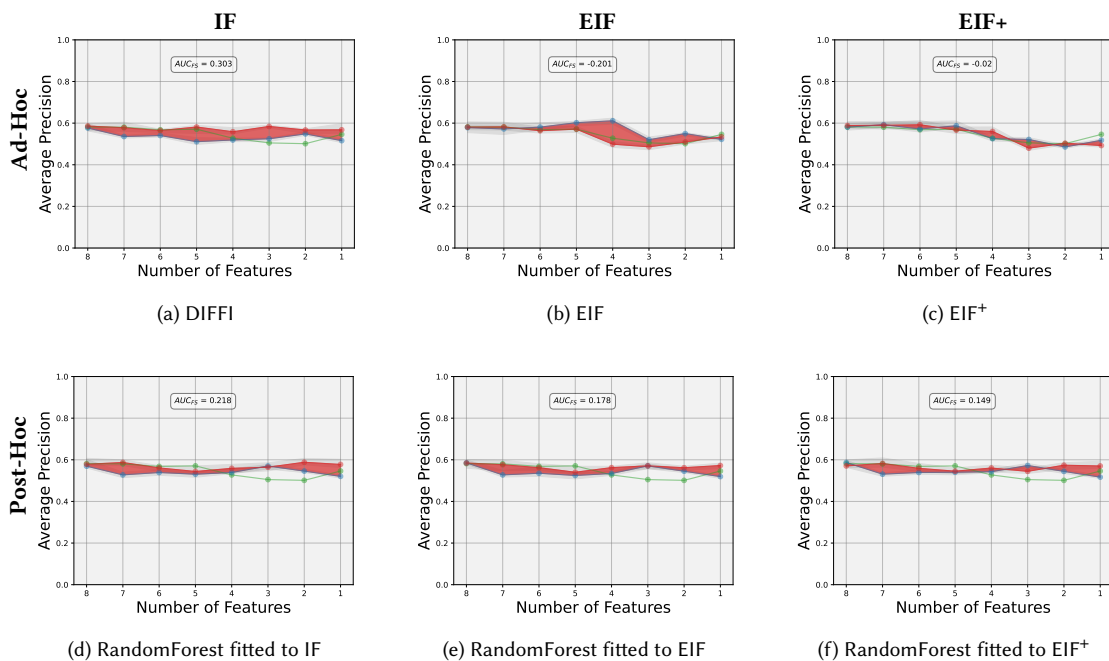


Fig. 51. Feature Selection of the different Ad-Hoc and Post-Hoc methods applied to the 3 Isolation Forest models: IF, EIF and EIF⁺. The blue line is the values of average precision, calculated with the EIF⁺ model in the Scenario II, dropping the most important feature at each step, the red line is the values of average precision dropping the least important feature at each step and the green line is the value of the feature selection dropping a random feature at each step.

As a consequence of the flat shapes observed in the Feature Selection plots the values of the AUC_{FS} metric grouped together in Table 33 are close to zero and negative in most of the cases.

Table 33. Quantitative evaluation of the effectiveness of 6 different interpretation algorithms on Pima through the AUC_{FS} metric, introduced in 5.2. In the last column the average time taken by the different models to produce the importance scores is reported. The highest AUC_{FS} and lowest Importance time values are highlighted in bold.

| Interpretation | Evaluation with EIF | | Evaluation with EIF ⁺ | | Importance time |
|----------------|--------------------------|---------------------------|----------------------------------|---------------------------|-----------------|
| | Scenario I AUC_{FS} | Scenario II AUC_{FS} | Scenario I AUC_{FS} | Scenario II AUC_{FS} | |
| DIFFI | -0.489 | 0.256 | -0.497 | 0.303 | 0.57 |
| EXIFFI | -0.316 | -0.214 | -0.324 | -0.201 | 0.067 |
| EXIFFI+ | -0.309 | -0.037 | -0.272 | -0.02 | 0.06 |
| IF_RF | -0.369 | 0.191 | -0.301 | 0.218 | 0.43 |
| EIF_RF | -0.443 | 0.127 | -0.416 | 0.178 | 0.43 |
| EIF+_RF | -0.288 | 0.063 | -0.286 | 0.149 | 0.43 |

3693 **Shuttle**
 3694
 3695
 3696
 3697
 3698
 3699
 3700

A.5.19 *Performance.* Figure 52a displays changes in the Average Precision metric as the contamination level of the training set used for the fitting process of the AD models considered in this study increased from 0 to 10 %. The EIF⁺ and DIF model present a decreasing trend proving once again how these methods, EIF⁺ in particular, are more suitable for datasets in which the contamination is limited. As it can be observed in Figure 52b the EIF model achieves slightly better performances than EIF⁺ in this particular dataset.

3701

3702

3703

3704

3705

3706

3707

3708

3709

3710

3711

3712

3713

3714

3715

3716

3717

3718

3719

3720

3721

Fig. 52. Figure 52a illustrates the average precision as the contamination level in the training set increases. Figure 52b compares the performance graphs of EIF and EIF⁺, using the difference of their scores in various contamination levels.

3722

3723

3724

3725

3726

3727

3728

3729

3730

3731

3732

3733

3734

3735

3736

3737

3738

3739

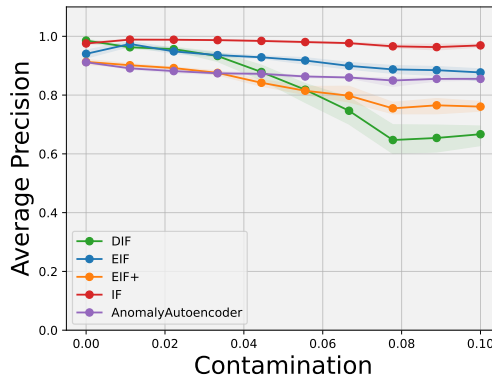
3740

3741

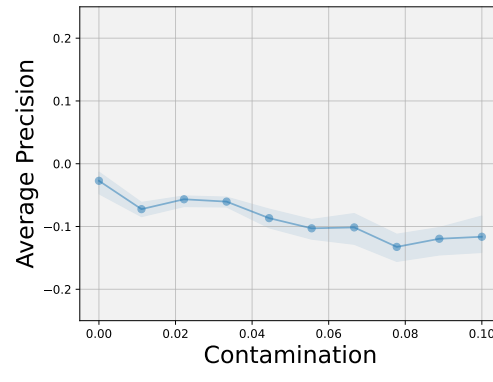
3742

3743

3744



(a) Models evaluation, varying the contamination levels

(b) Difference between EIF⁺ and EIF average precision

A comparison between Classification reports of the AD models in Scenario I and Scenario II is reported in Table 34. The IF model can be considered the best according to the metric values but it is worth noticing the significant improvement of the proposed EIF⁺ model passing from Scenario I to Scenario II.

Table 34. Performances of 5 different Anomaly Detection models over Shuttle are compared using classical Classification metrics. Moreover, the last two columns contain the average time for a fit and predict operation. The highest metric values and the lowest execution times are highlighted in bold

| AD Model | Scenario I | | | Scenario II | | | Time | |
|-------------|-------------|-------------|-------------|-------------|-------------|-------------|-------------|-------------|
| | Avg Prec | Prec | ROC AUC | Avg Prec | Prec | ROC AUC | fit | pred |
| IF | 0.98 | 0.96 | 0.97 | 0.98 | 0.97 | 0.98 | 0.21 | 0.06 |
| EIF | 0.9 | 0.87 | 0.93 | 0.97 | 0.95 | 0.97 | 0.16 | 0.54 |
| EIF+ | 0.7 | 0.71 | 0.84 | 0.91 | 0.96 | 0.97 | 0.2 | 0.36 |
| DIF | 0.54 | 0.6 | 0.78 | 0.99 | 0.97 | 0.98 | 10.5 | 9.02 |
| AutoEncoder | 0.9 | 0.95 | 0.97 | 0.9 | 0.94 | 0.97 | 19.6 | 0.25 |

A.5.20 *Importance Plots.* Similarly to the Pima dataset also in Shuttle anomalies are superimposed to the inliers distribution, as observable in the Local Scoremaps depicted in Figures 53c and 53f thus also for this dataset the explanations produced by ExIFFI+ should be evaluated with care. Comparing the feature rankings produced in the

Score Plots in Figure 53b and 53e a feature that should be considered as relevant is Feature 0 since it is placed in second position in both Scenario I and II.

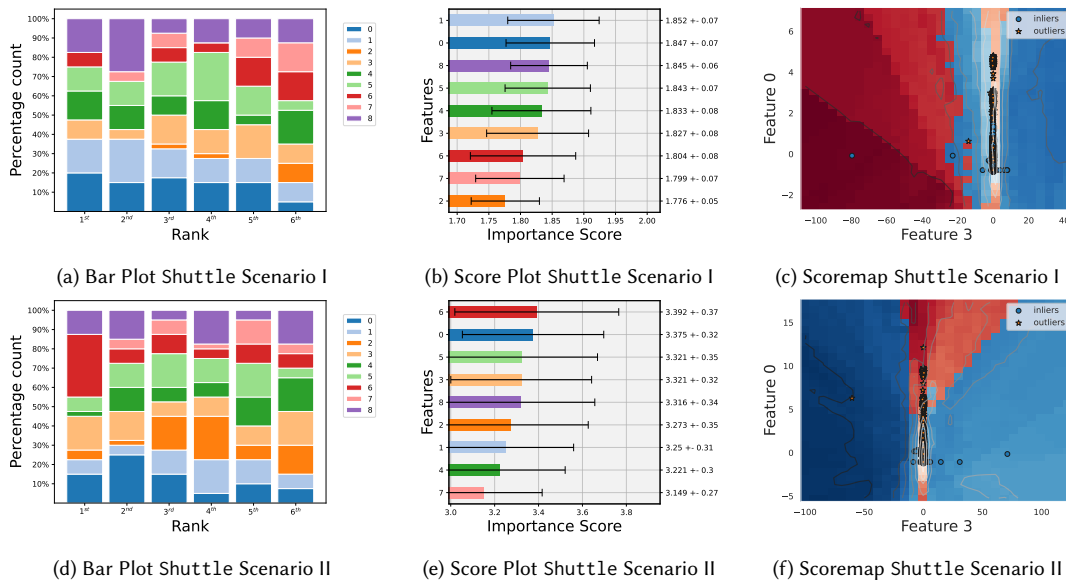


Fig. 53. Bar Plot, Score Plot and Scoremap for Shuttle in the two different Scenarios, using the ExIFFI algorithm applied to the EIF⁺ model.

A.5.21 Feature Selection. Feature Selection plots for the Shuttle dataset are grouped together in Figure 54 . Because of the peculiar distribution of the data points, that violates the typical properties anomalies are intended to have, post-hoc interpretation methods achieve better results than Isolation-based models. In fact in Figures 54d, 54e, 54f are associated with a constant trend in Average Precision as features are removed in increasing order of importance (red line) while precision decreases as features are excluded from the input space in decreasing order or relevance (blue line). On the other hand in Figures related to the ExIFFI and ExIFFI + models (Figures 54b, 54c) the red line presents a decreasing trend leading to small (if not negative) values of the AUC_{FS} metric.

Table 35 contains the AUC_{FS} metrics values for all the combinations of interpretation and evaluation model both for Scenario I and Scenario II. As already discussed in A.5.21 using a post-hoc interpretation model based on Random Forest as a surrogate is the best choice for the Shuttle dataset. The AUC_{FS} values of the proposed interpretation algorithms ExIFFI and ExIFFI +, even though faster than post-hoc methods, are lower and in some cases also negative.

Wine

A.5.22 Performance. The Contamination plot, depicted in Figure 55a, shows how the Average Precision of all the Anomaly Detection models considered diminishes as outliers are progressively included as part of the training set. EIF⁺ is the model with the best metric values for low values of the contamination parameter confirming another time its effectiveness in datasets with a limited number of outliers as Wine. Moreover Figure 55b , that represents the difference in the Average Precision values of the EIF and EIF⁺, enhances the superiority of the proposed model with the respect to its counterpart.

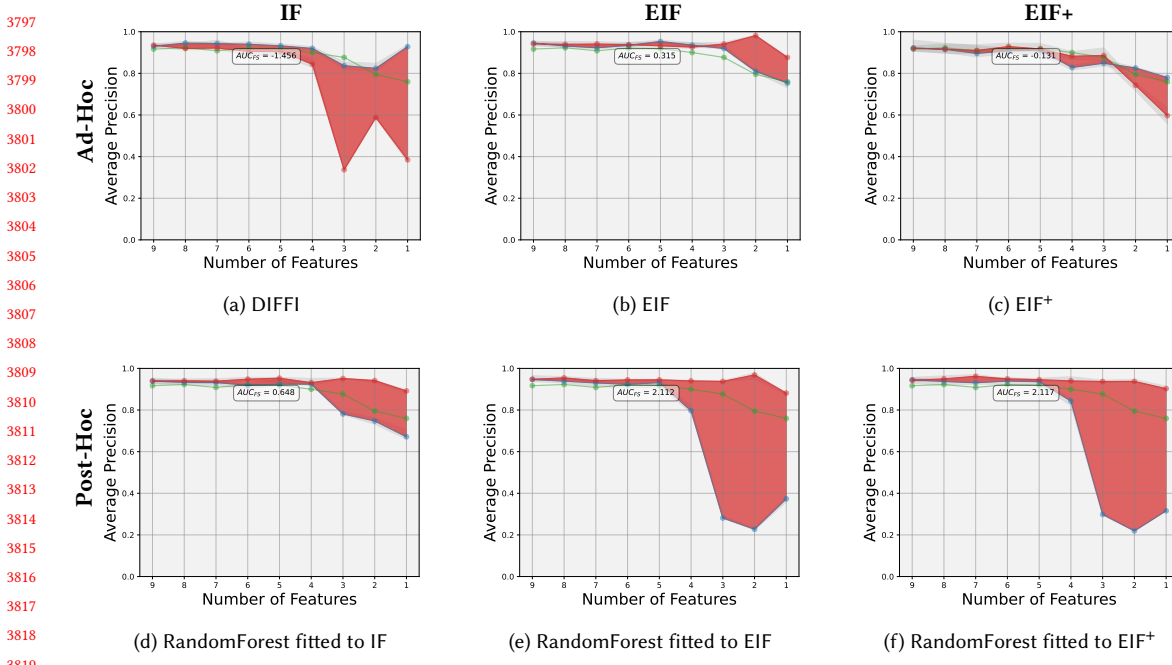


Fig. 54. Feature Selection of the different Ad-Hoc and Post-Hoc methods applied to the 3 Isolation Forest models: IF, EIF and EIF⁺. The blue line is the values of average precision, calculated with the EIF⁺ model in the Scenario II, dropping the most important feature at each step, the red line is the values of average precision dropping the least important feature at each step and the green line is the value of the feature selection dropping a random feature at each step.

Table 35. Quantitative evaluation of the effectiveness of 6 different interpretation algorithms on Shuttle through the AUC_{FS} metric, introduced in 5.2. In the last column the average time taken by the different models to produce the importance scores is reported. The highest AUC_{FS} and lowest Importance time values are highlighted in bold.

| Interpretation | Evaluation with EIF | | Evaluation with EIF ⁺ | | Importance time |
|----------------|--------------------------|---------------------------|----------------------------------|---------------------------|-----------------|
| | Scenario I AUC_{FS} | Scenario II AUC_{FS} | Scenario I AUC_{FS} | Scenario II AUC_{FS} | |
| DIFFI | -0.514 | -1.487 | -0.693 | -1.456 | 0.95 |
| EXIFFI | -1.432 | 0.766 | 1.223 | 0.315 | 1.38 |
| EXIFFI+ | 0.459 | 0.019 | 0.736 | -0.131 | 1.39 |
| IF_RF | 0.44 | 0.904 | 0.36 | 0.648 | 2.33 |
| EIF_RF | 1.692 | 2.747 | 1.733 | 2.112 | 2.33 |
| EIF+_RF | 1.904 | 2.138 | 1.628 | 2.117 | 2.33 |

Table 36 provides a comprehensive comparison of the performances of the different methods analyzed in this study in the two different evaluation scenarios described in 5.2. In Scenario I the performances of Isolation based models (i.e. IF, EIF and EIF⁺) overcome the ones of deep learning based approaches (i.e. DIF and Autoencoder) while in Scenario II EIF⁺ stands out as the best performing model. Referring to the computational efficiency argument there is a clear separation between Isolation based and deep learning based models with the first ones being the fastest in fitting the model and providing predictions on new samples.

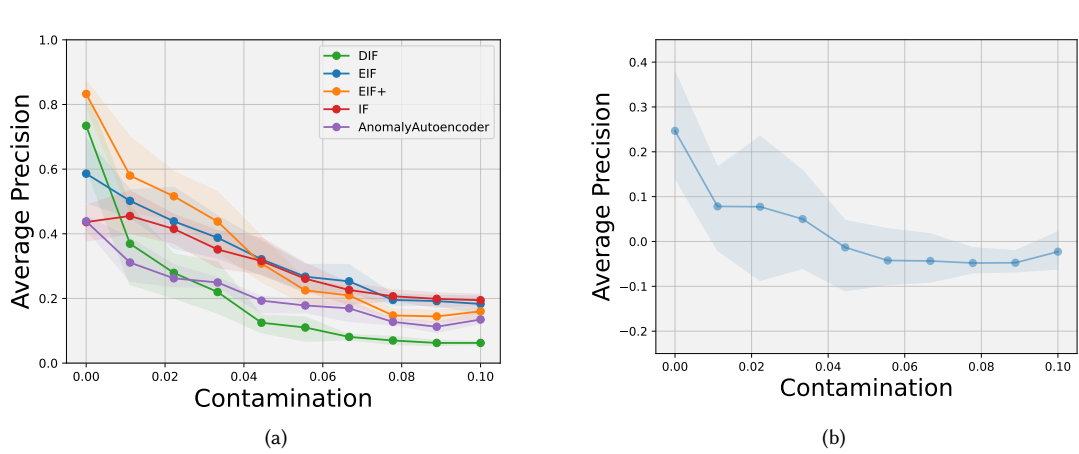


Fig. 55. Fig. 55a Represent the average precision the more the level of contamination of the train set is increased. The Fig. 55b Give show specifically the graphs of the EIF and EIF+

Table 36. Performances of 5 different Anomaly Detection models over Wine are compared using classical Classification metrics. Moreover the last two columns contain the average time for a fit and predict operation. The highest metric values and the lowest execution times are highlighted in bold

| AD Model | Scenario I | | | Scenario II | | | Time | |
|-------------|-------------|------------|-------------|-------------|------------|-------------|-------------|--------------|
| | Avg Prec | Prec | ROC AUC | Avg Prec | Prec | ROC AUC | fit | pred |
| IF | 0.26 | 0.2 | 0.56 | 0.61 | 0.5 | 0.72 | 0.10 | 0.002 |
| EIF | 0.21 | 0.2 | 0.56 | 0.57 | 0.6 | 0.78 | 0.09 | 0.005 |
| EIF+ | 0.17 | 0.0 | 0.45 | 0.79 | 0.7 | 0.83 | 0.10 | 0.002 |
| DIF | 0.07 | 0.0 | 0.45 | 0.72 | 0.7 | 0.83 | 0.57 | 0.21 |
| AutoEncoder | 0.14 | 0.1 | 0.51 | 0.45 | 0.5 | 0.72 | 2.13 | 0.04 |

A.5.23 *Importance Plots.* Figure 56 provides a qualitative and quantitative evaluation of the proposed interpretation algorithm on the Wine dataset. In Scenario I ExIFFI+ is not able to identify, as shown in 56a, an attribute dominating the others in terms of relevance for pursuing the Anomaly Detection task. On the other hand, exploiting the characteristics of EIF⁺ when the training set is composed of solely inliers, feature Proline is indicated as the most important feature in Scenario II as depicted in 56e. The relevance of the Proline variable can be assesed observing the Local Scoremap reported in Figure 56f.

A.5.24 *Feature Selection.* Figure 57 shows the superiority of the EExIFFI and ExIFFI + interpretation algorithm, illustrated in Figures 57b and 57c. Using the feature ranking derived from the importance scores provided by these two methods, in fact, guarantees an increasing Average Precision as non relevant attributes are progressively removed from the feature space (red line) reaching almost perfect scores of 1. On the other hand following the blue line it is possible to notice an instantaneous drop in performance as the most important features are removed from the training set. On the other hand the DIFFI interpretation algorithm produces a clearly incorrect feature ranking, as observable in Figure 57a, where the blue line overcomes the red one leading to a negative value of AUC_{FS} .

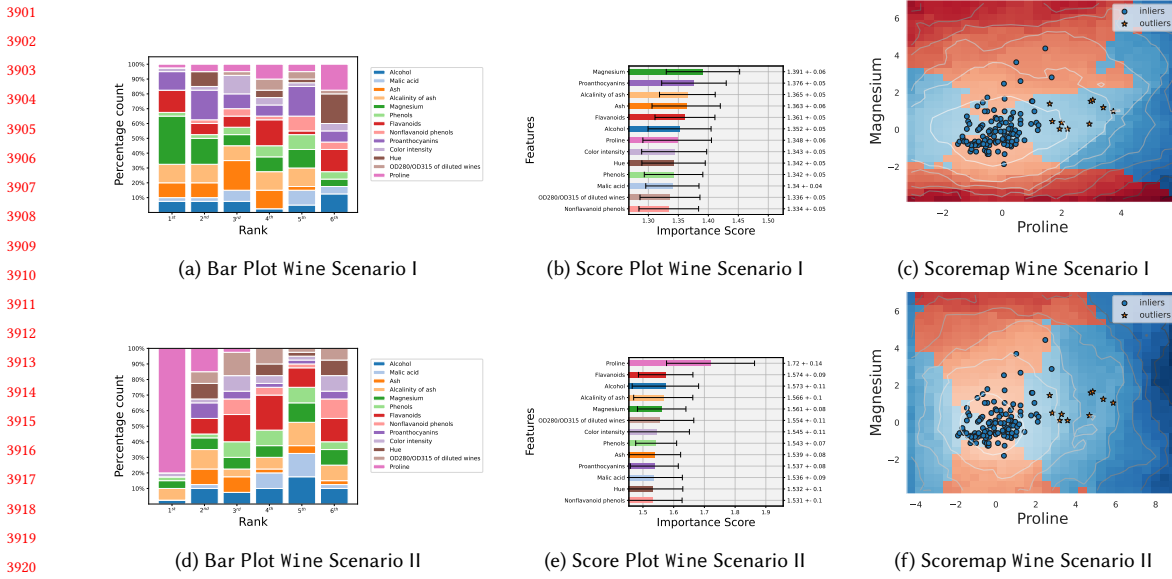


Fig. 56. Bar Plot, Score Plot and Scoremap for Wine in the two different Scenarios, using the ExIFFI algorithm applied to the EIF⁺ model.

The summary reported in 37 confirm the effectiveness of the proposed approach in providing explainability to the EIF and EIF⁺ AD methods surpassing DIFFI and ad-hoc interpretability approaches such as Random Forest that showcase negative values of the Feature Selection AUC.

Table 37. Quantitative evaluation of the effectiveness of 6 different interpretation algorithms on Wine through the AUC_{FS} metric, introduced in 5.2. In the last column the average time taken by the different models to produce the importance scores is reported. The highest AUC_{FS} and lowest Importance time values are highlighted in bold.

| Interpretation | Evaluation with EIF | | Evaluation with EIF ⁺ | | Importance time |
|----------------|--------------------------|---------------------------|----------------------------------|---------------------------|-----------------|
| | Scenario I AUC_{FS} | Scenario II AUC_{FS} | Scenario I AUC_{FS} | Scenario II AUC_{FS} | |
| DIFFI | 0.176 | -3.799 | 0.437 | -3.491 | 0.33 |
| EXIFFI | 0.451 | 7.122 | 0.459 | 8.12 | 0.01 |
| EXIFFI+ | 0.127 | 9.0 | 0.18 | 9.25 | 0.01 |
| IF_RF | -3.093 | 4.413 | -2.339 | 4.539 | 0.18 |
| EIF_RF | -2.415 | 3.946 | -1.57 | 4.369 | 0.18 |
| EIF+_RF | -2.816 | 4.873 | -2.056 | 5.642 | 0.18 |

A.6 EIF⁺: the effects of η

In this section the results of the ablation study on the η hyperparameter of the EIF⁺ model for the datasets covered in this Appendix are reported. The Yaxis dataset, presented in A.4, is excluded from this analysis because of its high similarity to the Xaxis dataset that lead to essentially identical outcomes.

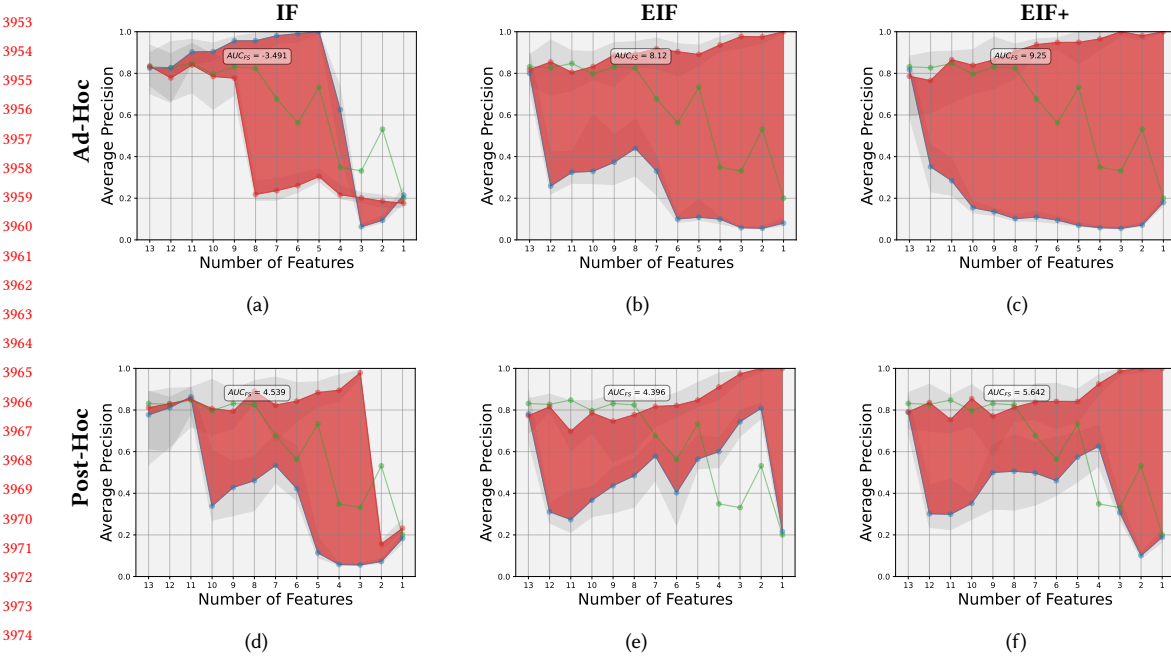


Fig. 57. Feature Selection of the different Ad-Hoc and Post-Hoc methods applied to the 3 Isolation Forest models: IF, EIF and EIF⁺. The blue line is the values of average precision, calculated with the EIF⁺ model in the Scenario II, dropping the most important feature at each step, the red line is the values of average precision dropping the least important feature at each step and the green line is the value of the feature selection dropping a random feature at each step.

The ablation study consists in evaluating the performance of the EIF⁺ model, through the Average Precision metric, for 25 linearly spaced values between 0.5 and 5 of the parameter η , whose interpretation is given in 3.3.

After a careful observation of the plots collected in Figure 58 it is possible to conclude that for the Bisect, Breastw, Ionosphere and Shuttle the Average Precision of EIF⁺ is not affected by the value of the parameter η . In fact, as it can be noticed comparing to the blue line inserted in the plot to represent the Average Precision value achieved by the EIF model, in these sets of data the improvement achieved by EIF⁺ on its counterpart EIF is minimal since both models already achieve almost perfect precision scores. As a consequence the model remain unchanged independently on the η value since anomalies are detectable utilizing the traditional oblique cuts employed by EIF.

For other datasets, where the data distribution is intricate and EIF-like partitions are not as effective as the novel partition approach introduced with EIF⁺, the effect of η is more visible in the sense that there are some contained oscillations on the Average Precision values as the hyperparameter is varied.

Concluding, comparing the diverse plots produced it is possible to infer that the optimal value for the parameter analysed in this section is highly dependent on the specific dataset structure and thus the suggested approach is to perform an hyperparameter optimization through a validation set in order to optimal value of η .

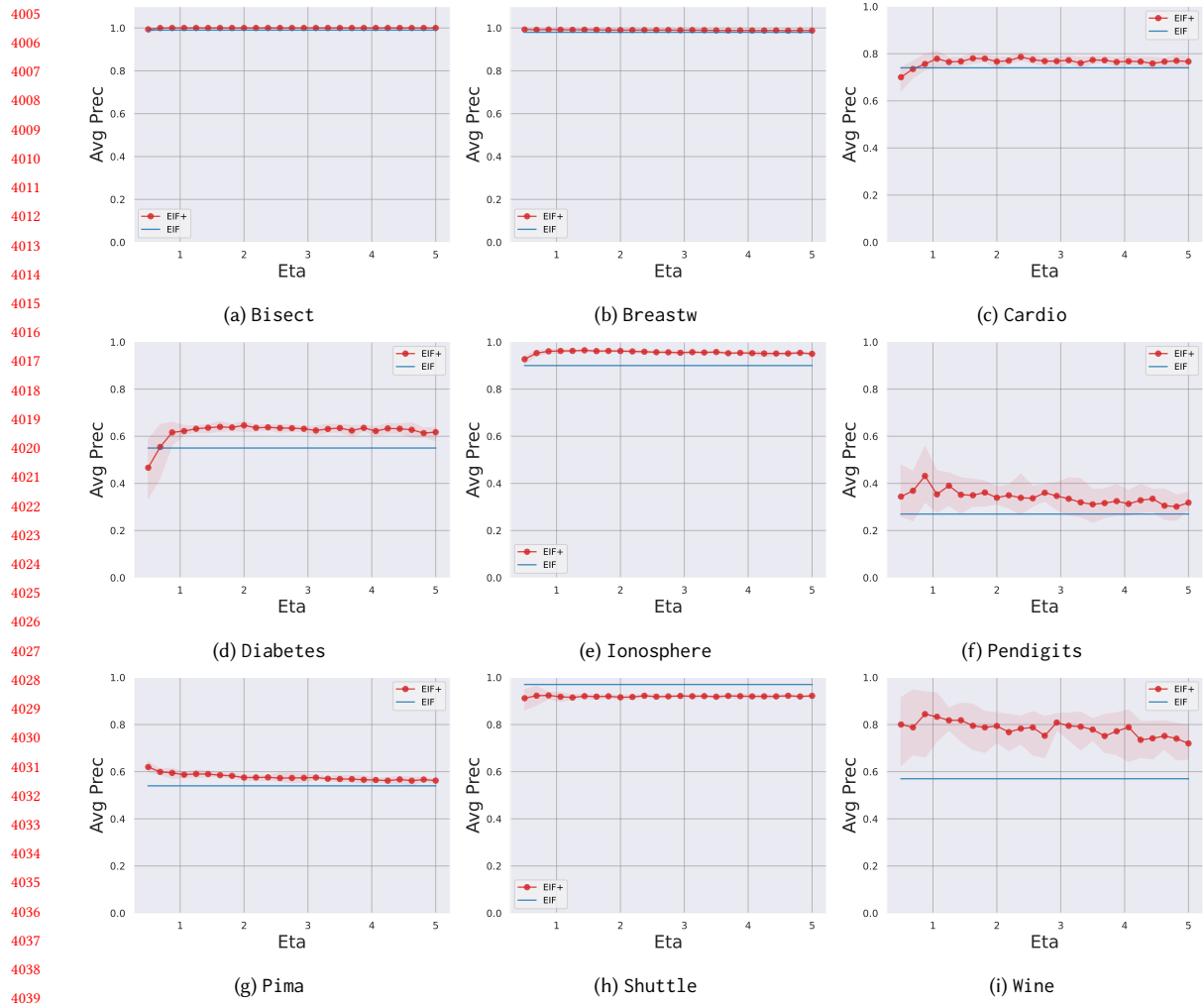


Fig. 58. Exploration of how average precision changes with variations in the η parameter.